DOKUZ EYLÜL UNIVERSITY

GRADUATE SCHOOL OF NATURAL AND APPLIED SCINCES

VIBRATION ANALYSIS OF COMPLEX STRUCTURES SUBJECTED TO MOVING LOADS

by

Salih DEMİRTAŞ

January, 2020

İZMİR

VIBRATION ANALYSIS OF COMPLEX STRUCTURES SUBJECTED TO MOVING LOADS

A Thesis Submitted to the
Graduate School of Natural and Applied Sciences of Dokuz Eylül University
In Partial Fulfillment of the Requirements for the Degree of Doctor of Philosophy in Mechanical Engineering, Machine Theory and Dynamics Program

by

Salih DEMİRTAŞ

January, 2020

İZMİR

Ph.D. THESIS EXAMINATION RESULT FORM

We have read the thesis entitled "**VIBRATION ANALYSIS OF COMPLEX STRUCTURES SUBJECTED TO MOVING LOADS**" completed by **SALİH DEMİRTAŞ** under supervisor of **PROF. DR. HASAN ÖZTÜRK** and we certify that in our opinion it is fully adequate, in scope and in quality, as a thesis for the degree of Doctor of Philosophy.

Prof. Dr. Hasan ÖZTÜRK

Supervisor

Prof. Dr. Zeki KIRAL

Thesis Committee Member

Prof. Dr. Hasan YILDIZ

Thesis Committee Member

Assoc. Prof. Dr. Levent ÇETİN

Examining Committee Member

Prof. Dr. Lale Canan DÜLGER

Examining Committee Member

Prof. Dr. Kadriye ERTEKİN

Director

Graduate School of Natural and Applied Sciences

ACKNOWLEDGEMENTS

I would like to thank my academic supervisors Professor Dr. Hasan Ozturk for his guidance. His support and patience has been invaluable in helping me to learn how to do research.

I am sincerely grateful to Professor Dr. Mustafa Sabuncu who was my supervisor at the beginning of the Ph.D. study and passed away before the end of my doctoral thesis. Without his valuable contributions, we would not have been able to complete this study.

I would also like to thank Professor Dr. Zeki Kıral and Professor Dr. Hasan Yıldız who have offered guidance, feedback and suggestions along the way.

I am forever indebted to my master thesis supervisor Professor Dr. Metin Gürgöze for their guidance, and unrelenting support throughout this process.

Salih DEMİRTAŞ

VIBRATION ANALYSIS OF COMPLEX STRUCTURES SUBJECTED TO MOVING LOADS

ABSTRACT

In this doctoral thesis, dynamic responses of the complex structure subjected to vehicles moving at a constant speed V have been studied. The complex structure, that is, multi- bay and multi- storey frames, is thought to be as a model of a viaduct. The dynamic response of the viaduct under passage of the high-speed train is important issue for design of the structures, passenger comfort, derailment of the train, etc. Various vehicle as a model of a train are used: (1) the moving load model, (2) moving oscillator model, (3) the moving 2-axle vehicle with 4 degrees-of-freedom (DOF), (4) the moving 10 DOF multi-body system consisting of 2-bogies and 4-axle.

The dynamic analysis of the vehicle-structure interaction (or moving load-structure) system is performed by using the finite element method. The beams and columns forming the frame structure are modelled by the Bernoulli-Euler beam theory. The presence of cracks in the structure is also examined. This is significant because the structure is subjected to high amplitude vibrations for a long time, the fatigue-induced crack formation can occur. The presence of a crack changes the stiffness of the structure. The stiffness is decreased and this implies a reduction of the natural frequency of the structure. Depending on the location of the crack, the reduction effect in stiffness or natural frequency varies. In order to obtain the stiffness matrix of the cracked element, the total elasticity matrix is first calculated. The stiffness matrix of the cracked element in the free-free state is then determined from the condition of equilibrium.

The equations of motion are determined by the generalized Lagrange's equation. The equations of motion corresponding to the vehicle-structure system is a coupled second-order differential equations with variable coefficient. The Newmark method and Wilson-theta method of direct integration are used to integrate those equations.

In this thesis, the effects of the crack location, the velocity of moving vehicle/load, number of bays/storeys, force span length and mode shapes on the dynamic response of complex structures have been investigated. In order to validate the finite element model, code developed with MATLAB software has been compared with a study in the literature or ANSYS software. Three-dimensional(3D) graphics have been used to evaluate the results.

Keywords: Viaduct, moving vehicle, finite element method, vehicle-structure interaction, cracked beam

HAREKETLİ YÜKLERE MARUZ KALAN KOMPLEKS YAPILARIN TİTREŞİM ANALİZİ

ÖZ

Bu doktora tezinde, V sabit hızıyla hareket eden taşıtlara maruz kalan kompleks yapıların dinamik analizleri incelenmiştir. Çok bölmeli ve çok katlı çerçeveler bir viyadük modeli olarak düşünülmüştür. Hızlı tren geçişi altındaki viyadüklerin dinamik tepkisi, yapıların tasarımı, yolcu konforu, trenin raydan çıkması, vb. bakımından önem taşır. Bir tren modeli olarak çeşitli yükleme tipleri kullanılmıştır. Bunlar: (1) hareketli yük modeli, (2) hareketli osilatör modeli, (3) 4 serbeslik dereceli 2 akslı araç modeli, (4) 10 serbestlik dereceli 2 boji ve 4 akstan oluşan çoklu gövdeli araç sistemidir.

Araç-yapı etkileşimi (veya hareketli yük-yapı) sisteminin dinamik analizinde, sonlu elemanlar yöntemi kullanıldı. Çerçeve yapısını oluşturan kirişler ve sütunlar Bernoulli-Euler kiriş teorisi ile modellenmiştir. Yapıda çatlak bulunması durumu da incelenmiştir. Bu durum, yapının yüksek genlikli titreşimlere uzun süre maruz kalması halinde yorulma kaynaklı çatlak oluşabileğinden dolayı önemlidir. Bir çatlağın varlığı, yapının katılığını değiştirir. Katılık azalır ve bu da yapının doğal frekansının azalmasına sebep olur. Çatlağın konumuna bağlı olarak, yapının katılığındaki veya doğal frekanslarındaki azalma etkisi değişir. Çatlak elemanın katılık matrisi kırılma mekaniği prensiplerinden faydalanılarak belirlenmiştir.

Hareket denklemleri genelleştirilmiş Lagrange denklemi ile belirlenmiştir. Taşıt-yapı sisteminin titreşimlerini temsil eden hareket denklemleri, değişken katsayılı, bağlı, ikinci mertebeden diferansiyel denklemlerdir. Bu denklemlerin integrasyonu için Newmark metodu ve Wilson-teta direkt integrasyon metodu kullanılmıştır.

Bu tez çalışmasında, çatlak yerinin, hareketli taşıt / yük hızının, çerçeve yapının bölme sayısının / kat sayısının, yük aralığının ve mod şekillerinin karmaşık yapıların dinamik tepkisi üzerindeki etkileri incelenmiştir. Sonlu elemanlar modelini

doğrulamak için, MATLAB yazılımı ile geliştirilen kod, literatürdeki bir çalışma ile veya ANSYS yazılımı kullanılarak oluşturulan sayısal model ile karşılaştırılmıştır. Sonuçları değerlendirmek için üç boyutlu (3B) grafikler kullanılmıştır.

Anahtar kelimeler: Viyadük, hareketli araç, sonlu elemanlar metodu, araç-yapı etkileşimi, çatlaklı kiriş

CONTENTS

Page

LIST OF FIGURES

Page

LIST OF TABLES

Page

CHAPTER ONE
INTRODUCTION

1.1 Introduction

Nowadays, the use of fossil fuels as the main reason for the increase of air pollution imposes higher demands for rail transportation. The importance of high-speed railway, due to its high-speed, comfortable riding, safe running, enhance inter-regional economic ties, promoting regional economic growth, has increased. The first high-speed rail system between Tokyo and Osaka began operation in 1964 in Japan. The train could reach a speed of 210 km/h. In 1977, this was followed by a high-speed train (HST) line between Rome and Florence, which became Europe's first high-speed railway, with a maximum speed of 250 km/h. Later, the first HST lines were inaugurated in Germany and France in the 1980s, and Spain in 1992 (Hughes, 2015).

Figure 1.1 HST lines in Turkey (Ministry of Transport and Infrastructure of the Republic of Turkey, 2018)

In Turkey, the first line opened in 2009 between Eskişehir and Ankara and is 245 km in length. Then, the 212 km HST line between Ankara and Konya was put into service in 2011. Finally, the 288 km HST line between Eskişehir and İstanbul was started the

operation in 2014. There is a total 594 km line in operation (Ministry of Transport and Infrastructure of the Republic of Turkey, 2018). The maximum speed of the trains, an example of such a train is shown in Figure 1.2 (a), used in these lines is approximately 250 km/h. The use of high-speed train (HST) lines and high-speed train in passenger transportation is increasing in Turkey. Ankara-Sivas and Ankara-İzmir HST lines are under construction (see Figure 1.1).

The high-speed railways require more viaducts/bridges (Figure 1.2 (b)-(c)) than a conventional railway. There are a total of 24 viaducts and 579 bridges on the HST line between Ankara and İstanbul and total length is 32.908 km (Turkish State Railways [TCDD], 2018). The ratio of viaducts and bridges' length to the total HST line length is 6.17 percent. It can be said that this ratio is small compared to the examples, such as 21.5 percent in TGV Northern line, 32.2 percent TGV Southern line, the average percentage in Japan is 48 percent, in the world (Guo et al., 2012).

(a)

(b)

(c)

Figure 1.2 (a) A high-speed train (Siemens, 2019), (b) Ankara-İstanbul HST line (TCDD, 2019), (c) Cikurutug bridge (Orangesmile, 2019)

The effects of dynamic interaction between vehicle and structure are important

issue due to the structural safety of the bridge, risk of derailment and deterioration of passenger comfort. Vehicle-structure interaction is a complex dynamic phenomenon depending on several factors, such as the traffic speed, bridge span and modal characteristics of the structure, the number and type of the vehicles, vehicle characteristics. The predominant parameter among them is the traffic speed especially when the traffic speed exceeds 200 km/h. Vehicle induced resonance effect must be taken into consideration in those speed values.

The wheel loads are repetitive in nature. Resonance takes place when the exciting frequency of wheel load coincides with a multiple of one of the structure's undamped natural frequency. Structural resonance is a phenomenon encountered in such a way the dynamic amplitudes are progressively increasing when the free vibration oscillations of the structure are large. If the structure is subjected to high amplitude vibrations for a long time, the fatigue-induced crack formation can occur. The presence of a crack changes the stiffness and damping of the structure. The stiffness is decreased and this implies a reduction of the natural frequency of the structure. Depending on the location of the crack, the reduction effect in stiffness or natural frequency varies.

1.2 Aims and Objectives

The main objectives of this thesis are to investigate the dynamic interaction between train and structure. It is aimed to understand better the dynamic interaction between the structure and the train. Viaducts are modelled as a multi-bay frame or multi-storey frame. The presence of cracks in the structure is also examined. Various models for the train are used. They comprise simplified models a series moving forces, moving undamped oscillators, and the sophisticated models including 2-axle 4 degrees of freedom (DOF) model and 10 DOF multi-body system with 4-axle 2-bogie (Figure 1.3).

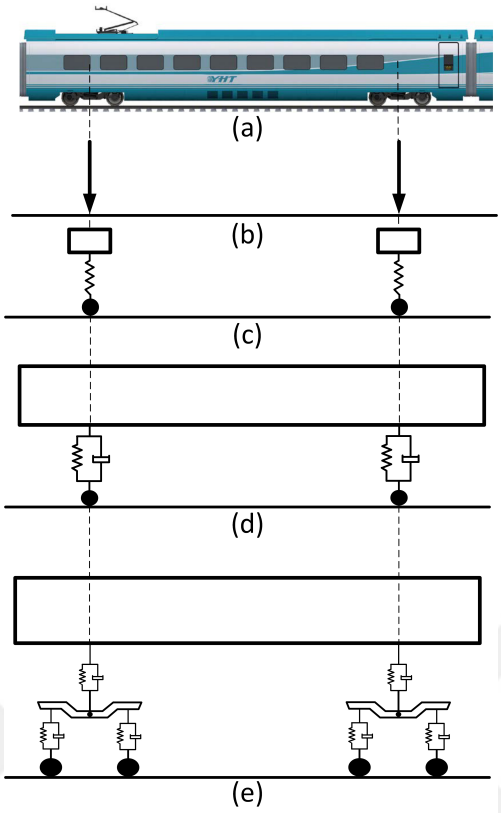

Figure 1.3 Models to represent a train: (a) A high-speed train carriage (Siemens, 2019), (b) the moving force model, (c) the moving undamped oscillator model, (d) the moving 2-axle vehicle model, (e) the moving 4-axle 2-bogie model

The followings are limitations made in modelling vehicular load and structure:

- Rail irregularities are not considered.
- Two-dimensional (2D) numerical model for structures and exciting mechanisms are used.
- The wheel-sets always keep in contact with the structure.
- The coach body, bogie and wheel-sets are regarded as rigid components which mean elastic deformation during vibration is neglected.
- The suspension system is idealised as linear springs and viscous dashpots.
- Each coach is identical. There are no differences between locomotive and passenger carriages.

- The vehicular load runs on the structure at a constant speed.
- The vehicle-structure interacting force act in the vertical direction. Horizontal forces generating due to moving vehicles are neglected.

1.3 Literature Review

Dynamic characteristics of structures under the action of moving loads have seen considerable interest over the years. Extensive lists of references on the subject of moving loads over elastic structures are contained in the classical monograph by Fryba (1999). Fryba presented various analytical solutions for vibration problems of uniform, single span, simply supported beams under moving loads in his book.

Structures, for instance, gantry crane, bridges, viaducts, subjected to moving loads are often encountered in engineering applications. The concentrated moving load model is the simplest one considering only bridge response. Wu et al. (2000) have developed a technique for using standard finite element packages to analyse the dynamic responses of structures to moving loads. The calculation of the equivalent nodal forces to represent moving loads has been performed by three approximate methods. In the first "full" method, equivalent nodal forces and moments have been calculated. This requires the shape functions for the elements. The second method simply ignores the moments calculated using method 1. The third "simple" method ignores any moments applied at the nodes at the outset and therefore does not require knowledge of the shape functions. Wu et al. (2001) have presented a technique using combined finite element and analytical methods for determining the dynamic responses of the structures to moving bodies. In order to illustrate the methodology, and for validation purposes, the technique has been first applied to a clamped-clamped beam subjected to a single mass moving along the beam. Then it has been applied to predict the dynamic response of an experimental mobile gantry crane structure due to the two-dimensional motion of trolley. Lin & Chang (2006) have developed an analytical method to investigate the dynamic responses of cracked cantilever Euler-Bernoulli beam under the action of a concentrated moving force. Şimşek &

Kocatürk (2009) investigated the free vibration characteristics and the dynamic behavior of a functionally graded simply supported beam under a concentrated moving harmonic load. Khalili et al. (2010) have studied the dynamic responses of functionally graded beams subjected to a moving load using a mixed method which combines the Rayleigh-Ritz and the differential quadrature method. The Lagrange equations have been used to derive the governing equations of motion. Johansson et al. (2013) derived a closed-form solution for calculating the dynamic characteristics of a general multi-span Euler-Bernoulli beam under moving loads. Ozturk et al. (2015) have studied the effects of crack depth and crack location on the in-plane static and dynamic stability of cracked multi-bay frame structures subjected to periodic loading using the finite element method. In addition, the effect of the number of spans and static and dynamic load parameters on static and dynamic stability analysis have been investigated. Kumar et al. (2015) have introduced a new formula to obtain the free vibration responses of a uniform both lightly damped and heavily damped simply supported beam under a single moving load. Rostam et al. (2015) have implemented various vibration control strategies to attenuate both the flexural and torsional vibrations of a curved beam traversed by off-center moving loads. Dimitrovová (2016) has introduced a new formula for determining a more realistic estimate of the critical velocity of a load moving uniformly over a beam supported by a foundation of finite depth. Song et al. (2016) have proposed a new spectral element analysis method for a beam, based on Timoshenko beam theory, subjected to a moving force which is represented as a series of point loads in frequency domain. Thambiratnam & Zhuge (1996) have presented a study for determining the effects of some parameters, such as the foundation stiffness, travelling speed, length of beam and stiffness of the sprung mass, on the dynamic responses of beams under a concentrated moving load. Henchi et al. (1997) have investigated the dynamic response of multi-span structures under a convoy of moving loads employing a dynamic modal representation coupled with the FFT technique. Zheng et al. (1998) have used developed modified beam vibration functions as the assumed modes to analyse the vibration of a multi-span non-uniform beam subjected to a moving load. Kiral Z. & Kiral B. G. (2007) have investigated dynamic responses of a symmetric laminated composite beam under a concentrated

force with a constant velocity. Song et al. (2016) have proposed a frequency domain spectral element method (SEM) for a Timoshenko beam model subjected to a moving point force. Svedholm et al. (2016) have investigated the dynamic behaviour of a non-proportionally damped Bernoulli-Euler beam with general end conditions under a moving load. Ozturk et al. (2015) have studied the dynamic behaviour of cracked beam which is resting on elastic support subjected to concentrated moving force with constant velocity.

Dynamic analysis of a structure subjected to moving vehicular loads requires an accurate model of the force induced by the vehicle. Lou et al. (2005) have presented modal coordinate formulation for analysing the dynamic interaction between a simply supported bridge and a moving train. The train is modelled as two-stage suspension vehicles with 10 DOF. Bridge is modelled as a uniform simply supported beam, based on Euler-Bernoulli beam theory. Rayleigh damping is assumed for the bridge. In the literature, the dynamic behaviour of structures subjected to four-axle two-bogie train with 10 unconstrained degrees of freedom is investigated by authors (Duan et al., 2018; Hubbell & Gauvreau, 2018; Wu & Yang, 2003; Youcef et al., 2013; Biondi et al., 2005). Other train models, such as those 2-axle 6 DOF (Xiang et al., 2007), 4 DOF (Yang et al, 1999); moving suspension mass model (Lin et al., 2005).

Bridges (or viaducts) are used mainly for the purpose of connecting two points of the terrain which are similar in height in order to carry mostly rail and road traffic. Su et al. (2010) studied the dynamic responses of a viaduct subject to high-speed train. 3D dynamic analysis models for train-bridge system are developed. The train idealized as a four-axle two-bogie with 27 degrees of freedom (DOF) dynamic system. The dynamic responses have investigated using field measurement and numerical simulations. Track irregularities have been considered in this study. The authors (Romero et al., 2013; Xia et al, 2012; Majka & Hartnett, 2008; Dimitrakopoulos & Zeng, 2015; Lee & Kim, 2010) have modelled vehicles and structures as 3D dynamic systems in their papers. The resonant response of the train-bridge system is of particular interest due to the structural safety of the bridge, risk of derailment and deterioration of passenger comfort. Mao & Lu (2013) have

studied the resonance of railway bridge under train load excitation taking into account the frequency characteristics of the excitation. In addition, the change in resonance frequency when the vehicle mass is involved has also been investigated. Museros & Alarcón (2005) have discussed the contribution of the second bending mode to the dynamic behaviour of railway bridge modelled as simply supported Bernoulli-Euler beam. Ju & Lin (2003) have investigated the resonant characteristic of the three-dimensional vehicle-bridge system under the action of train loads. Multi-span bridge with high piers and simply supported beam models have been used in their paper. Xia et al. (2006) have studied the effect of the parameters such as span, total length, the lateral and vertical stiffness of the bridge, the compositions of the train, and the axle arrangements and natural frequencies of the vehicles, on bridge resonance.

1.4 Contribution/originality

The study on the dynamic analyses of the viaduct-like structures under the effects of moving vehicles are rare. There are not many studies on this subject in the existing literature. These doctoral thesis aims to fill the gap in the existing literature. In the thesis, the dynamic analysis of the vehicle-structure interaction (or moving load-structure) system was performed by using the finite element method. Various vehicle/coach model representing the train such as the moving load model, moving oscillator model, the moving 2-axle vehicle with 4 degrees-of-freedom(DOF), the moving 10 DOF multi-body system consisting of 2-bogies and 4-axle, were used. The beams and columns forming the frame structure were modelled by the Bernoulli-Euler beam theory. The Rayleigh damping assumption was also made for structure. The equations of motion were determined by the generalized Lagrange's equation. Those equations are a coupled second-order differential equations with variable coefficient. The Newmark method and Wilson-theta method of direct integration were used to integrate those coupled equations. Also, the presence of cracks in the structure was considered and the effects of the crack location on

dynamic displacements were examined utilizing 3D graphics. Effects of the parameters like the velocity of moving vehicle/load, number of bays/storeys, force span length and mode shapes on the dynamic response of complex structures were also studied.

1.5 Outline of the thesis

This thesis is divided into six chapters. Chapter 1 provides an introduction, literature review and aims and objectives which include scopes and limitations of the thesis.

Chapter 2 provides a dynamic analysis of complex structures subjected to moving loads. The theoretical background of the finite element method is given. The multi-bay frame subjected to a moving single force and successive moving loads with a constant interval is discussed and presented in the paper (Demirtas et al., 2019) . The effect of the mode shapes on the dynamic response of the multi-storey frame are determined.

Chapter 3 is devoted to the finite element-based formulation of the vehicle-structure interaction dynamic problem. The coupled second-order equations of motions are derived using the generalized Lagrange equation. Three vehicle models are used. Those models are undamped oscillator with 2 degrees of freedom (DOF), 2-axle four DOF and 4-axle 2-bogie multi-body system with ten DOF.

Two case studies are given in Chapter 4. The effective mode shapes are determined when the multi-bay frame is subjected to four and ten degrees of freedom vehicle models.

The effects of the crack location on the dynamic response are discussed in Chapter 5. Two case studies are presented. One is discussed the resonance response of a cracked multi-bay frame subjected to moving oscillator. The other is relating the effect of the crack location on the dynamic response of the multi-storey frame subjected to passage of the high-speed train.

Chapter 6 provides general results of the thesis, overview of the main conclusions

and suggestions for future research.

CHAPTER TWO
DYNAMIC RESPONSE OF THE COMPLEX STRUCTURES SUBJECTED TO MOVING LOADS

Moving loads modelled as a vehicle passing over a multi-bay/multi-storey frame have been studied. It is reasonable for using moving load models when the only response of the bridge is desired. The moving load models give satisfactory results if the mass of the vehicle is small relative to that of structure.

2.1 Theory

The equation of motion of an undamped multi-degree of freedom systems shown in Figure 2.1 is given by

$$\boldsymbol{M\ddot{U}} + \boldsymbol{KU} = \boldsymbol{f} \tag{2.1}$$

where $\boldsymbol{M}$ and $\boldsymbol{K}$ are the overall mass and stiffness matrices of the system, respectively. $\boldsymbol{\ddot{U}}$ and $\boldsymbol{U}$ are the respective acceleration and displacement vectors for the whole structure. $\boldsymbol{f}$ is the external time-dependent force vector.

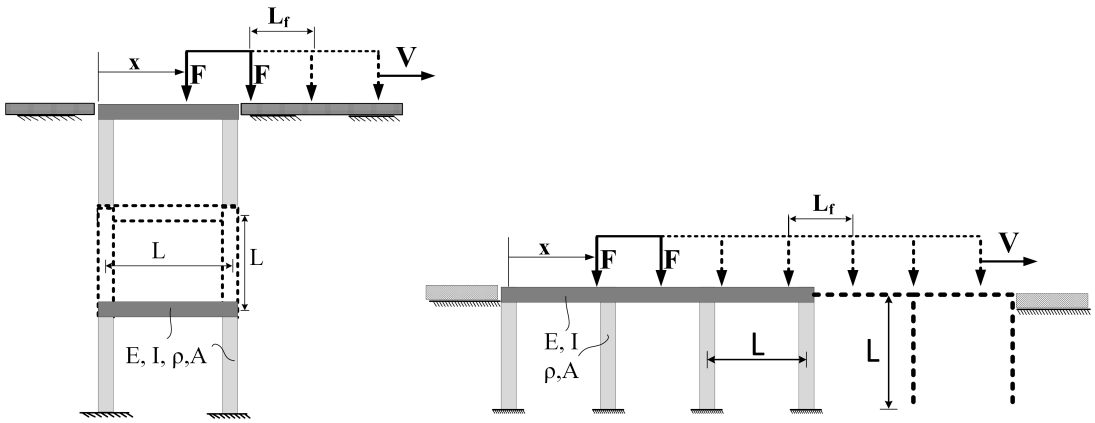

Figure 2.1 Multi-storey and multi-bay frames subjected to moving concentrated forces

2.1.1 Mass and Stiffness Matrices for a Frame Structure

Mass and stiffness matrices of the system shown in Figure 2.1 have been obtained by using the finite element method. A finite element model is used to represent a beam element of length h. The element has two nodes with three degrees of freedom at each node (2 translations and 1 rotation, see Figure 2.2).

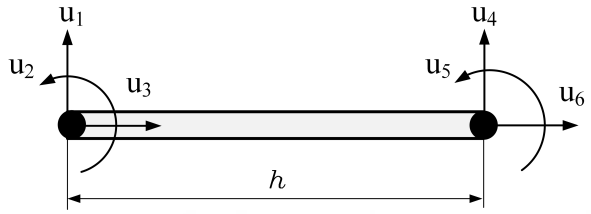

Figure 2.2 Six degrees of freedom (DOF) beam element

The mass and stiffness matrices of the uniform beam element can be computed from

$$\boldsymbol{m}_b = \rho A \int_0^h [N_b(x/h)][N_b(x/h)]^T dx \tag{2.2}$$

$$\boldsymbol{k}_b = EI \int_0^h [N_b''(x/h)][N_b''(x/h)]^T dx \tag{2.3}$$

for the bending vibration and

$$\boldsymbol{m}_a = \rho A \int_0^h [N_a(x/h)][N_a(x/h)]^T dx \tag{2.4}$$

$$\boldsymbol{k}_a = EA \int_0^h [N_a'(x/h)][N_a'(x/h)]^T dx \tag{2.5}$$

for the axial vibration where ρ, E, I, A and h are mass density, elastic modulus, area moment of inertia, cross-sectional area and beam length, respectively. Also, the prime sign represents a derivative with respect to x.

N_b and N_a are the shape functions and are defined as follows (Meirovitch, 1986):

$$\begin{gathered} \boldsymbol{N}_b = [N_{b1}\, N_{b2}\, N_{b3}\, N_{b4}]^T \\ N_{b1} = 1 - 3\xi^2 + 2\xi^3\,,\ \ N_{b2} = \xi - 2\xi^2 + \xi^3\,, \\ N_{b3} = 3\xi^2 - 2\xi^3\,,\ \ N_{b4} = -\xi^2 + \xi^3 \end{gathered} \tag{2.6}$$

$$\begin{gathered} \boldsymbol{N}_a = [N_{a1}\, N_{a2}]^T \\ N_{a1} = 1 - \xi\,,\ \ N_{a2} = \xi \end{gathered} \tag{2.7}$$

where $\xi = x/h$.

The element mass and stiffness matrices, shown in equations (2.2)-(2.5), are given by superposing the element matrices associated with the two-node elements:

$$\boldsymbol{m}_e = \begin{bmatrix} m_b(1,1) & m_b(1,2) & 0 & m_b(1,3) & m_b(1,4) & 0 \\ m_b(2,1) & m_b(2,2) & 0 & m_b(2,3) & m_b(2,4) & 0 \\ 0 & 0 & m_a(1,1) & 0 & 0 & m_a(1,2) \\ m_b(3,1) & m_b(3,2) & 0 & m_b(3,3) & m_b(3,4) & 0 \\ m_b(4,1) & m_b(4,2) & 0 & m_b(4,3) & m_b(4,4) & 0 \\ 0 & 0 & m_a(2,1) & 0 & 0 & m_a(2,2) \end{bmatrix} \tag{2.8}$$

$$\boldsymbol{k}_e = \begin{bmatrix} k_b(1,1) & k_b(1,2) & 0 & k_b(1,3) & k_b(1,4) & 0 \\ k_b(2,1) & k_b(2,2) & 0 & k_b(2,3) & k_b(2,4) & 0 \\ 0 & 0 & k_a(1,1) & 0 & 0 & k_a(1,2) \\ k_b(3,1) & k_b(3,2) & 0 & k_b(3,3) & k_b(3,4) & 0 \\ k_b(4,1) & k_b(4,2) & 0 & k_b(4,3) & k_b(4,4) & 0 \\ 0 & 0 & k_a(2,1) & 0 & 0 & k_a(2,2) \end{bmatrix} \tag{2.9}$$

where $a(i,j)$ defines $(i,j)^{th}$ element of matrix $\boldsymbol{a}$.

To ensure that the compatibility conditions are satisfied at the columns and top beams connections, the transformation of element matrices to a global coordinate system is necessary before the assembly is constructed. In the case of planar structures, all local systems have one axis parallel to one axis of the global system. Figure 2.3 shows the case in which axis u_2 of an arbitrary local system is parallel to axis U_2 of the global system. For a frame element oriented at angle α from the positive U_3 axis in the clockwise direction, the displacements in global coordinates are given by

$$\boldsymbol{u} = \boldsymbol{\Delta U} \tag{2.10}$$

For the element matrices

$$\boldsymbol{\Delta} = \begin{bmatrix} \boldsymbol{\Delta}_1 & \boldsymbol{0} \\ \boldsymbol{0} & \boldsymbol{\Delta}_1 \end{bmatrix} \tag{2.11}$$

where

$$\boldsymbol{\Delta}_1 = \begin{bmatrix} \cos\alpha & 0 & -\sin\alpha \\ 0 & 1 & 0 \\ \sin\alpha & 0 & \cos\alpha \end{bmatrix} \tag{2.12}$$

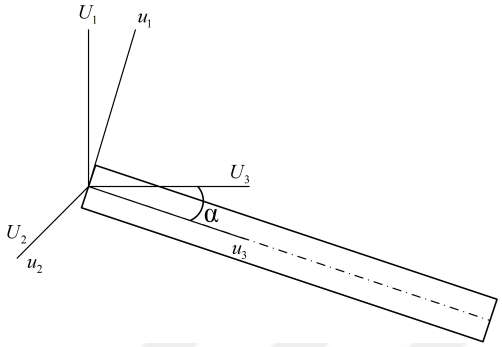

Figure 2.3 $u_1u_2u_3$: Local coordinate system, $U_1U_2U_3$: Global coordinate system

The element mass and stiffness matrices referred to as the global coordinates are then given by

$$\boldsymbol{M}_e = \boldsymbol{\Delta}^T \boldsymbol{m}_e \boldsymbol{\Delta}, \qquad \boldsymbol{K}_e = \boldsymbol{\Delta}^T \boldsymbol{k}_e \boldsymbol{\Delta} \tag{2.13}$$

2.1.1.1 Equivalent nodal forces

The equivalent nodal force of the s^{th} beam element, as shown in Figure 2.4, is taken the following form Wu et al. (2000):

$$\boldsymbol{f}_i^s = \left[f_1^s(t)\, f_2^s(t)\, f_3^s(t)\, f_4^s(t)\, f_5^s(t)\, f_6^s(t)\right]^T = -F\boldsymbol{N} \tag{2.14}$$

where $\boldsymbol{N}$ is defined as

$$\boldsymbol{N} = [N_{b1}\ N_{b2}h\ N_{a1}\ N_{b3}\ N_{b4}h\ N_{a2}]^T \tag{2.15}$$

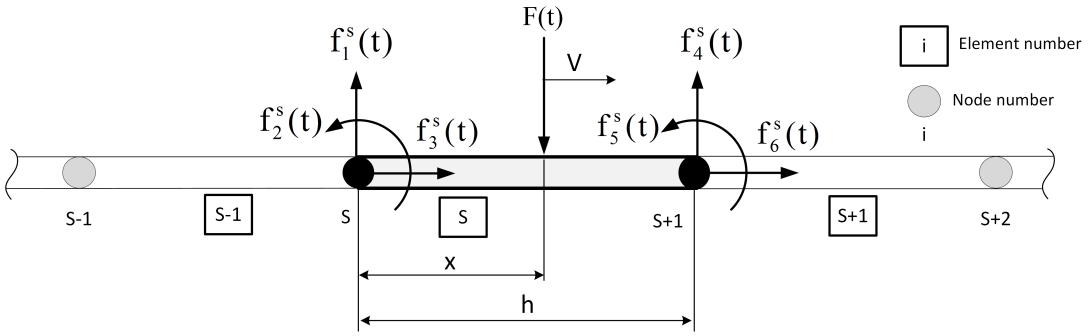

Figure 2.4 Equivalent nodal forces of the s^{th} beam element

Noting that $f_3^s(t) = f_6^s(t) = 0$, x is the application point of force along the beam element (s), h is element length and $\xi = x/h$ is the local coordinate. At time $t = 0$, the moving force starts to move with velocity V from left to right on the beam element. At a specific time $t_r = r\Delta t$, the moving force on the element is s, where s is found as

$$s = \text{Integer}\left[\frac{x_f}{h}\right] + 1\,, \quad x_f = Vt_r \tag{2.16}$$

2.2 Direct Integration Methods: The Newmark Method and Wilson-Theta Method

To integrate equation (2.1), the Newmark method and Wilson-theta method are commonly used methods in structural dynamics. These methods are briefly introduced in the following.

2.2.1 The Newmark Method

Newmark presented a integration method for the problem in the structural dynamics in 1959. Newmark method is an implicit integration method due to the solution ${}^{t+\Delta t}\boldsymbol{U}$ is based on the equilibrium conditions at time $t + \Delta t$. The equation of motion (2.1) are solved with parameters $\delta = 0.5$ and $\alpha = 0.25$, which results an unconditionally stable the constant-average-acceleration method. The Newmark integration algorithm is given in Figure 2.5 (Bathe, 1996).

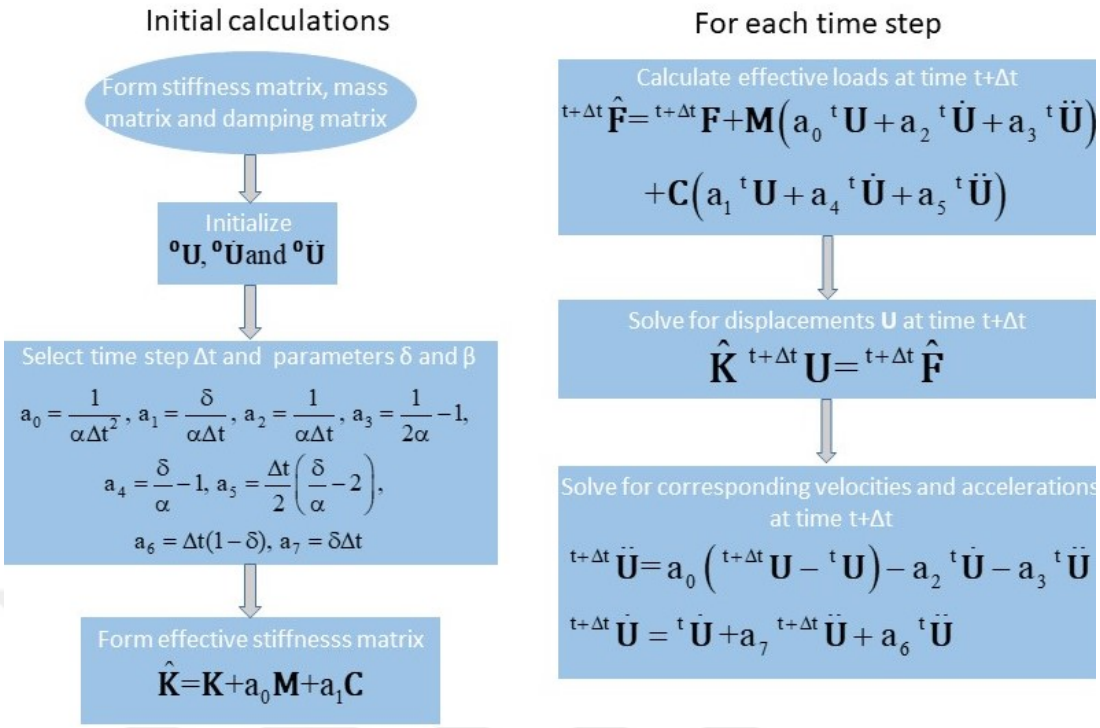

Figure 2.5 Newmark integration algorithm

2.2.2 The Wilson-theta Method

The Wilson-theta method is also an implicit integration scheme like Newmark's method. For unconditionally stability, which means that the solution for any initial disturbance does not grow without bound over time, θ should be selected as 1.4. Figure 2.6 summarizes the Wilson-theta algorithm (Bathe, 1996).

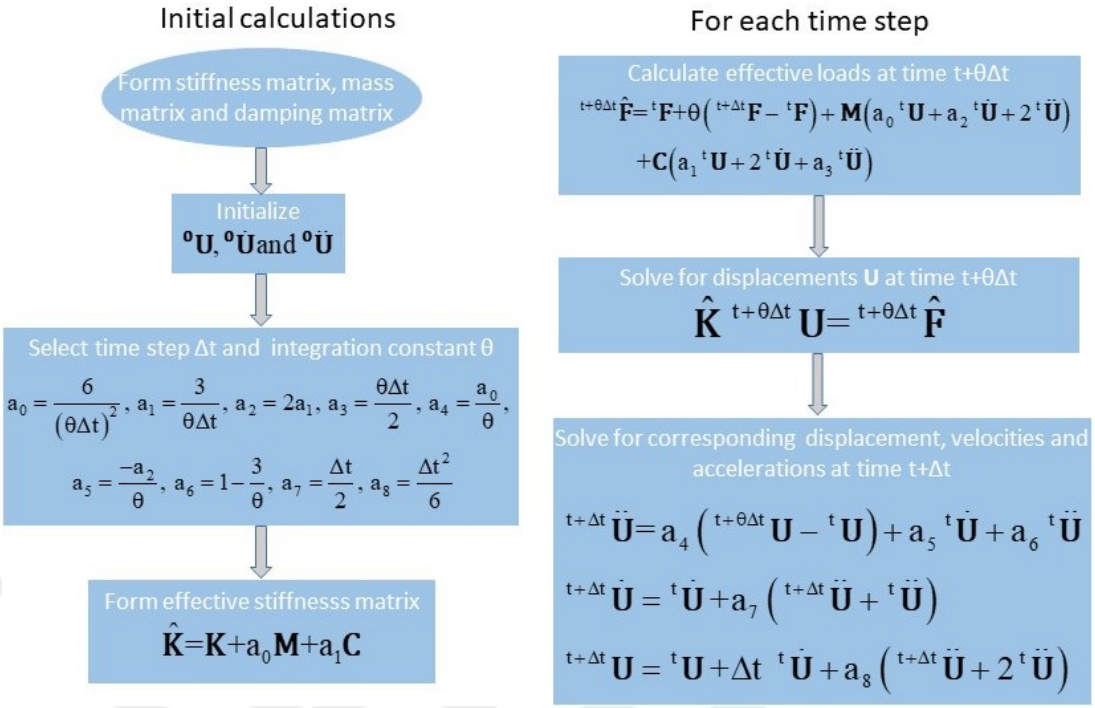

Figure 2.6 Wilson-theta integration scheme

2.3 Dynamic Response of Multi-bay Frames Subjected to Successive Moving Forces

Dynamic responses of multi-bay frame structures, based on the Bernoulli-Euler beam theory, subjected to concentrated single moving force and a series of equidistant loads with constant velocity have been investigated using the developed MATLAB code. For the purpose of validation of the developed MATLAB-FE (finite element) model, the results compared with those obtained by using ANSYS. This analysis can be considered as a simplified model of a gantry crane when the 1-bay frame is subjected to a single moving force with speed of $V < 5$ m/s. For the case of frame forming one or multi-bays and subjected to a sequence of moving loads of constant intervals with speed of $V > 50$ m/s, the problem can be considered as a train-induced vibration on a viaduct (Demirtas et al., 2019).

2.3.1 Numerical Results

The multi-bay frame structures, as shown in Figure 2.7, were analyzed for various cases in this study. The lengths of top beams and columns are L_1 and L_2, respectively. The moving force $F(t)$ starts to move with a velocity V (m/s) from left to right on the top beams (Demirtas et al., 2019).

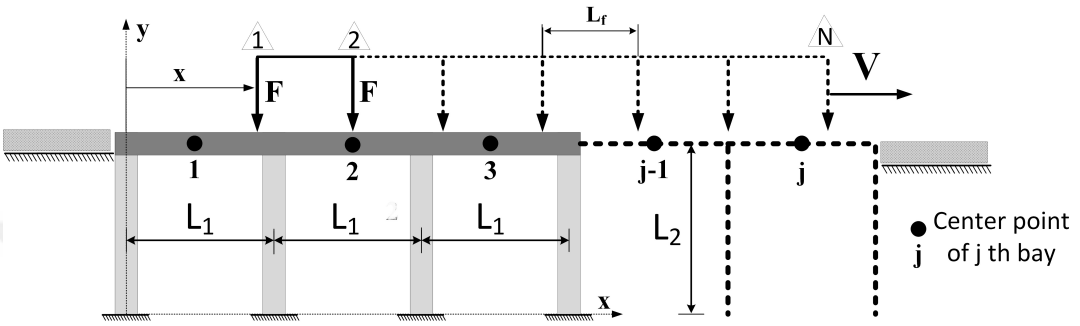

Figure 2.7 Multi-bay frame structure subjected to moving concentrated force with constant interval L_f

In the computations performed, the parameters given in Table 2.1 were used to calculate the dynamic responses of i-bay frame structure (i=1,2,⋯,n) to concentrated moving force, unless stated otherwise (Demirtas et al., 2019).

Table 2.1 Physical parameters of the frame structure

Description	Notation	Value
Top beam length	L_1	1 m
Column length	L_2	1 m
Force	F	50 N
Elastic modulus	E	200×10^9 N/m^2
Mass density	ρ	7800 kg/m^3
Cross-section		2×2 $(cmxcm)$

2.3.1.1 Effect of Moving Load Speed on the Dynamic Response of Multi-bay Frame

A i-bay frame ($i = 1,2,3$) subjected to a concentrated moving force (N=1 in Figure 2.7) is considered here. The element size and column length used in the finite element model are 0.25 m and 1 m, respectively. The effect of velocity on the dynamic response was investigated by plotting the impact factor with respect to the speed parameter. The impact factor ($I(x)$) and the speed parameter (S_v) are calculated by formulas given in Yang et al. (1997)

$$I(x) = \frac{R_d(x) - R_s(x)}{R_s(x)}, \quad S_v = \frac{\pi V}{\omega_2 L_1} \tag{2.17}$$

where $R_d(x)$ and $R_s(x)$ denote the maximum dynamic and static displacements calculated for position x where it corresponds to midpoints of the top beam of each bay, respectively. The maximum static displacements at points j ($j = 1,2,3$) in the i-bay frame ($i = 1,2,3$) are the displacements determined from the force F applied at point j. The ω_2 is the second circular natural frequency of frame (The second mode of vibration dominates the vibration response when the structure is subjected to moving load (Demirtas et al., 2019). This issue will be examined later in detail).

Figure 2.8 (a)-(f) show the variation of $I(x)$ with respect to S_v. The E, I and L_2 are remaining unchanged in the subsequent analysis and taken from Table 2.1. The top beam lengths (L_1) $1, 1.5, 2$ m are considered and graphs are plotted for the i-bay frame at different EI/L_1 values. It is evident from the figure that even though the structure has a different number of bays, it is clear that point i of the i-bay frame ($i = 1,2,3$) has similar dynamic characteristics to each other. The maximum impact factor is obtained for a speed parameter of approximately 0.58 for the 1-bay frame and multi-bay frames at point 1. Moreover, the maximum impact factor for a multi-bay frame at point j (j=2,3,...,N) was obtained approximately at $S_v = 0.73$. These values are independent of the number of bays forming the frame (Demirtas et al., 2019).

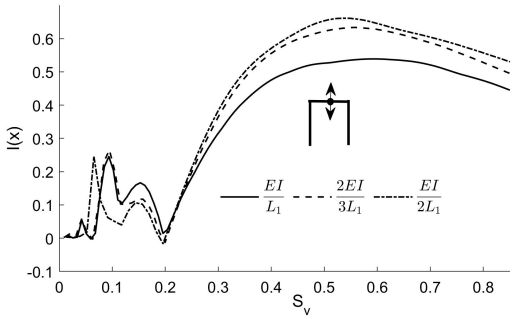

(a) 1-bay frame, point 1.

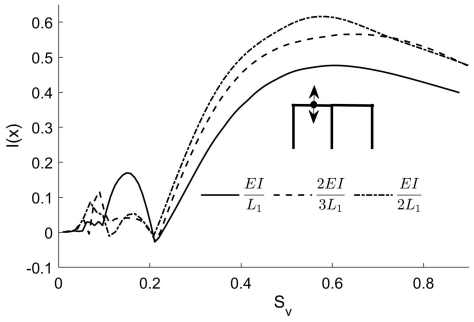

(b) 2-bay frame, point 1.

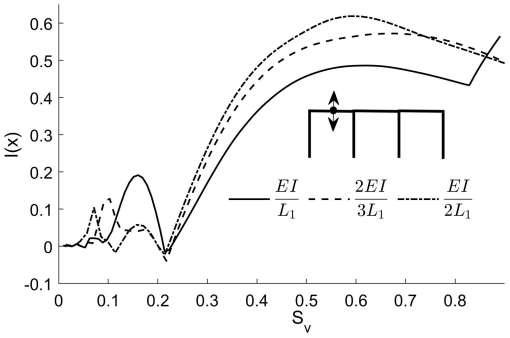

(c) 3-bay frame, point 1.

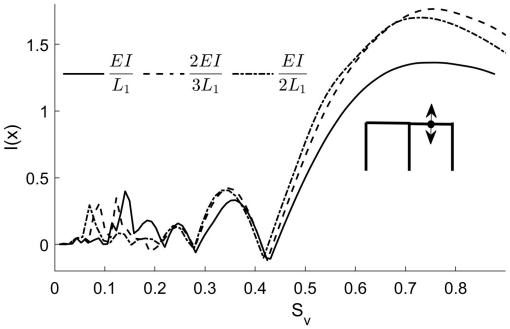

(d) 2-bay frame, point 2.

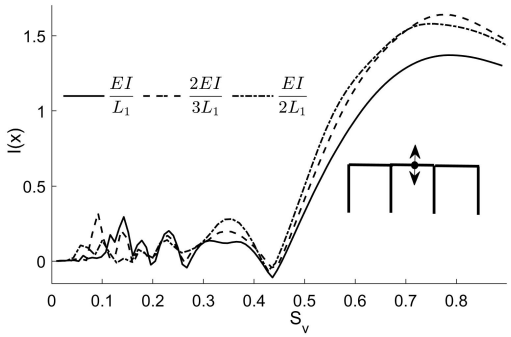

(e) 3-bay frame, point 2.

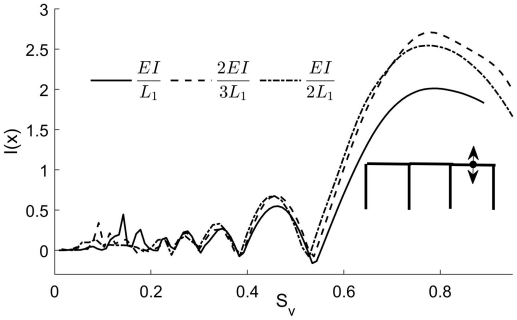

(f) 3-bay frame, point 3.

Figure 2.8 The impact factor - Speed parameter plot.

The second natural frequency of the 1-bay frame for the top beam lengths of 1 m, 1.5 m and 2 m are 58.8334 Hz, 31.7320 Hz and 19.1612 Hz, respectively. The speed of the moving load corresponding to the maximum impact factors are computed using equation (2.17) as 68, 55.2 m/s and 44.5 m/s for the top beam lengths of 1 m, 1.5 m and 2 m, respectively (Demirtas et al., 2019).

For 2 and 3-bay frames and $L_1 = 1$ m, the second natural frequencies are 56.9094 Hz and 56.1213 Hz, respectively. The maximum impact factors of 2 and 3-bay frames are obtained as 66 m/s and 65 m/s at point 1 and 83.1 m/s and 81.94 m/s at point 2, respectively. The second natural frequencies get to each other as the number of bay increases. Therefore, the difference between the speeds is also reduced (Demirtas et al., 2019).

The minimum impact factor is obtained at point 1 for a 3-bay frame, as seen in Figure 2.8 (c). When comparing Figure 2.8 (e) to Figure 2.8 (c) it is clear that point 2 has a greater value than point 1. The trend continued in this way and the impact factor got its maximum value at point 3, as seen in Figure 2.8 (f). In the j-bay frame ($j = 2, 3, ..., N$), the largest maximum impact value is obtained at point j corresponding to the midpoint N of the last top beam over which the load has passed (Demirtas et al., 2019).

From Figure 2.8, the difference between static and dynamic displacement values is small up to about $S_v = 0.085$ or $V \approx 10$ m/s of moving load speed.

2.3.1.2 Effect of Top Beam Length

The i-bay frames (i=1,2,3,4) were examined in order to determine the influence of the lengths of top beams on dynamic responses. The moving load moves with a speed of 10 m/s from the left end of the top beam to the right end. The fixed element size of 0.125 m is used for all computations made here. The column length is fixed and equals to $L_2 = 1$ m in all structures. MATLAB results (present work) were compared with ANSYS results to verify the calculations made. BEAM54 beam element with 6 degrees of freedom is used in ANSYS finite element model. The element size is also the same as that used in the present model (Demirtas et al., 2019).

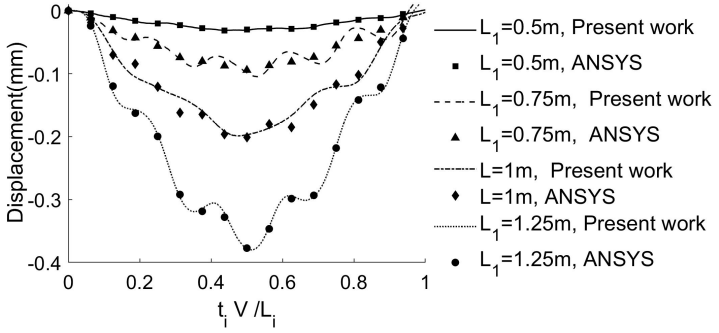

(a) 1-bay frame, point 1

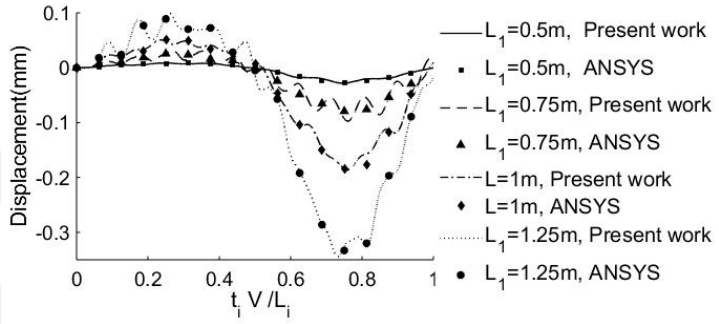

(b) 2-bay frame, point 2

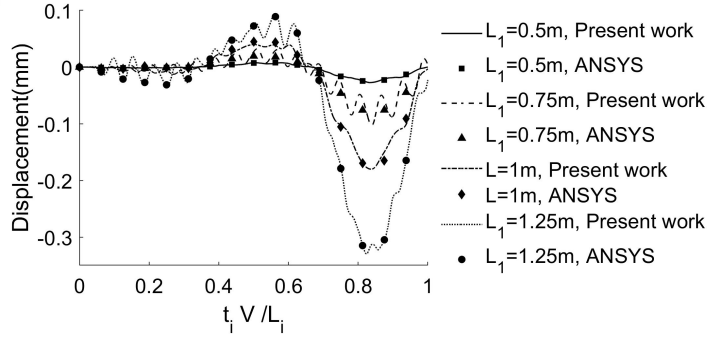

(c) 3-bay frame, point 3

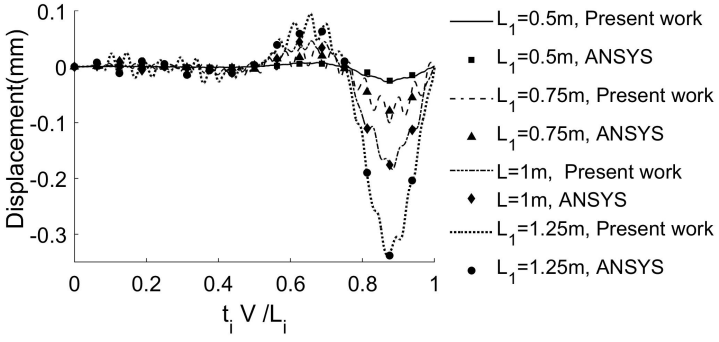

(d) 4-bay frame, point 4

Figure 2.9 Effect of top beam length on dynamic response of i-bay frame at point i (i=1,2,3,4)

The dynamic responses of center point deflections of top beams are shown in Figure 2.9 using the dimensionless time axis ($t_i V/L_i$, $i = 1,2,3,4$). Only the results of these displacements have been given since the maximum dynamic displacement in the multi-bay frame, observed from the results of the previous section, occurred in the mid-point of the top beam of the last bay. The displacements of the top beam on which the force moves are in the direction of the force, but the displacements of the adjacent top beams are upwards. It can be inferred from the figure that the longer the top beam lengths are taken, the more flexible the frames become. As a consequence, as the flexibility increases, the center point deflections of the top beams also increases. On whatever the bay structure the load is, the adjacent bays are affected. This effect increases as the beam length increases. For the further bays, this effect dies out. From Figure 2.9, it is also seen that the results of present work and ANSYS are close to each other (Demirtas et al., 2019).

2.3.1.3 Multi-bay Frame Subjected to Moving Successive Forces with Constant Interval

The problem considered is a multi-bay frame subjected to a moving successive force with a constant interval. The properties of the multi-bay frame and the moving force are listed in Table 2.1 with N=10 and constant span length of L_f (m), see also Figure 2.7.

2.3.1.3.1 Single-bay frame. Figure 2.10 depicts the dynamic deflections at point 1 of 1-bay frame subjected to a moving force train with $L_f = 1$ m and $V = 2$ m/s. When $L_f = L_1$, there are ten peaks with $L_f/V = 0.5$s spacing. It is also seen that the results obtained with MATLAB and ANSYS finite element models are close to each other (Demirtas et al., 2019).

Figure 2.11 shows the 3D relationship of the non-dimensional speed parameter (S_v)-force span length to the top beam length ratio ($\overline{L}$)-dynamic magnification factor (DMF) plot. Here, $\overline{L}(L_f) = L_f/L_1$ ($L_f = 0, 0.2, 0.4, ..., 2$ m) and $S_v(V) = \pi V/(\omega_2 L_1)$

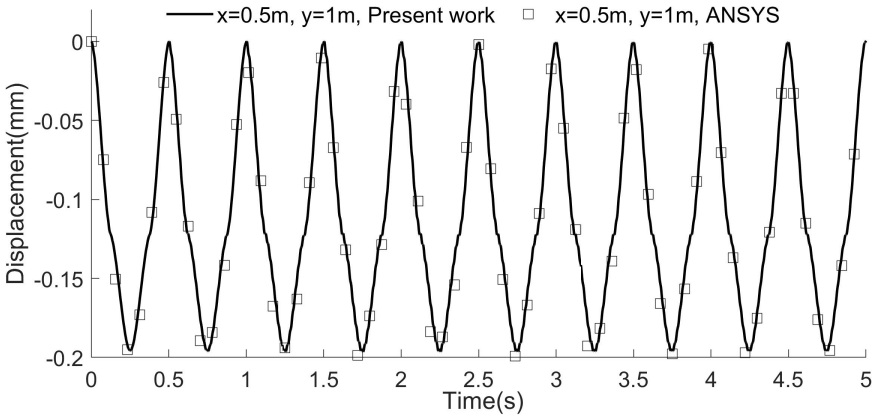

Figure 2.10 Time response of 1-bay frame at point 1

($V = 1, 2, ..., 100$ m/s) where ω_2 represents the second circular natural frequency (see Table 2.2). The DMF is obtained as the ratio of the maximum dynamic deflection to the maximum static deflection. The maximum static deflection is computed at the midpoint of the top beam. The load is applied separately to the center of each beam and taken as $10 \times F$ (Demirtas et al., 2019). It can be deduced from Figure 2.11 (a) that for the small values of L_f, the ten loads with equidistant intervals, modelled as the moving load, behave as a single point force with a magnitude of $10 \times F$ (Demirtas et al., 2019). It is clearly seen from Figures 2.11 (a) and 2.11 (b) that the $\overline{L}$ and S_v have a significant effect on the dynamic response. As the value of $\overline{L}$ increases, the DMF gradually decreases and at a special value of $\overline{L}$, it takes a minimum value. The L_f value which corresponds to the minimum dynamic response is analytically calculated for simply supported beams and is given by the following equation (Yang et al., 1997)

$$\frac{L}{L_f} = i - 0.5 \quad i = 1, 2, 3, ... \tag{2.18}$$

In order to compare the numerical results obtained by the present work to the analytical solution (equation (2.18)), the mean DMF can be calculated using the equation

$$X_m(\overline{L}(L_f)) = \frac{1}{N} \sum_{V=1}^{N} X(\overline{L}(L_f), S_v(V)) \tag{2.19}$$

where $N = 100$, $L_f = 0, 0.02, 0.04, ..., 2$ m and $V = 1, 2, ..., 100$ m/s. Figure 2.12 shows the $\overline{L}$ - mean DMF graph. It is clear that the minimum displacement is obtained at $L_f/L_1 = 0.67$ m. L_1/L_f is 1.5 and the same result is obtained using equation (2.18) for $i = 2$ (Demirtas et al., 2019).

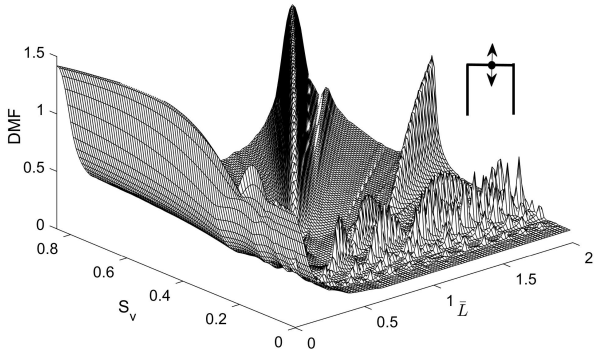

(a) S_v-$\overline{L}$-DMF

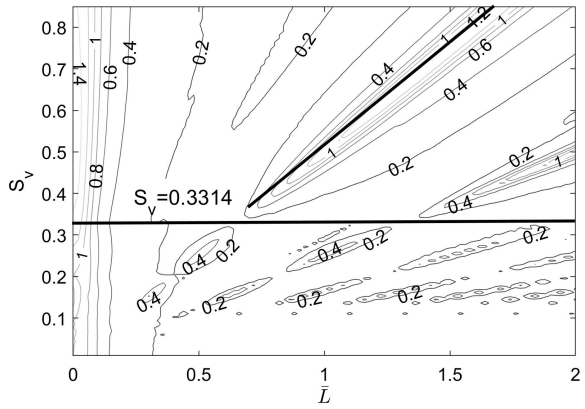

(b) Contour lines.

Figure 2.11 3D S_v-$\overline{L}$-DMF plot and its contour lines of 1-bay frame at point 1

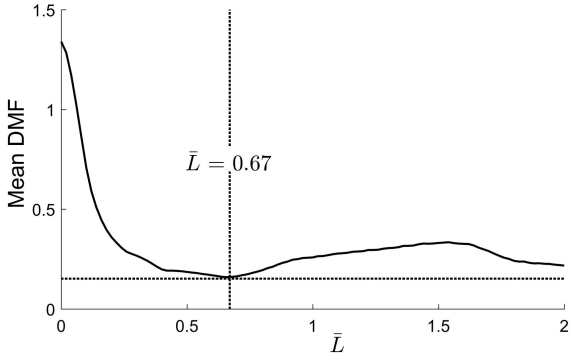

Figure 2.12 Mean DMF with $\overline{L}$

Repeated loads at some specific speeds can cause resonance. The detrimental effects on the structure are increased by increasing the number of loads at these speeds. The critical velocities causing the resonance phenomenon are determined by

the well-known formula given for a simple beam in Yang et al. (1997)

$$V_{cr} = \frac{f_n L_f}{k}, \qquad k = 1, 2, ... \tag{2.20}$$

V_{cr} and L_f in equation (2.20) can be selected from the inclined thick black line in Figure 2.11 (b). For example if $\overline{L} = 0.72$ and $S_v = 0.365$, then the critical velocity is calculated as $V_{cr} = \omega_2 S_v/(\pi L_1) = 43$ m/s. Similarly, 59 m/s and 93 m/s can be computed for $\overline{L} = 1, 1.58$, respectively (Demirtas et al., 2019).

The resulting time responses for these L_f and V_{cr} values are shown in Figure 2.13 (a). As can be seen from this figure, the amplitude of the vibration increases with the increase of the L_f value. Once the amplitude becomes maximum at a certain L_f value, after that as the L_f value increases, the amplitude decreases and, it gets a minimum value at a speed at which the free vibrations are cancelled (Demirtas et al., 2019).

By taking the Fourier transform of the displacement response, the dominant mode at these speeds and L_f values can be determined. Yang & Lin (2005) have shown that solutions of sufficient accuracy for a simply supported beam can be obtained by considering only the first mode of vibration (Demirtas et al. (2019)).

The first few natural frequencies of the i-bay frame (i=1,2,3,4) are given in Table 2.2. In Table 2.2, the first and the last of the natural frequencies given for each bay frame correspond to the dominant column modes, while the ones given separated between them correspond to the dominant beam modes (Demirtas et al., 2019).

As seen in Figure 2.13 (b), due to the flexibility of the columns in the structure, it is determined that the second mode dominates the dynamic response (see Table 2.2). From equation (2.20), k can be determined

$$k \approx \frac{58.8334(0.72)}{43} \approx \frac{58.8334(1)}{59} \approx \frac{58.8334(1.58)}{93} \approx 1 \tag{2.21}$$

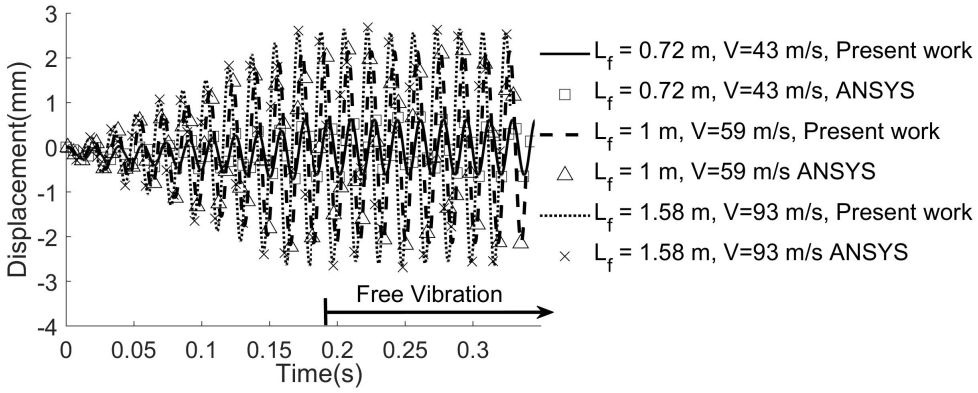

(a)

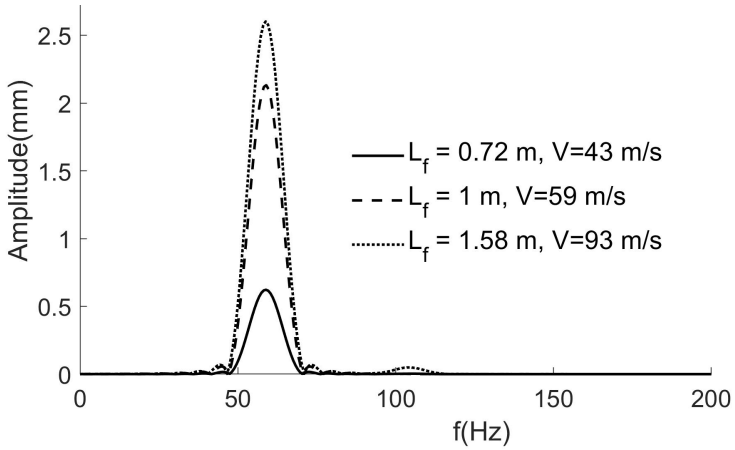

(b)

Figure 2.13 Forced-free vibration response of 1-bay frame at point 1 for various critical speeds and L_f values. (a) Time history response, (b) Frequency response

Table 2.2 First few natural frequencies in Hz for i-bay frame (i=1,2,3,4)

1-Bay		2-Bay		3-Bay		4-Bay	
Present work	ANSYS	Present work	ANSYS	Present work	ANSYS	Present work	ANSYS
14.9095	14.909	13.8145	13.814	13.4512	13.451	13.2444	13.244
58.8334	58.828	56.9094	56.899	56.1213	56.090	55.7224	55.692
		71.6759	71.662	64.6308	64.587	61.1623	61.124
				79.1602	79.085	71.7695	71.712
						83.0051	82.920
96.0673	96.042	96.7276	96.703	97.0375	96.919	97.2106	97.091

The cancellation is a phenomenon, in which the free vibration caused by all previous forces except for the N^{th} force passing over the beam has been suppressed. The cancellation speed is determined from Figure 2.11 (b) as $S_v = 0.3314$ or $V = 39$ m/s. The dynamic deflections take the minimum value at this speed. Figures 2.14 (a), (b) and (c) show that the free vibration part of the response approaches zero when the moving load speed of $V = 39$ m/s and the L_f values, which leads to resonance at critical speed values are chosen as $L_f = 0.72, 1, 1.58$ m (Demirtas et al., 2019).

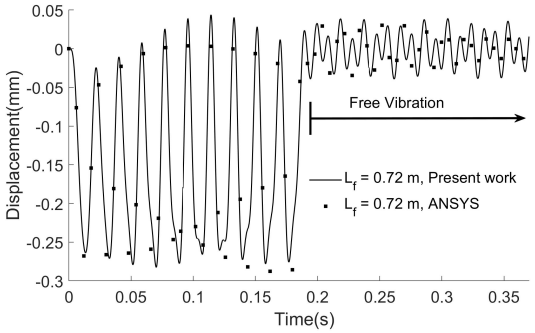

(a) $L_f = 0.72$ m.

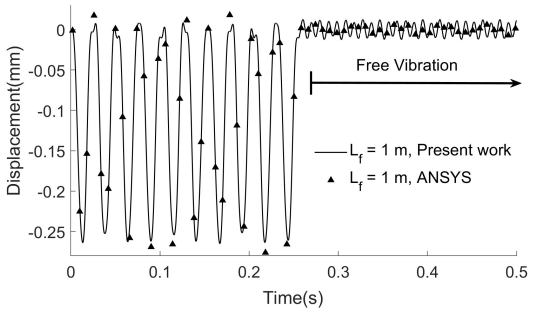

(b) $L_f = 1$ m.

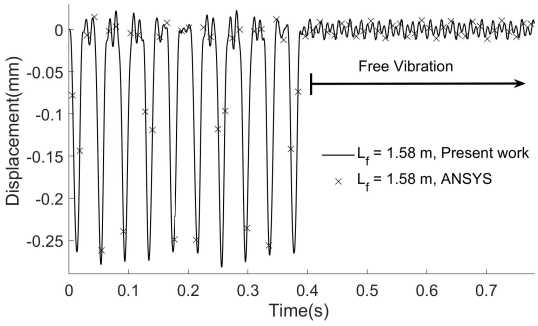

(c) $L_f = 1.58$ m.

Figure 2.14 Forced and free time responses at cancellation speed.

As a result, it is observed that the analytical solution and the results obtained by using the finite element method are in close agreement. As it can be seen from the graphs obtained by the finite element method solution, the equations obtained using the analytical solution remain valid in some special cases (Demirtas et al., 2019).

2.3.1.3.2 Multi-bay frame. Consider a 2-bay frame subjected to successive loads with constant intervals moving at speed V, as shown in Figure 2.7 with $N = 10$. Figures 2.15 (a) and 2.15 (c) show the S_v-L-DMF curves of the 2-bay frame at points 1 and 2 with their contour lines given in Figures 2.15 (b) and 2.15 (d).

From Figure 2.15, it can be observed that the two center points of the top beam have similar trends of dynamic displacements.

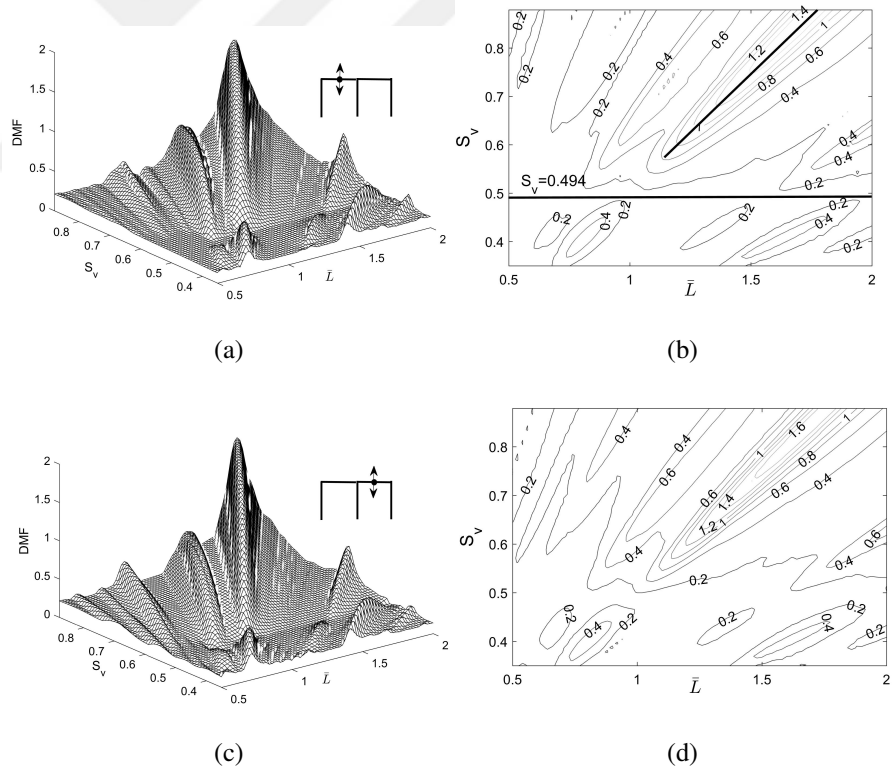

(a) (b)

(c) (d)

Figure 2.15 (a)-(c) and (b)-(d) are S_v-$\bar{L}$-DMF plots and its contour lines, respectively. (a)-(b) are the plots of point 1 and (c)-(d) are the plots of point 2

The value of $\bar{L}$ corresponding to the minimum displacement is approximately

determined as $\overline{L}$ = 0.67 from the $\overline{L}$ - mean DMF graph shown in Figure 2.16.

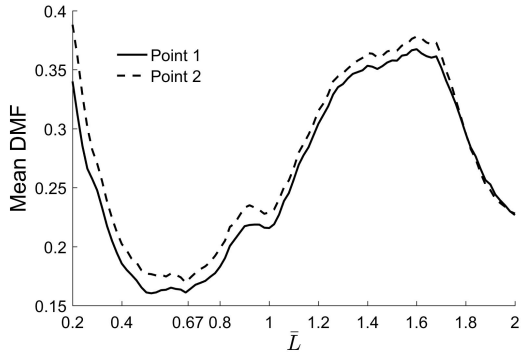

Figure 2.16 Mean displacement-L_f plot at points 1 and 2 of the 2-bay frame

The relationship between V_{cr} and L_f values, which excite the structure in the resonance conditions, is linear as can be seen from equation (2.20). The three points ($\overline{L}$, S_v) that cause resonance response are taken over the inclined thick black line from Figure 2.15 (b). Then, L_f and the critical speeds can be computed as $(1.1, 65), (1.34, 77)$ and $(1.68, 95)$, as it was done in the previous section (Demirtas et al., 2019).

Figure 2.17 (a) shows the dynamic deflection with the time in the resonance case of the 2-bay frame at point 1 for the selected (L_f, V_{cr}) values. Figure 2.17 (b) shows the frequency response obtained by taking the Fourier transform of the free vibration response, which has been calculated after the load has just passed over the structure. It is clear that the second mode with the frequency of f_{n2} = 56.9094 Hz has dominated the response (Demirtas et al., 2019).

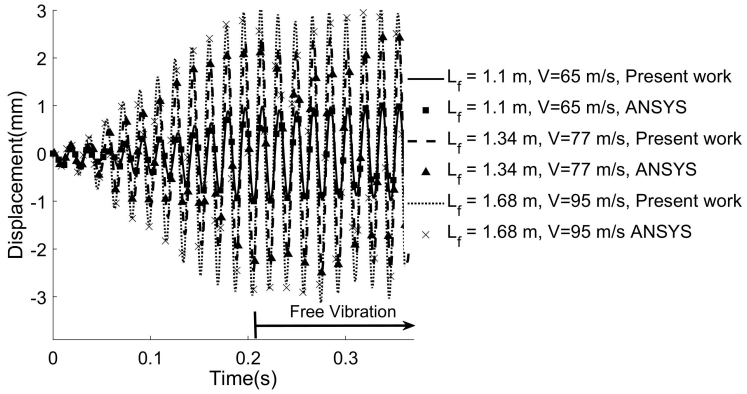

(a)

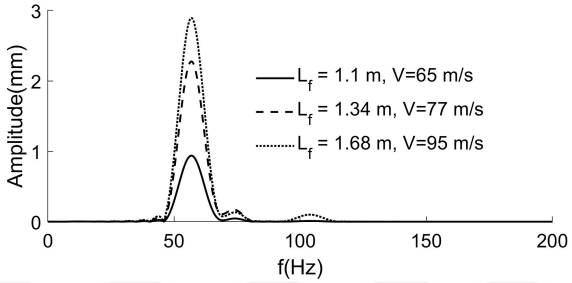

(b)

Figure 2.17 Vibration response of the 2-bay frame at point 1 for various critical speeds and L_f values.(a) Time history response, (b) Frequency response

It can be observed from Figure 2.15 (b) or 2.15 (d) that the cancellation speed corresponds to $S_v = 0.494$ or $V = 56$ m/s. Figure 2.18 shows the time response plotted for $L_f = 1.1, 1.34, 1.68$ values at cancellation velocity of $V = 56$ m/s. Note that the resonance response is obtained, as shown in Figure 2.17, for the same L_f and the corresponding V_{cr} values. When the cancellation phenomenon is happened, the dynamic response can be calculated by taking into account the final load that is still on the structure, since free vibrations are suppressed (Demirtas et al., 2019).

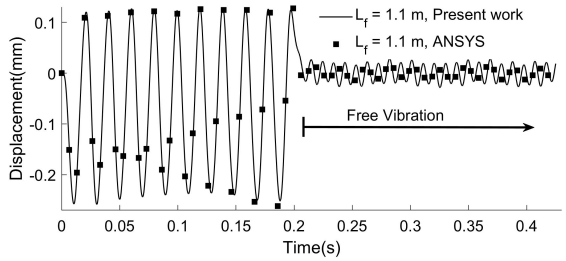

(a)

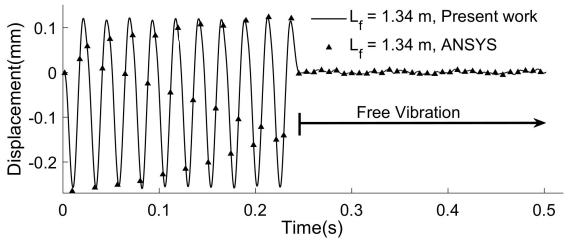

(b)

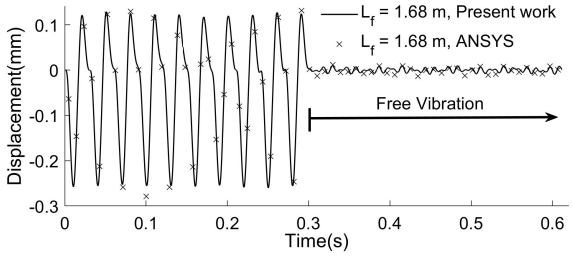

(c)

Figure 2.18 Time response of free and forced vibration showing cancellation phenomenon of 2-bay frame at point 1 for various L_f values

Figure 2.19 illustrates the 3D S_v-$\overline{L}$-DMF plot and their contour lines of the 3-bay frame at center points 1, 2 and 3 of the top beams. It is seen in Figure 2.19 that the midpoints of 1 and 3 have similar dynamic behavior due to the structural symmetry (Demirtas et al., 2019).

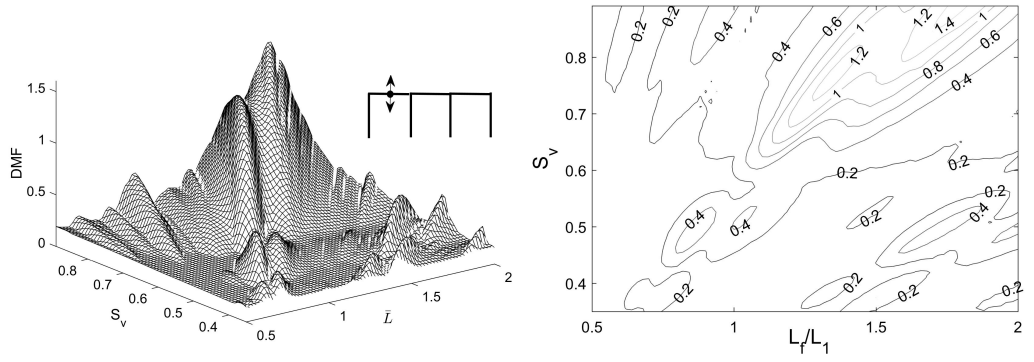

(a) (b)

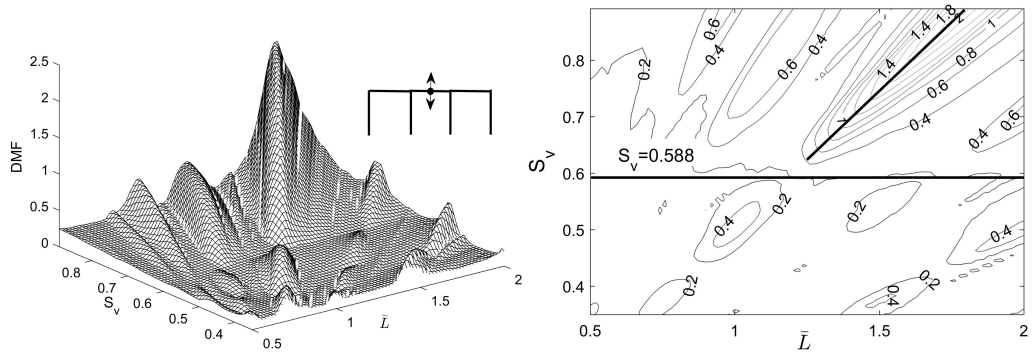

(c) (d)

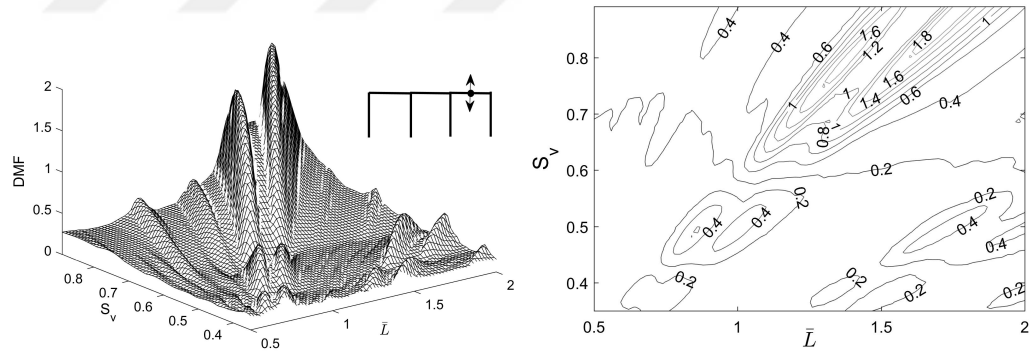

(e) (f)

Figure 2.19 (a)-(b), (c)-(d) and (e)-(f) are 3D S_v-$\overline{L}$-DMF and its contour lines at points 1,2 and 3, respectively

The 2^{nd} and 3^{rd} natural frequencies of the 3-bay frame are 56.1213 and 64.6308 Hz, respectively (See Table 2.2). Due to the fact that these two modes are close to each other, two dominant peaks appear in Figures 2.19 (a) and e. It is seen in Figure 2.19 (c) that, as observed in 1 and 2 bay frames, a single peak, and thus a single mode,

dominates the response. These are all related to the frequencies dominated by the top beam.

The values of (S_v, $\overline{L}$) which force the frame in the resonance conditions are depicted over the inclined thick black line in Figure 2.19 (d). Then, (L_f,V_{cr}) values are computed as (1.28 m, 74 m/s), (1.44 m, 81 m/s) and (1.76 m, 98 m/s) (Demirtas et al., 2019).

The mean DMF for each $\overline{L}$ value at points 1, 2 and 3 are calculated and the mean DMF - $\overline{L}$ graph is plotted as shown in Figure 2.20. A similar characteristic behavior is determined at points 1 and 3. The average maximum displacement trends at points 1 and 3 are similar. However, the $\overline{L}$ value corresponding to the minimum response is the same at all points and is obtained at about $\overline{L}$ = 0.67 m, as in the case of 1 and 2 bay frames (Demirtas et al., 2019).

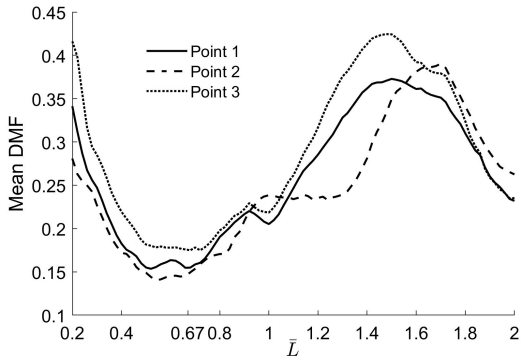

Figure 2.20 Mean MDF-$\overline{L}$ plot of 3-bay frame at points 1,2 and 3

Figure 2.21 (a) shows the displacement-time curve at point 2 for both free and forced vibration response obtained for the critical velocities and L_f values given above. Figure 2.21 (b) shows the frequency response obtained by taking the Fourier transform of the free response given in Figure 2.21 (a). It is seen in Figure 2.21 (b) that the 3-bay frame is excited at its second mode with natural frequency f_n = 56.1213 Hz (Demirtas et al., 2019).

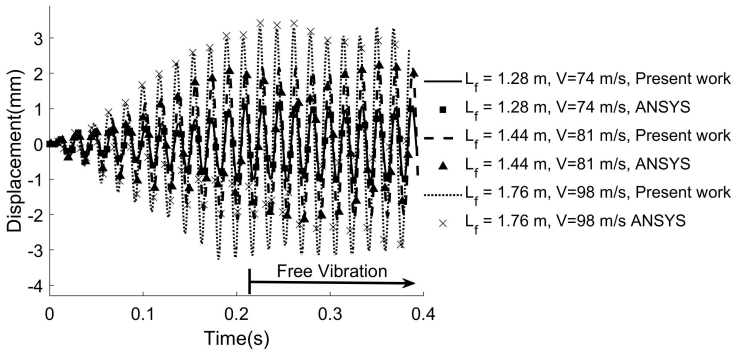

(a)

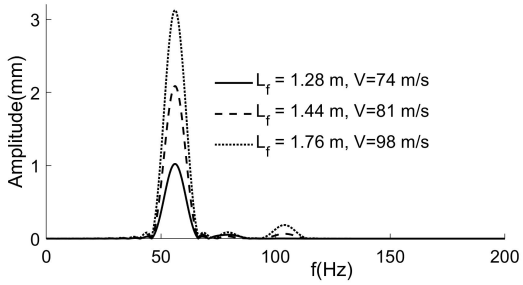

(b)

Figure 2.21 Forced-free vibration response of 3-bay frame at point 2 for various critical speeds and L_f values.(a) Time history response (b) Frequency response

The cancellation speed is obtained as $S_v = 0.588$ or $V = 64$ m/s by using the contour curves given in Figure 2.19 (d). To determine the effect of L_f on the dynamic response and to compare it with the resonance response, the same L_f values are selected as in Figure 2.21 (a). Figures 2.22 are plotted for values of $L_f = 1.28, 1.44$ and 1.76 m, respectively. Because the speed sensitivity is 1 m/s in numerical computations carried out, the free vibration part of the response is very close but not exactly equal to zero, even though it is equal to zero in analytical solutions. If the free vibration oscillations of the structure are large, the dynamic amplitudes are triggered after the passage over of each load. Then the resonance state occurs, as seen in Figure 2.21 (a). However, the resonance phenomenon is not encountered at the cancellation speeds which cause a small free oscillation amplitude, regardless of the value of L_f (Demirtas et al., 2019).

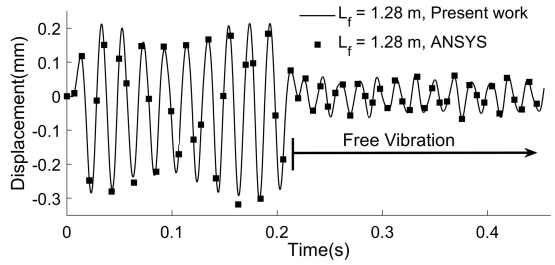

(a)

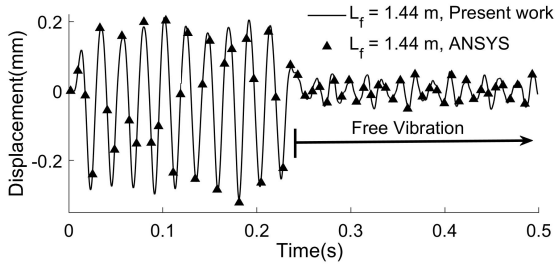

(b)

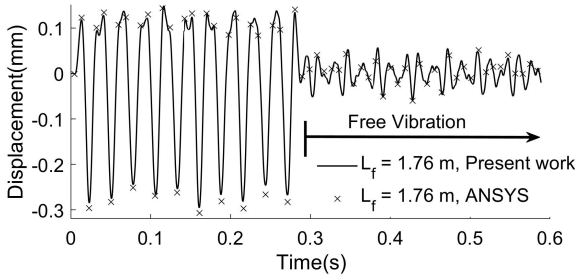

(c)

Figure 2.22 Time history of the 3-bay frame at point 2 for various L_f values at cancellation speed

2.4 Effect of Mode Shapes on the Dynamic Response of a Multi-storey Frame Subjected to Moving Train Loads

The train loads are modelled as loads of constant intervals with constant velocity. The case where the concentrated load speed takes small values, can be considered as a gantry crane, and the case of high speed values of successive moving force with constant interval can be considered as a train induced vibration of railway bridges. In addition, the structure having more than one storeys is also examined. It is assumed that the boundary conditions of the frame are zero horizontal and vertical

displacements and zero rotations at bases of columns.

2.4.1 Problem Description

The system considered, shown schematically in Figure 2.23, is a multi-storey frame subjected to train moving forces having a magnitude of F with a constant velocity of V. The Bernoulli-Euler beam theory is used in the analysis. It is assumed that beams and columns have length L, elastic modulus E, mass per unit length m, area moment of inertia I, cross-section area A, respectively. The distance between successive loads is the same and denoted as L_f.

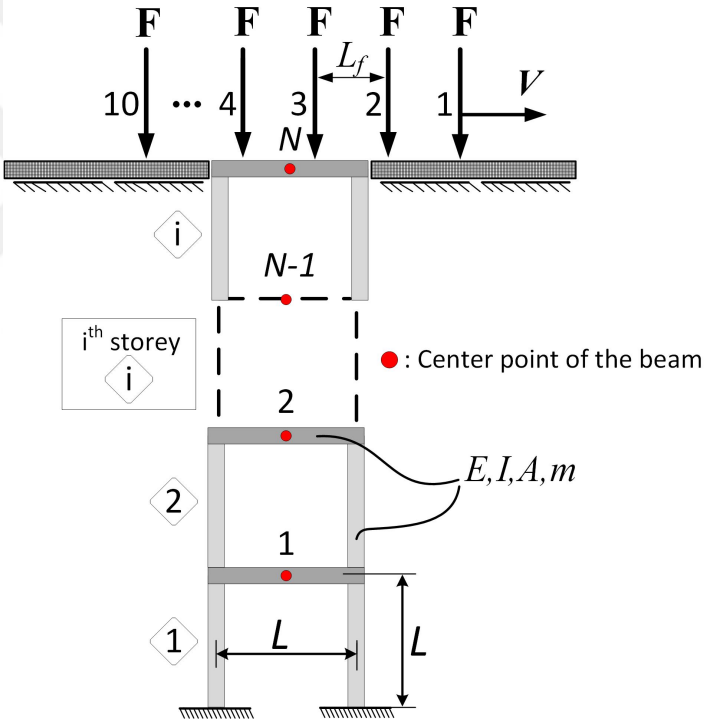

Figure 2.23 A multi-storey frame

2.4.2 Modal Analysis of the Multi-storey Frame

All the parameters which are used in subsequent computations are given in Table 2.3. The values of physical properties are taken from Yang et al. (1997).

Table 2.3 Physical and geometric properties of the multi-storey frame

Description	Notation	Value
Beam/column length	L	30 m
Force	F	60822 N
Elastic modulus	E	2.87×10^{9} N/m^2
Area moment of inertia	I	2.9 m^4
Cross-section area	A	8.7 m^2
Mass per unit length	m	2303 kg/m
Element size of FE model	l	5 m

The first few natural frequencies are determined using both ANSYS and the developed MATLAB programs (present work). The beams and columns are modelled using BEAM54 element. ANSYS BEAM54 is used because it has the same nodal degrees of freedom with the model developed by present work. Element size is taken as 5 m to generate the same finite element mesh those of the developed model. Table 2.4 shows the natural frequencies of i-storey frame (i=1,2,3,4).

Table 2.4 The first few natural frequencies (f) of i-storey frame (i=1,2,3,4)

	1-Storey		2-Storey		3-Storey		4-Storey	
f(Hz)	Present work	ANSYS	Present work	ANSYS	Present work	ANSYS	Present work	ANSYS
f_1	1.0762	1.0760	0.5020	0.5020	0.3176	0.3176	0.2307	0.2307
f_2	4.2178	4.2100	1.6503	1.6493	1.0518	1.0515	0.7479	0.74780
f_3			3.6168	3.6102	1.9017	1.9004	1.3843	1.3837
f_4			4.9873	4.9784	3.4572	3.4510	2.0335	2.0320
f_5					4.3706	4.3626	3.3939	3.3878
f_6							3.9822	3.9752
f_7							4.4549	4.4511

The mode shapes for those natural frequencies given in Table 2.4 is determined. The first modes of the structure shown in Figures 2.24 (a)-(d) correspond to the first bending modes of the columns forming the frame. The displacement of the beam in the vertical

direction has become important in the second mode of the 1-bay frame. This mode corresponds to the first mode in which the vertical direction of the beam is effective. Therefore, the natural frequency of the structure in this mode is shown in Table 2.4 with a dark background. The 2^{nd} mode of the 2, 3 and 4-storey frames corresponds to the 2^{nd} bending mode of the columns. The 3^{rd} mode of the 3 and 4-storey frame corresponds to the 3^{rd} bending mode of the columns. Finally, the 4^{th} mode of the 4-storey frame corresponds to the 4^{th} bending mode of the columns. The displacement of the top beam in the vertical direction is negligible in the above-mentioned modes.

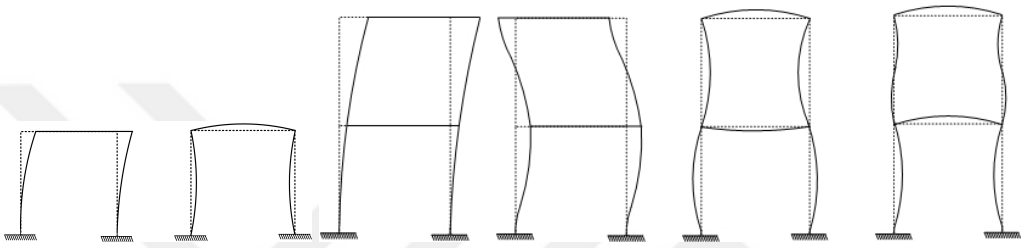

(a) 1-storey frame (b) 2-storey frame

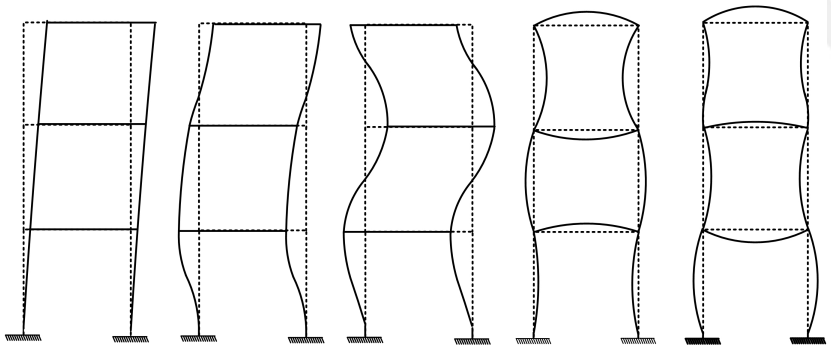

(c) 3-storey frame

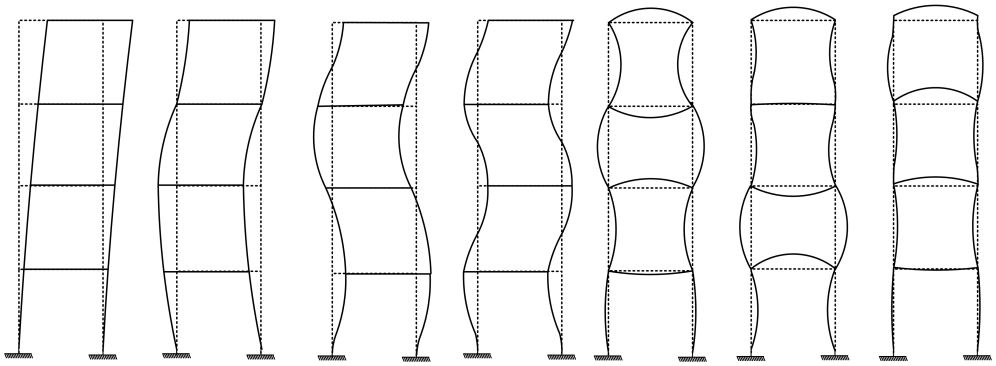

(d) 4-storey frame

Figure 2.24 The first few mode shapes of i-storey frame (i=1,2,3,4). The modes corresponding to the natural frequencies listed in Table 2.4 are given in increasing order from left to right

The load moves on the top beam of the structure. The study will be limited to the vertical vibrations of the structure. Therefore, the displacements of the top beam in the vertical direction are important in the resonance behaviour of the structure under the influence of the successive moving loads. Hence, the 2^{nd} mode for 1-storey frame, the 3^{rd} or 4^{th} mode of the 2-storey frame, the 4^{th} or 5^{th} mode of the 3-storey frame and the 5^{th}, 6^{th} or 7^{th} mode of the 4-storey frame can be expected to be dominant in the resonance behavior.

2.4.3 Effect of Mode Shape on the Dynamic Response

It is known that structures vibrate under resonance conditions in certain situations due to the passage of repeated groups of loads. The load velocity and force span length are important parameters on the resonance vibrations. The resonance vibrations can be observed in some values of these parameters.

2.4.3.1 Validation

In order to prove the validity of the finite element model (present work), it is reasonable to compare the results with those of ANSYS software. The loads consist of a succession of 4 concentrated moving loads of constant intervals L_f = 30m travelling at constant speed V = 2m/s (see Figure 2.25).

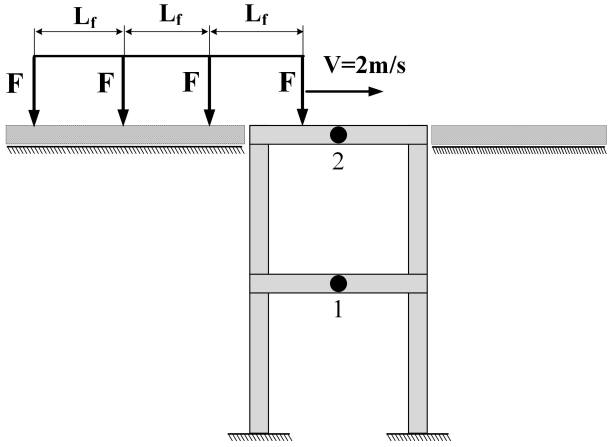

Figure 2.25 2-storey frame under train moving load

The vertical vibration response for center points 1 and 2 of the 2-storey frame are shown in Figure 2.26. The time delay of successive forces are the same and its value equals L_f/V = 15s. Because of beam length $L = L_f$, the displacement/time plot, given in Figure 2.26, has four peaks. Very good agreement is observed.

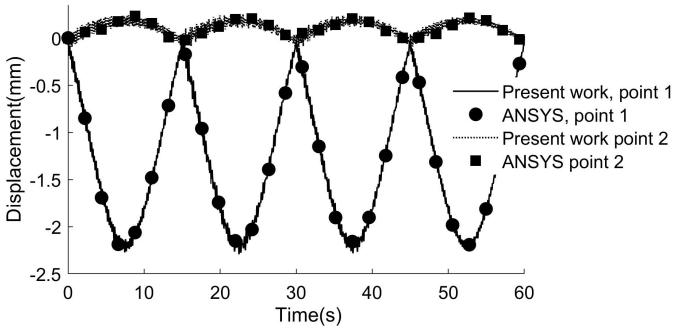

Figure 2.26 Transverse deflections at points 1 and 2

2.4.3.2 Velocity-Force Span Length to Beam Length Ratio-Dynamic Magnification Factor (V-$\overline{L}$-DMF)

A i-bay frame (i = 1,2,3,4) subjected to successive moving forces with constant interval (Figure 2.23) is considered here. The effect of velocity and force span length on the dynamic response was investigated by plotting the velocity (V)-force span length to beam length ratio ($\overline{L}$)-dynamic magnification factor (DMF) plot. The DMF is defined as the ratio of the maximum dynamic deflection to the maximum static deflection. The maximum static deflection is computed at the midpoint of the top beam, as shown in Figure 2.27. The static forces were defined in such a way that one of the forces was applied at the center of the beam.

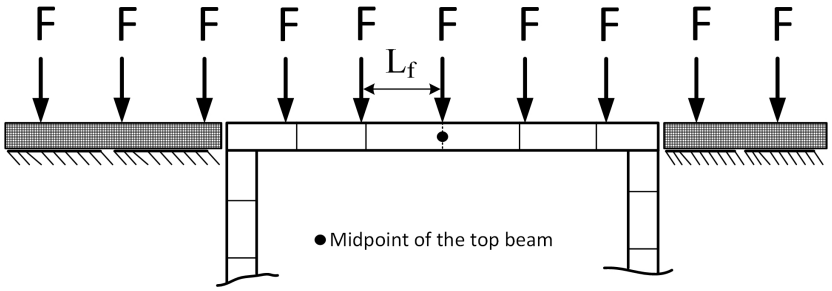

Figure 2.27 Maximum static deflection calculated at midpoint of the top beam

Figure 2.28 (a) shows 3D views of V-$\overline{L}$-DMF plot of 1-storey frame. Three typical points (P_1, P_2 and P_3) that correspond to the maximum DMF are selected. The values $V = 64$ m/s, $\overline{L} = 0.5$; $V = 44$ m/s, $\overline{L} = 0.7$; and $V = 32$ m/s, $\overline{L} = 0.75$ are read from these three points, respectively.

The maximum DMF values of the 3D V-$\overline{L}$-DMF curves shown in Figures 2.28 (a) - 2.31 (a) depend on $\overline{L}$ and V. If $\overline{L}$ changes the specific velocity (critical velocity, V_{cr}), which causes the largest maximum displacement also changes. As can be seen in Figures 2.28 (b) - 2.31 (b), the variation of V_{cr} with $\overline{L}$ is linear. Figures 2.28 (b)- 2.31 (b) provide directions corresponding to critical speeds. The most important of these directions is the solid line because it gives the largest maximum DMF values. Figure 2.28 (b) shows that the other two directions are below the solid line.

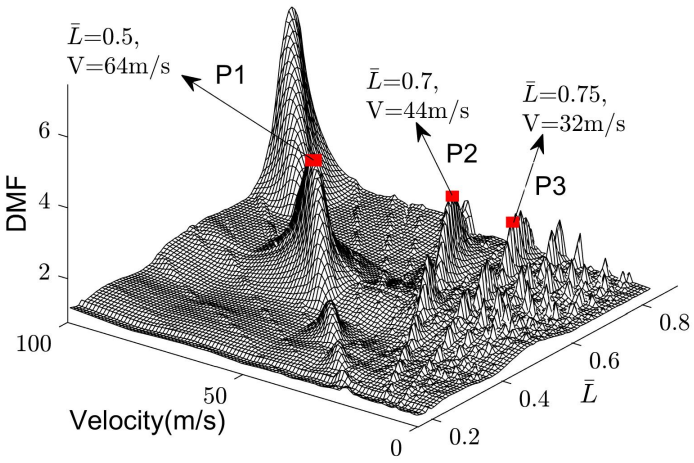

(a)

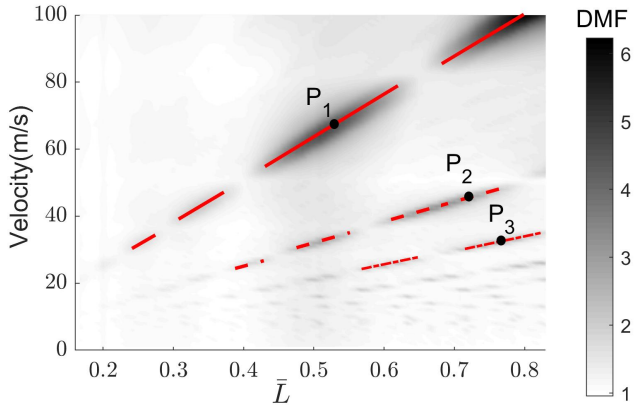

(b)

Figure 2.28 1-storey frame, (a) 3D V-$\overline{L}$-DMF plot, (b) its 2D projection

Figure 2.29 (a) illustrates 3D V-$\overline{L}$-DMF plot of 2-storey frame. The points P_1, P_2 and P_3 have values of V = 54 m/s, $\overline{L}$ = 0.5; V = 83 m/s, $\overline{L}$ = 0.5417; and V = 38 m/s, $\overline{L}$ = 0.7, respectively. Figure 2.29 (b) is a two-dimensional representation of Figure 2.29 (a). Here the color bar shows DMF. The three directions corresponding to the critical speed are shown in this figure. From these directions, the dashed-dotted line is above the solid line and the dashed line is below.

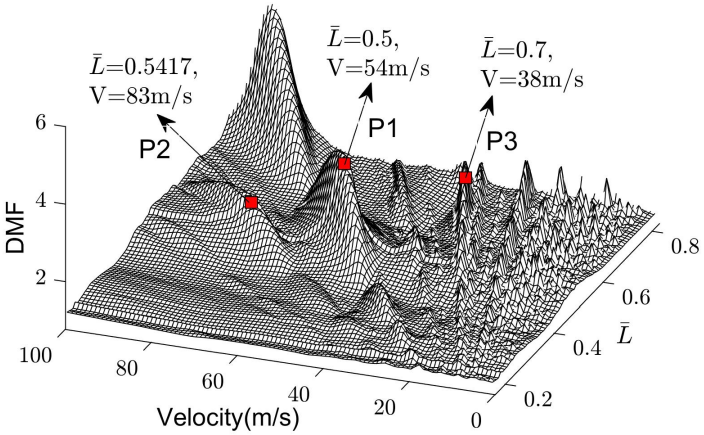

(a)

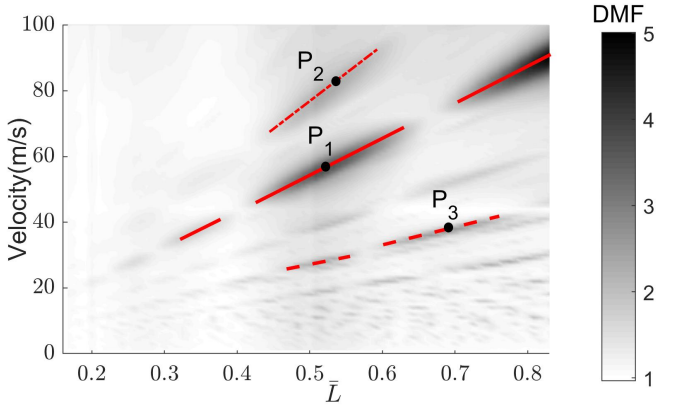

(b)

Figure 2.29 2-storey frame, (a) 3D V-$\overline{L}$-DMF plot, (b) its 2D projection

The 3D V-$\overline{L}$-DMF is plotted for the 3-storey frame, as shown in Figure 2.30 (a). The three points selected on this figure are as follows: V = 51 m/s, $\overline{L}$ = 0.5 at point P_1; V = 71 m/s, $\overline{L}$ = 0.5417 at point P_2; and V = 38 m/s, $\overline{L}$ = 0.7 at point P_3. Figure 2.30 (b) shows the directions giving the critical speeds. It is observed that the solid line and

dashed-dotted line approaching each other when compared to the case of the 2-storey frame.

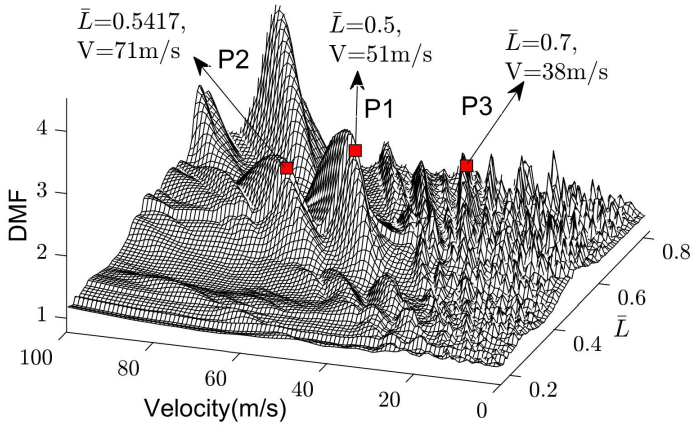

(a)

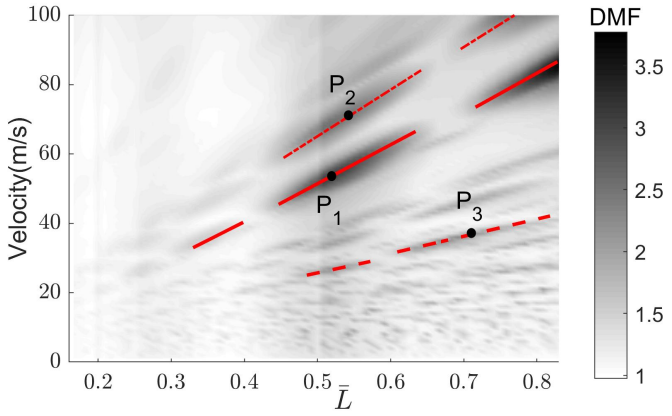

(b)

Figure 2.30 3-storey frame, (a) 3D V-$\overline{L}$-DMF plot, (b) its 2D projection

From Figure 2.31 (a), the points P_1, P_2 and P_3 for the 4-storey frame are taken as $V = 51$ m/s, $\overline{L} = 0.5$; $V = 64$ m/s, $\overline{L} = 0.5417$; and $V = 47$ m/s, $\overline{L} = 0.7$, respectively. As a result of the increase of storey number of the structure, the difference between the consecutive natural frequencies of the structure decreased. Therefore, as seen in Figure 2.31 (b), the dashed-dotted line and the solid line are getting closer to each other.

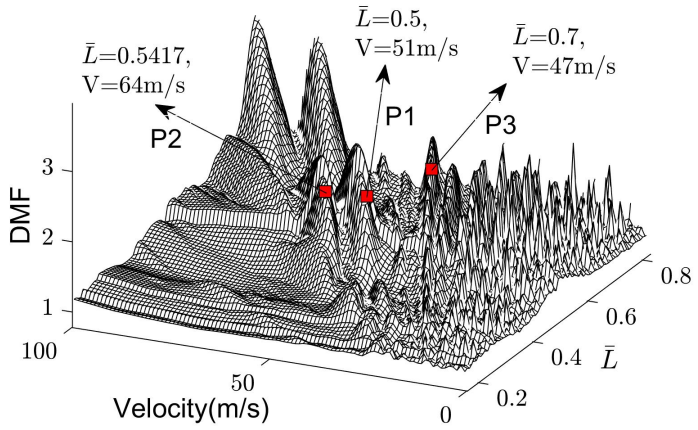

(a)

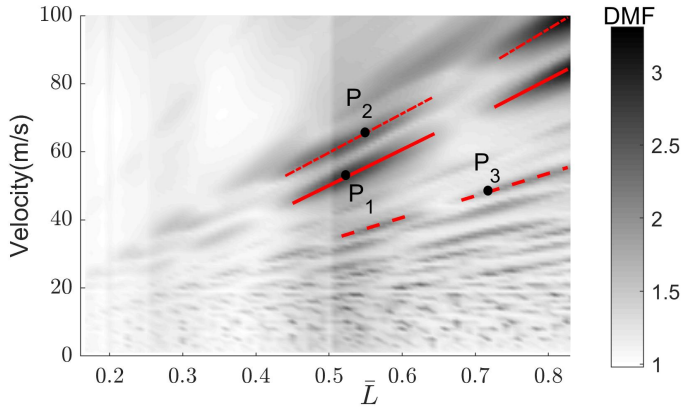

(b)

Figure 2.31 4-storey frame, (a) 3D V-$\overline{L}$-DMF plot, (b) its 2D projection

2.4.4 Time and Frequency Responses

To show which mode is dominating the dynamic responses of multi-storey frames, the Fourier transform of the free response is calculated. The graphs are plotted for the three points indicated in Section 2.4.3.2 for each frame. The graphs plotted below are the displacements (or frequency) in the vertical direction of the point N (see also Figure 2.23) for the N-storey frame.

Figure 2.32 (a) shows the time history graphs for the V and $\overline{L}$ values at the point P_1 of the i-storey frame (i=1,2,3,4). Here, the t_f in the dimensionless time axis indicates the time that the load leaves the structure. It is clear that the values t/t_f greater than 1

illustrate free vibrations. By taking the Fourier transform of the free vibration responses, the frequency responses, as shown in Figure 2.32 (b), were obtained.

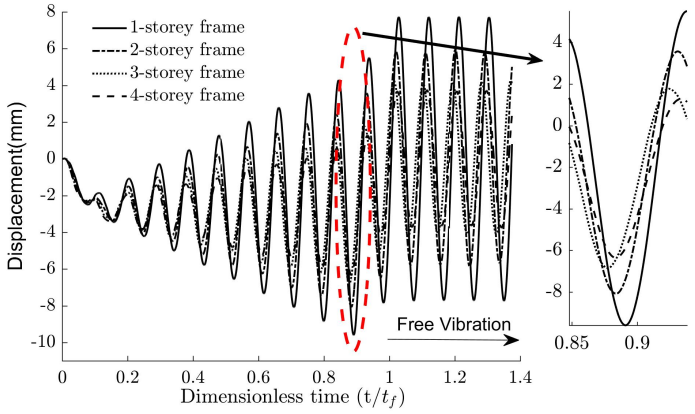

(a)

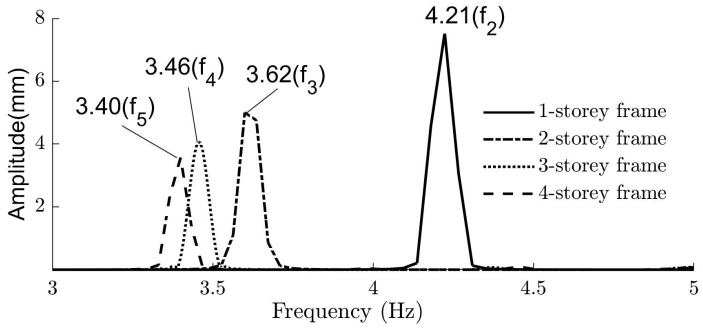

(b)

Figure 2.32 (a) Time history curves of free and forced response for point P_1. (b) Frequency response

In Figure 2.32 (b), it is seen that the values taken from point P_1 for 1-storey frame excite the 2^{nd} mode of vibration with the natural frequency of 4.21 Hz. A similar situation can be said to be the 3^{rd} mode of the 2-storey frame, the 4^{th} mode of the 3-storey frame and the 5^{th} mode of the 4-storey frame. Furthermore, if P_1 is considered to be a point on the solid line shown in Figures 2.28 (b)-2.31 (b), it can be concluded that the points taken on the solid line will again excite the same modes.

Figure 2.33 (a) depicts displacements against dimensionless time plots for those values taken at point P_2 of the i-storey frame (i=1,2,3,4). From Figure 2.33 (b), as in P_1, the 2^{nd} mode of the 1-storey frame dominates the resonance response. In contrast, the 4^{th} mode of the 2-storey frame, the 5^{th} mode of the 3-storey frame, and the 6^{th}

mode of the 4-storey frame are excited at this point. Also, this point is a typical point taken on the dashed line in Figures 2.28 (b)-2.31 (b). Note that these dashed lines for the 1-storey frames are below the solid line, while they are above the solid line for 2-4 storey frames.

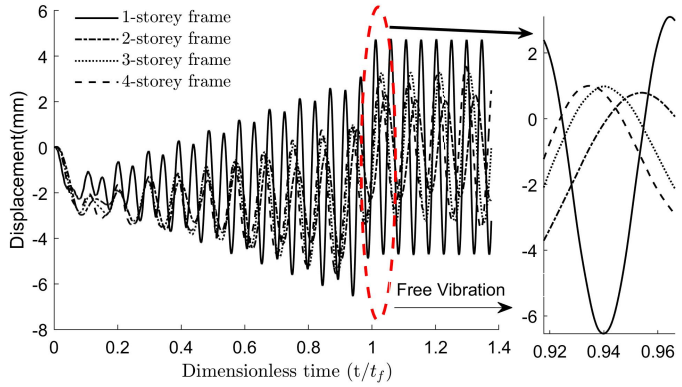

(a)

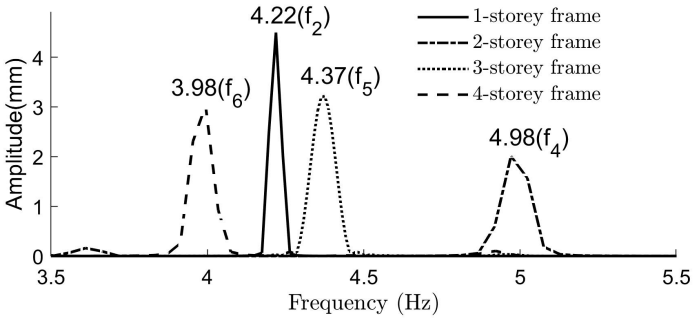

(b)

Figure 2.33 (a) Time history curves of free and forced response for point P_2. (b) Frequency response

Figure 2.34 shows the time history and frequency response plots for the values picked at point P_3. For the 1, 2 and 3-storey frames, just like point P_1, the excited modes are the 2^{nd}, 3^{rd} and 4^{th} modes, respectively (Figure 2.34 (b)). However, the resonance response of the 4-storey frame seems to be related to the 7^{th} mode of the structure. These modes are effective in the resonance response of the structures at a value from any point on the dashed-dotted line in Figure 2.31 (b). The flexibility of the structure increases with the increase in storey number. This means that higher modes may have an effect on the resonance response, depending on the mode shape of the structure.

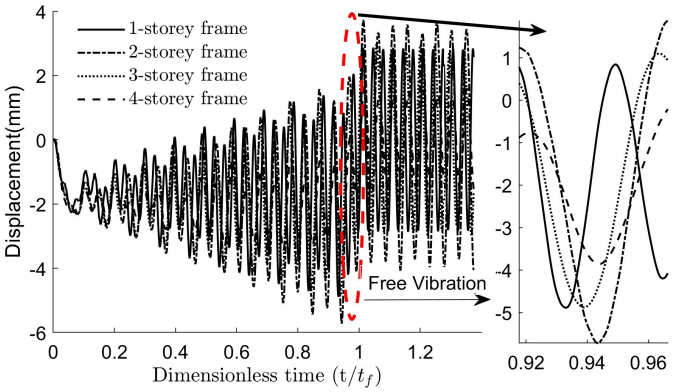

(a)

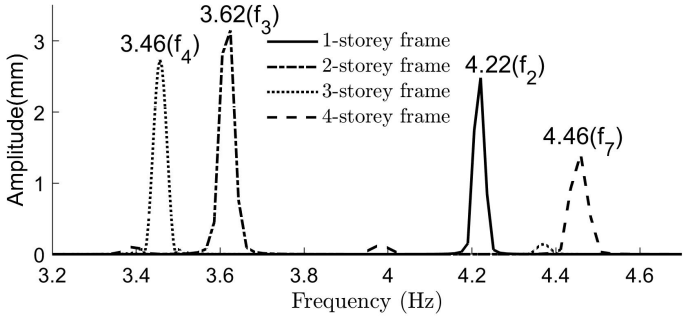

(b)

Figure 2.34 (a) Time history curves of free and forced response for point P_3. (b) Frequency response

It has been mentioned in Refs. (Yang et al., 1997; Yang et al., 2004) that solutions of sufficient accuracy can be obtained for the bridge which modelled as simply supported beam if only the first mode of vibration is considered. However, this situation is different in multi-storey frame structures. As a result of the elasticity of the columns, for N-storey frame, $N+1$ modes at least should be considered.

CHAPTER THREE
VEHICLE-STRUCTURE INTERACTION DYNAMICS: THEORETICAL BACKGROUND

Dynamic analysis of multi-bay/multi-storey frame under the action of the moving undamped oscillator, the moving vehicle 2-axle with 4 DOF and moving vehicle model with 4-axle 2-bogie having 10 DOF models are studied. The moving force model, presented in Chapter 2, is the simplest one which is ignored the interaction effects between vehicle and structure. The moving undamped oscillator model enables us analyzing displacements in the vertical direction of a vehicle's body. The 2-axle with 4 DOF moving vehicle model considers the pitching motion of the vehicle's body. The 4-axle 2-bogie vehicle model is the more sophisticated multi-body system having primary and second suspension units and 2 bogies.

3.1 The Moving Undamped Oscillator Model

3.1.1 Mathematical Model

A Bernoulli-Euler simply supported beam of length L and oscillators moving from left end to right end with constant speed V is shown in Figure 3.1. $r(x)$ is the rail irregularity function. The discussion here covers the general case. However, the equations of motion for a beam subjected to a moving single oscillator problem will be obtained with the aim of simplifying the formulation and confirming the results obtained in the literature.

Let the moving oscillator is on the element p having nodes i and $i+1$ at a given instant of time (Figure 3.1). It is assumed that the wheel of the vehicle always keeps in contact with the structure.

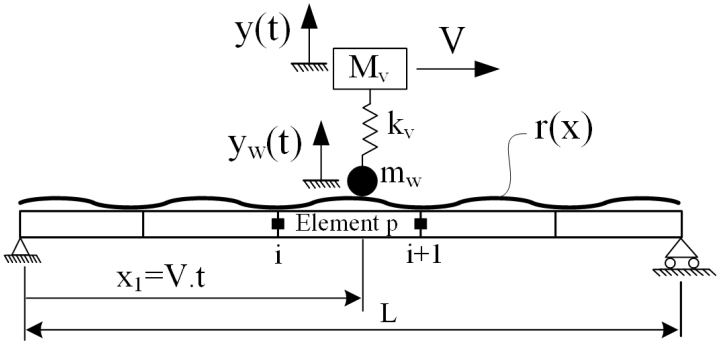

Figure 3.1 Simply supported beam subjected to a moving oscillator

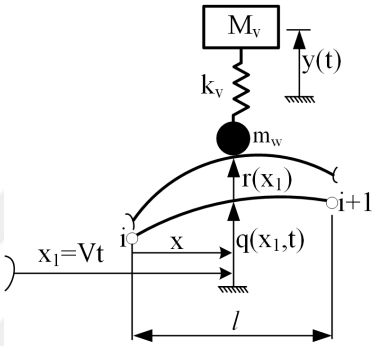

Figure 3.2 Deflected beam element p

Consider the element p of length l as shown in Figure 3.2. The kinetic and potential energy of the system can be written as

$$\begin{aligned} T &= \frac{1}{2}\left[M_v\dot{y}(t)^2 + m_w\dot{y}_w(t)^2\right] + \frac{1}{2}\dot{\boldsymbol{q}}_f^T\boldsymbol{M}_f\dot{\boldsymbol{q}}_f \\ V &= \frac{1}{2}k_v\left[y(t) - y_w(t)\right]^2 + \frac{1}{2}\boldsymbol{q}_f^T\boldsymbol{K}_f\boldsymbol{q}_f \end{aligned} \tag{3.1}$$

where $\boldsymbol{K}_f$ and $\boldsymbol{M}_f$ are the respective stiffness and mass matrices of the frame (see Section 2.1.1). $q(x,t)$, $\dot{q}(x,t)$ and $\ddot{q}(x,t)$ are the transverse displacement, velocity and acceleration at any point x and time t. Those can be expressed as the vertical displacements of element nodes as follows:

$$q(x,t) = N_1(\xi)q_j^{(p)} + N_2(\xi)q_{j+3}^{(p)} \tag{3.2}$$

$$\dot{q}(x,t) = N_1(\xi)\dot{q}_j^{(p)} + VN_1(\xi)_{,x}q_j^{(p)} + N_2(\xi)\dot{q}_{j+3}^{(p)} + VN_2(\xi)_{,x}q_j^{(p)} \tag{3.3}$$

$$y_w(t) = q(x,t) + r(x) \tag{3.4}$$

$$\dot{y}_w(t) = N_1(\xi)\dot{q}_j^{(p)} + VN_1(\xi)_{,x}q_j^{(p)} + N_2(\xi)\dot{q}_{j+3}^{(p)} + VN_2(\xi)_{,x}q_j^{(p)} + Vr(x)_{,x} \tag{3.5}$$

where the derivative of a function $f(x)$ with respect to x is denoted by $f(x)_{,x}$, $\xi = x/l$ and $N_i (i = 1,2)$ are interpolation functions:

$$N_1 = 1 - 3\xi^2 + 2\xi^3\,,\;\; N_2 = 3\xi^2 - 2\xi^3 \tag{3.6}$$

and nodal displacement vector $\boldsymbol{q}$ is following:

$$\boldsymbol{q}_f = \{q_1\; q_2\; \ldots\; q_j^{(p)} q_{j+1}^{(p)}\; q_{j+2}^{(p)}\; q_{j+3}^{(p)}\; q_{j+4}^{(p)}\; q_{j+5}^{(p)}\; \ldots\; q_N\} \tag{3.7}$$

where $q_j^{(p)}$ defines the nodal degrees of freedom of the element p.

The equations of motion are derived from Lagrange's equation given by

$$\frac{d}{dt}\left(\frac{\partial L}{\partial u_k}\right) - \frac{\partial L}{\partial u_k} = f_k\,, \quad L = T - V\,, \quad k = 1,2,...(N+1) \tag{3.8}$$

Substituting equation (3.1) into (3.8), one obtains, after some algebraic manipulations, the following differential equation:

$$\boldsymbol{M\ddot{u}} + \boldsymbol{C\dot{u}} + \boldsymbol{Ku} = \boldsymbol{f} \tag{3.9}$$

where $\boldsymbol{C}$, $\boldsymbol{K}$, $\boldsymbol{M}$ and $\boldsymbol{f}$ are, respectively, defined by

$$\begin{pmatrix}
0 & 0 & \ldots & \vdots & \ldots & \ldots & \vdots & \ldots & \ldots & 0 \\
0 & 0 & \ldots & \vdots & \ldots & \ldots & \vdots & \ldots & \ldots & 0 \\
\vdots & \vdots & \ddots & \vdots & \ldots & \ldots & \vdots & \ldots & \ldots & \vdots \\
\ldots & \ldots & \ldots & c_{11}^{(p)} & \ldots & \ldots & c_{14}^{(p)} & \ldots & \ldots & 0 \\
\vdots & \vdots & \ldots & \vdots & \ddots & & \vdots & \ldots & \ldots & \vdots \\
\vdots & \vdots & \ldots & \vdots & & \ddots & \vdots & \ldots & \ldots & \vdots \\
\ldots & \ldots & \ldots & c_{41}^{(p)} & \ldots & \ldots & c_{44}^{(p)} & \ldots & \ldots & 0 \\
\vdots & \vdots & \ldots & \vdots & \ldots & \ldots & \vdots & \ddots & \ldots & \vdots \\
0 & \vdots & \ldots & \vdots & \ldots & \ldots & \vdots & \ldots & 0 & 0 \\
0 & 0 & \ldots & 0 & \ldots & \ldots & 0 & \ldots & 0 & 0
\end{pmatrix} \tag{3.10}$$

$$\begin{aligned}
c_{11}^{(p)} &= 2m_w V N_1 N_{1,x}\,, \quad c_{14}^{(p)} = 2m_w V N_1 N_{2,x} \\
c_{41}^{(p)} &= 2m_w V N_{1,x} N_2\,, \quad c_{44}^{(p)} = 2m_w V N_2 N_{2,x}
\end{aligned} \tag{3.11}$$

$$\begin{pmatrix}
k_{11} & k_{12} & \dots & \vdots & \dots & \dots & \vdots & \dots & \dots & 0 \\
k_{21} & k_{22} & \dots & \vdots & \dots & \dots & \vdots & \dots & \dots & 0 \\
\vdots & \vdots & \ddots & \vdots & \dots & \dots & \vdots & \dots & \dots & \vdots \\
\dots & \dots & \dots & k_{11}^{(p)} & \dots & \dots & k_{14}^{(p)} & \dots & \dots & -k_v N_1 \\
\vdots & \vdots & \dots & \vdots & \ddots & & \vdots & \dots & \dots & \vdots \\
\vdots & \vdots & \dots & \vdots & & \ddots & \vdots & \dots & \dots & \vdots \\
\dots & \dots & \dots & k_{41}^{(p)} & \dots & \dots & k_{44}^{(p)} & \dots & \dots & -k_v N_2 \\
\vdots & \vdots & \dots & \vdots & \dots & \dots & \vdots & \ddots & \dots & \vdots \\
k_{N1} & \vdots & \dots & \vdots & \dots & \dots & \vdots & \dots & k_{NN} & 0 \\
0 & 0 & \dots & -k_v N_1 & \dots & \dots & -k_v N_2 & \dots & 0 & k_v
\end{pmatrix} \tag{3.12}$$

$$k_{11}^{(p)} = k_{jj} + k_v N_1^2 + m_w V^2 N_1 N_{1,xx}\,, \quad k_{14}^{(p)} = k_{j(j+3)} + k_v N_1 N_2 + m_w V^2 N_1 N_{2,xx}$$
$$k_{41}^{(p)} = k_{(j+3)j} + k_v N_1 N_2 + m_w V^2 N_{1,xx} N_2\,, \quad k_{44}^{(p)} = k_{(j+3)(j+3)} + k_v N_2^2 + m_w V^2 N_2 N_{2,xx} \tag{3.13}$$

$$\begin{pmatrix}
m_{11} & m_{12} & \dots & \vdots & \dots & \dots & \vdots & \dots & \dots & 0 \\
m_{21} & m_{22} & \dots & \vdots & \dots & \dots & \vdots & \dots & \dots & 0 \\
\vdots & \vdots & \ddots & \vdots & \dots & \dots & \vdots & \dots & \dots & \vdots \\
\dots & \dots & \dots & m_{11}^{(p)} & \dots & \dots & m_{14}^{(p)} & \dots & \dots & \dots \\
\vdots & \vdots & \dots & \vdots & \ddots & & \vdots & \dots & \dots & \vdots \\
\vdots & \vdots & \dots & \vdots & & \ddots & \vdots & \dots & \dots & \vdots \\
\dots & \dots & \dots & m_{41}^{(p)} & \dots & \dots & m_{44}^{(p)} & \dots & \dots & \dots \\
\vdots & \vdots & \dots & \vdots & \dots & \dots & \vdots & \ddots & \dots & \vdots \\
m_{N1} & \vdots & \dots & \vdots & \dots & \dots & \vdots & \dots & m_{NN} & 0 \\
0 & 0 & \dots & \vdots & \dots & \dots & \vdots & \dots & 0 & M_v
\end{pmatrix} \tag{3.14}$$

$$m_{11}^{(p)} = m_{jj} + m_w N_1^2\,, \quad m_{14}^{(p)} = m_{j(j+3)} + m_w N_1 N_2$$
$$m_{41}^{(p)} = m_{(j+3)j} + m_w N_1 N_2\,, \quad m_{44}^{(p)} = m_{(j+3)(j+3)} + m_w N_2^2 \tag{3.15}$$

$$\boldsymbol{f} = \{0 \ \dots \ f_1^{(p)} \ 0 \ 0 \ f_4^{(p)} \ 0 \ 0 \ \dots \ k_v r(x)\}^T \tag{3.16}$$

$$
\begin{aligned}
f_1^{(p)} &= -(M_v + m_w)gN_1 - k_v N_1 r - m_w V^2 N_1 r_{,xx} \\
f_4^{(p)} &= -(M_v + m_w)gN_2 - k_v N_2 r - m_w V^2 N_2 r_{,xx}
\end{aligned}
\tag{3.17}
$$

where g is the acceleration due to gravity.

The damping of the structure is neglected. However, the reason for the damping matrix is that Coriolis forces are taken into account.

The structure has N degrees of freedom and the vehicle is one. Thus, the integrated system, in this case, has $N+1$ degrees of freedom. Therefore, $\boldsymbol{C}$, $\boldsymbol{K}$ and $\boldsymbol{M}$ are $(N+1)\times(N+1)$ matrices and $\boldsymbol{f}$ is a $(N+1)\times 1$ vector. The m_{ij} and k_{ij} elements of matrices seen above correspond to $(i,j)^{th}$ element of overall inertia and stiffness matrices.

Also, $\ddot{\boldsymbol{u}}$ and $\boldsymbol{u}$ are the respective acceleration and displacement vectors for the whole structure. $\boldsymbol{u}$ is

$$
\boldsymbol{u} = \{q_1\ q_2\ \ldots\ q_j^{(p)} q_{j+1}^{(p)}\ q_{j+2}^{(p)}\ q_{j+3}^{(p)}\ q_{j+4}^{(p)}\ q_{j+5}^{(p)}\ \ldots\ q_N\ y\}^T \tag{3.18}
$$

When the vehicle runs on the structure, $\boldsymbol{C}$, $\boldsymbol{K}$ and $\boldsymbol{M}$ matrices and the vector of $\boldsymbol{f}$ are always changing. As a consequence of this, equation 3.9 becomes a second-order differential equation with variable coefficients. Those time-variable coefficients, shown in the box in equations 3.10, 3.12, 3.14 and 3.16 , should be updated every time interval before the numerical integration process apply. Equation 3.9 can then be solved by using the Newmark's time integration scheme with $\delta = 0.5$ and $\alpha = 0.25$ (Bathe (1996)).

3.1.1.1 Validation model

The example model, shown in Figure 3.1, has been studied by Neves et al. (2012). They proposed direct method for the dynamic analysis of the vertical vehicle-structure interaction. Physical and geometric properties are given in Table 3.1. The first natural frequency of the beam is $\omega_1 = 30.02$ rad/s, the natural frequency of the spring-mass system is $\omega_v = 16.66$ rad/s and the mass ratio is $M_v/(mL) = 0.1$. The sprung mass moves at a constant speed $V = 100$ km/h. In Figures 3.3 and 3.4, the results obtained

by the present model are compared with the results from Ref. Neves et al. (2012). Also, it is seen that the moving load model can be used in the displacement of the beam.

Table 3.1 Physical and geometric properties of the simply supported beam

Description	Notation	Value
Beam length	L	$25\ m$
Force	F	$60822\ N$
Elastic modulus	E	$2.87\times10^{9}\ N/m^{2}$
Area moment of inertia	I	$2.9\ m^{4}$
Mass per unit length	m	$2303\ kg/m$
Spring stiffness	k_v	$1595\ kN/m$
Suspended mass	M_v	$5750\ kg$

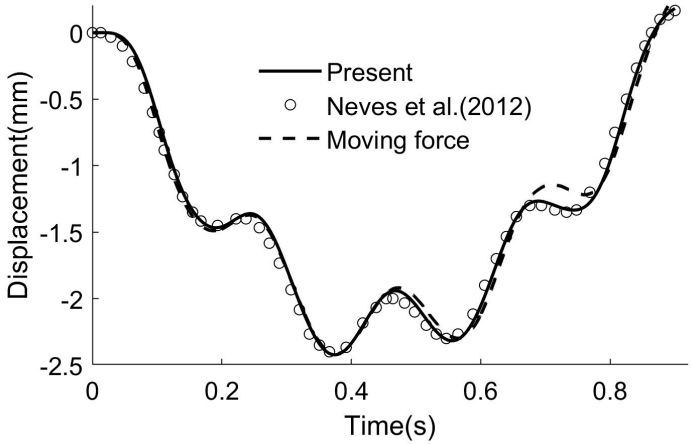

Figure 3.3 Vertical displacement at the midpoint of the beam

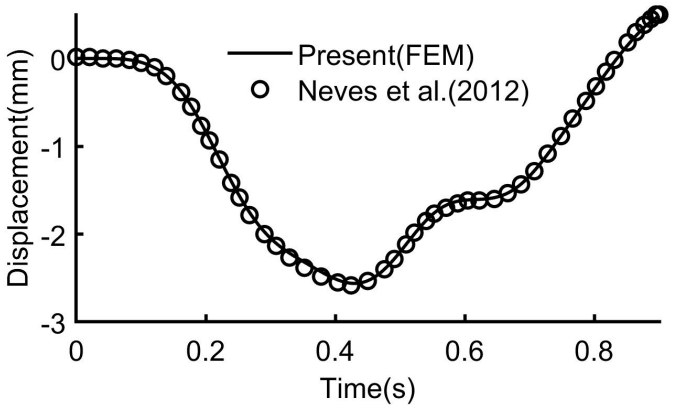

Figure 3.4 Vertical displacement of the sprung mass (y)

Let us now consider the case of a simply supported beam subjected to 50 moving sprung masses with constant speed V = 47.7 km/h. The L_f is 3 m, being M_v and k_v unaltered. The rail irregularity function is

$$r(x) = a_0 \sin\left(\frac{2\pi x}{\lambda}\right) \tag{3.19}$$

where a_0 = 0.5 mm and λ = 5 m. The parameters V and λ have chosen such that the frequency of excitation is equal to the natural frequency of the spring-mass system.

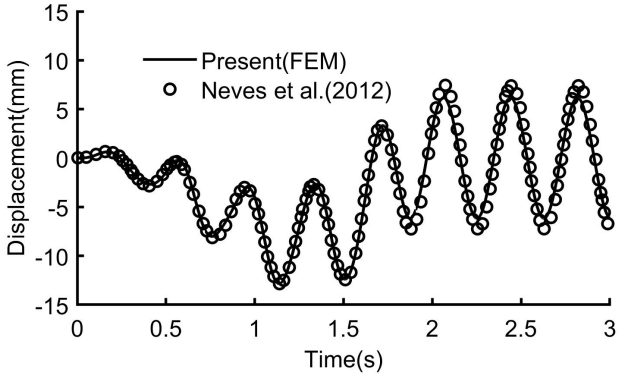

Figure 3.5 Vertical displacement of the first sprung mass (y_1)

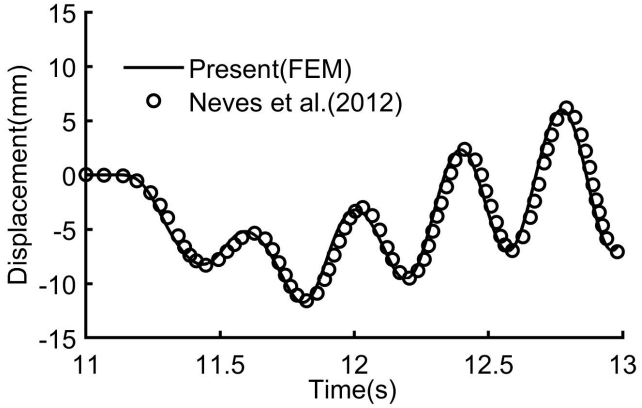

Figure 3.6 Vertical displacement of the last sprung mass (y_{50})

The present finite element model for dynamic displacement results of the first and the last sprung masses and the corresponding results of the direct method are plotted in Figures 3.5 and 3.6.

It is observed in Figures 3.3-3.6 that the vertical displacements of both midpoint of the beam and sprung mass(es) obtained with the present model have shown a good agreement. These figures validate the accuracy of the present model.

3.2 The Moving 2-axle 4 DOF Vehicle Model

3.2.1 System Description

The problem to be dealt with in the present study is a multi-bay frame subjected to a moving train, shown in Figure 3.7. Bernoulli-Euler beams forming the frame have the beam (column) length L, the elastic modulus E_{be}, the area moment of inertia I_{be}, the mass per unit length m_{be}. Points p_1 and p_2 correspond to the midpoint of the column and top beam, respectively.

The vehicle thought to be a model of the train consist of a suspension system having stiffness k and damping c. The m_w and m_v are the respective, the mass of a wheelset and mass of a vehicle body. J_v is the corresponding mass moment of inertia of a bogie and vehicle body. L_d is the longitudinal distance between the center of gravity of the bogie

and the nearest side of the vehicle body. d_1 (d_2) is the horizontal distance between the center of gravity of vehicle body and of the rear (front) bogie. G is the center of gravity of the vehicle body.

As seen Figure 3.7 (b), $y_{wi}(t)$ (i=1,2) denote the vertical displacement of the i^{th} wheelset. y_v is the vertical displacement of the vehicle body. Also, θ_v is the rotation of the vehicle body. The vehicle has four unconstrained degrees of freedom. It is assumed that the upward vertical displacements are taken as positive. They are measured from the respective static equilibrium positions.

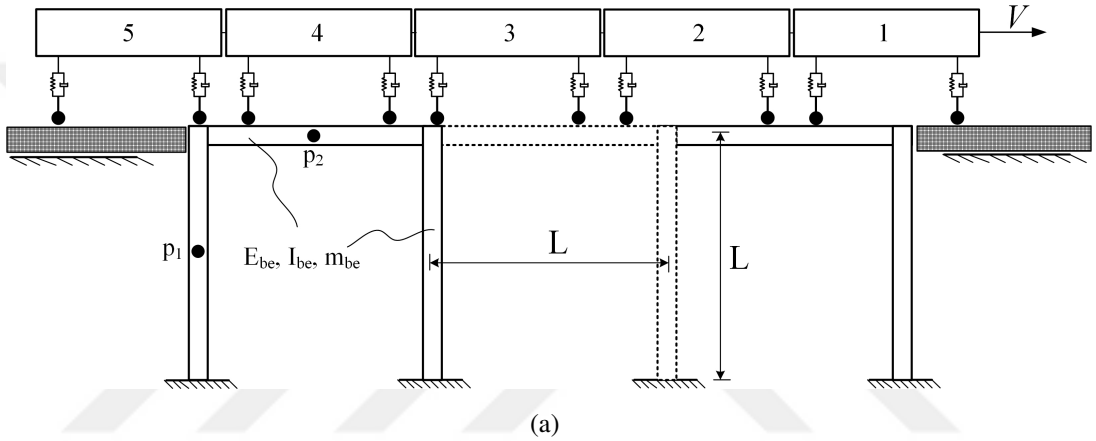

(a)

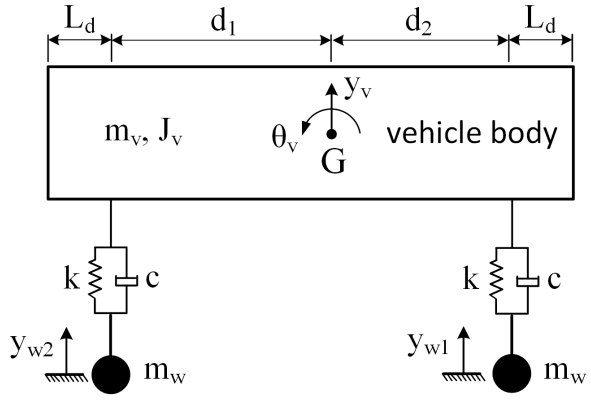

(b)

Figure 3.7 Vehicle-structure system: (a) structure model (b) vehicle model

3.2.2 Mathematical Formulation

A two-axle vehicle travelling at a uniform speed V on a frame was investigated, shown in Figure 3.8. x_i(t)(i=1,2) is the contact point between the frame and i^{th} axle measured from the left end of the top beam. It is assumed that two wheelsets and frame are in contact with elements e_i (i=1,2) at a time t. q_1^{ei} and q_4^{ei} (i=1,2) denote the vertical displacements at nodes of element e_i.

The equation of motion of the frame and vehicle are derived from the following generalized Lagrangian equation:

$$\frac{d}{dt}\left(\frac{\partial T}{\partial \dot{u}_k}\right) - \frac{\partial T}{\partial u_k} + \frac{\partial V}{\partial u_k} + \frac{\partial D}{\partial \dot{u}_k} = f_k, \quad k = 1, 2, \ldots \tag{3.20}$$

where $\dot{u}$ and u are respective generalized velocity and displacement of the whole system.

The kinetic, potential energy and dissipation function of the integrated system can be written as

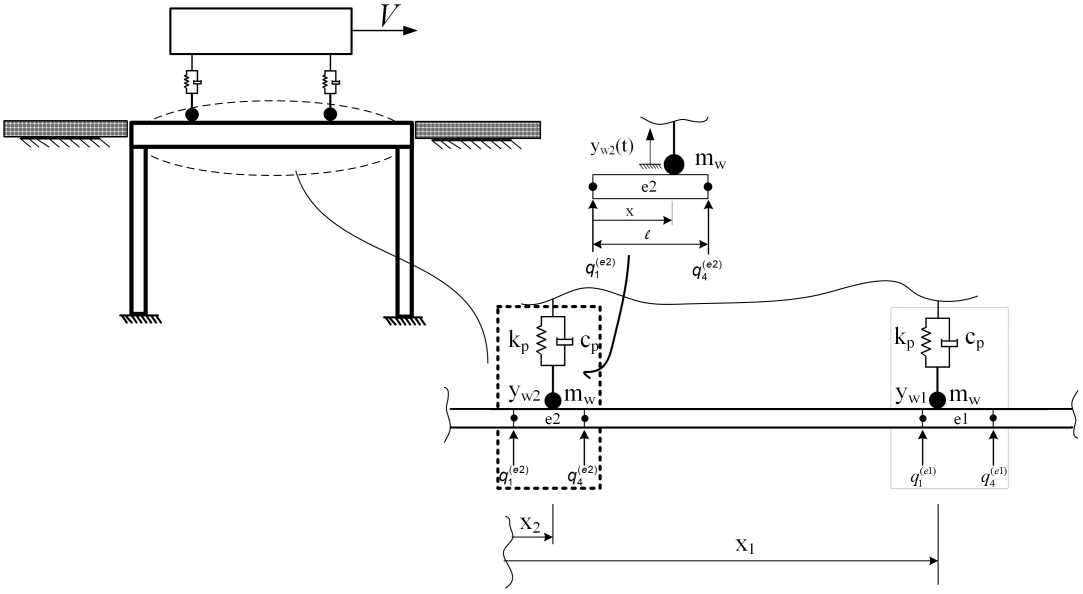

Figure 3.8 A vehicle travelling on a 1-bay frame

$$T = \frac{1}{2}\sum_{i=1}^{2} m_{wi}\dot{y}_{wi}^2 + \frac{1}{2}J_v\dot{\theta}_c^2 + \frac{1}{2}m_v\dot{y}_v^2 + \dot{\boldsymbol{q}}_f^T\boldsymbol{M}_f\dot{\boldsymbol{q}}_f \tag{3.21}$$

$$V = \frac{1}{2}k_s\left[(y_v + d_2\theta_v - y_{w1})^2 + (y_v - d_1\theta_v - y_{w2})^2\right] + \boldsymbol{q}_f^T\boldsymbol{K}_f\boldsymbol{q}_f \tag{3.22}$$

$$D = \frac{1}{2}c_s\left[\left(\dot{y}_v + d_2\dot{\theta}_v - \dot{y}_{w1}\right)^2 + \left(\dot{y}_v - d_1\dot{\theta}_v - \dot{y}_{w2}\right)^2\right] \tag{3.23}$$

where $\boldsymbol{M}_f$ and $\boldsymbol{K}_f$ are the mass and stiffness matrices of the frame as given in Section 2.1.1. $\boldsymbol{q}_f$ and $\dot{\boldsymbol{q}}_f$ are the vectors of nodal displacement and velocity of the frame, respectively.

The total number of degrees of freedom of vehicle is four. It is assumed that the wheels always keep in contact with the structure. This indicates that the structure and wheelsets do not move independently of each other. Therefore, the vertical displacement/velocity of each wheelset is equal to the vertical displacement/velocity of the point where it contacts the frame:

$$y_{w_i} = N_1(\xi)q_1^{e_i} + N_2(\xi)q_4^{e_i},\ i = 1,2 \tag{3.24}$$

$$\dot{y}_{w_i} = N_1(\xi)\dot{q}_1^{e_i} + VN_1(\xi)_{,x}q_1^{e_i} + N_2(\xi)\dot{q}_4^{e_i} + VN_2(\xi)_{,x}q_4^{e_i},\ i = 1,2 \tag{3.25}$$

where the derivative of a function $f(x)$ with respect to x is denoted by $f(x)_{,x}$, $\xi = x/l$ (see Figure 3.9) and $N_i(i = 1,2)$ are interpolation functions:

$$N_1 = 1 - 3\xi^2 + 2\xi^3,\ N_2 = 3\xi^2 - 2\xi^3 \tag{3.26}$$

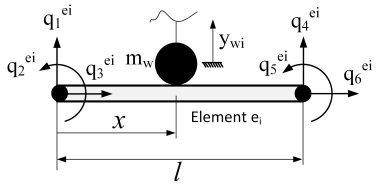

Figure 3.9 Nodal degrees of freedom of the beam element e_i

Nodal degrees of freedom of the element e_i is shown in Figure 3.9. The nodal displacement vector are as follows:

$$\boldsymbol{q}_f^{e_i} = \{q_1^{e_i}, q_2^{e_i}, q_3^{e_i}, q_4^{e_i}, q_5^{e_i}, q_6^{e_i}\},\ i = 1,2 \tag{3.27}$$

and the displacement vector of the vehicle is following:

$$\boldsymbol{q}_v = \{y_v, \theta_v\} \tag{3.28}$$

After some algebraic manipulations, the following equations of motion for the system can be obtained

$$\begin{bmatrix} \boldsymbol{M}_f + \sum_{i=1}^{2} \boldsymbol{M}_{fv}^{i} & \boldsymbol{0} \\ \boldsymbol{0} & \boldsymbol{M}_v \end{bmatrix} \begin{Bmatrix} \ddot{\boldsymbol{q}}_f \\ \ddot{\boldsymbol{q}}_v \end{Bmatrix} + \begin{bmatrix} \sum_{i=1}^{2} \boldsymbol{C}_{fv}^{i} & \bar{\boldsymbol{C}}_{vf} \\ \bar{\boldsymbol{C}}_{vf}^{T} & \boldsymbol{C}_v \end{bmatrix} \begin{Bmatrix} \dot{\boldsymbol{q}}_f \\ \dot{\boldsymbol{q}}_v \end{Bmatrix} + \begin{bmatrix} \boldsymbol{K}_f + \sum_{i=1}^{2} \boldsymbol{K}_{fv}^{i} & \bar{\boldsymbol{K}}_{vf} \\ \bar{\boldsymbol{K}}_{vf}^{T} & \boldsymbol{K}_v \end{bmatrix} \begin{Bmatrix} \boldsymbol{q}_f \\ \boldsymbol{q}_v \end{Bmatrix} = \begin{Bmatrix} \boldsymbol{f} \\ \boldsymbol{0} \end{Bmatrix} \quad (3.29)$$

where the subscripts v and f represent the vehicle and the frame, respectively. The index vf (or fv) in matrices is the result of the interaction between the structure and the vehicle. $\boldsymbol{M}_{fv}$, $\boldsymbol{C}_{fv}$ and $\boldsymbol{K}_{fv}$ are the $N \times N$ matrices and $\bar{\boldsymbol{C}}_{vf}$ and $\bar{\boldsymbol{K}}_{vf}$ are $N \times 2$ matrices. The non-zero columns of these matrices are given as follows:

In equation (3.29), the following abbreviations have been introduced:

$$\boldsymbol{M}_{fv}^{i} < q_1^{e_i} >= \begin{bmatrix} 0 & . & . & m_w N_1^2 & 0 & 0 & m_w N_1 N_2 & 0 & 0 & .. & 0 \end{bmatrix}^T \quad (3.30)$$

$$\boldsymbol{M}_{fv}^{i} < q_4^{e_i} >= \begin{bmatrix} 0 & . & . & m_w N_1 N_2 & 0 & 0 & m_w N_1^2 & 0 & 0 & . & . & 0 \end{bmatrix}^T \quad (3.31)$$

$$\boldsymbol{C}_{fv}^{i} < q_1^{e_i} >= \begin{bmatrix} 0 \\ . \\ . \\ 2V m_w N_1 N_{1,x} + c N_1^2 \\ 0 \\ 0 \\ 2V m_w N_{1,x} N_2 + c N_1 N_2 \\ 0 \\ 0 \\ . \\ . \\ 0 \end{bmatrix}, \quad \boldsymbol{C}_{fv}^{i} < q_4^{e_i} >= \begin{bmatrix} 0 \\ . \\ . \\ 2V m_w N_1 N_{2,x} + c N_1 N_2 \\ 0 \\ 0 \\ 2V m_w N_2 N_{2,x} + c N_2^2 \\ 0 \\ 0 \\ . \\ . \\ 0 \end{bmatrix} \quad (3.32)$$

$$\boldsymbol{K}^{i}_{fv} < q_1^{e_i} >= \begin{bmatrix} 0 \\ . \\ . \\ m_w V^2 N_1 N_{1,xx} + cV N_1 N_{1,x} + k N_1^2 \\ 0 \\ 0 \\ m_w V^2 N_1 N_{2,xx} + cV N_1 N_{2,x} + k N_1 N_2 \\ 0 \\ 0 \\ . \\ . \\ 0 \end{bmatrix},$$

$$\boldsymbol{K}^{i}_{fv} < q_4^{e_i} >= \begin{bmatrix} 0 \\ . \\ . \\ m_w V^2 N_{1,xx} N_2 + cV N_{1,x} N_2 + k N_1 N_2 \\ 0 \\ 0 \\ m_w V^2 N_2 N_{2,xx} + cV N_2 N_{2,x} + k N_2^2 \\ 0 \\ 0 \\ . \\ . \\ 0 \end{bmatrix} \tag{3.33}$$

where $i = 1, 2$.

$$\bar{\boldsymbol{A}}_{vf} = \begin{bmatrix} 0 & 0 \\ \vdots & \vdots \\ -aN_1 & d_1 aN_1 \\ 0 & 0 \\ 0 & 0 \\ -aN_2 & d_1 aN_2 \\ 0 & 0 \\ 0 & 0 \\ \vdots & \vdots \\ -aN_1 & -d_2 aN_1 \\ 0 & 0 \\ 0 & 0 \\ -aN_2 & -d_2 aN_2 \\ 0 & 0 \\ 0 & 0 \\ \vdots & \vdots \\ 0 & 0 \end{bmatrix} \tag{3.34}$$

$$\boldsymbol{M}_v = diag(m_v, J_v) \tag{3.35}$$

$$\boldsymbol{A}_v = \begin{bmatrix} 2a & (d_2 - d_1)a \\ (d_2 - d_1)a & (d_1^2 + d_2^2)a \end{bmatrix} \tag{3.36}$$

$$\boldsymbol{f} = \begin{bmatrix} 0 & . & . & f_1^{e_i} & 0 & 0 & f_4^{e_i} & 0 & 0 & . & . & 0 \end{bmatrix}^T \tag{3.37}$$

where $f_1^{e_i}$ and $f_4^{e_i}$ represent the vehicle loads exerted by each wheelset on the contacting element i and those are determined as follows:

$$\begin{aligned} f_1^{e_i} &= -\left(m_w + m_v \frac{d_2}{d_1 + d_2}\right) gN_1 \\ f_4^{e_i} &= -\left(m_w + m_v \frac{d_1}{d_1 + d_2}\right) gN_2 \end{aligned} \tag{3.38}$$

where g is the acceleration due to gravity.

Notation $\boldsymbol{A} < q_j^{e_i} >$ represents the j^{th} column of the element e_i in the matrix $\boldsymbol{A}$. If $\boldsymbol{A}$ and a in matrices $\bar{\boldsymbol{A}}_{vf}$ and $\boldsymbol{A}_v$ in Eqs. (3.34) and (3.36) are replaced by $\boldsymbol{C}$ and c (or $\boldsymbol{K}$ and k), matrices $\bar{\boldsymbol{C}}_{vf}$ and $\boldsymbol{C}_v$ (or matrices $\bar{\boldsymbol{K}}_{vf}$ and $\boldsymbol{K}_v$) can be determined.

When the vehicle runs on the structure, matrices with double subscript and the vector of $\boldsymbol{f}$ are always changing. As a consequence of this, equation (3.29) becomes a second-order differential equation with variable coefficients. Those time-variable coefficients should be updated every time interval before the numerical integration process is applied. equation (3.29) can then be solved by using the Wilson-theta time integration scheme with $\theta = 1.4$ (Bathe, 1996).

3.2.2.1 Validation of the Model

The model considered here has been studied by Yang et al. (1999) and shown in Figure 3.10. The properties of the vehicle are listed in Table 3.2.

Table 3.2 Physical and geometric properties of the simply supported beam and vehicle

Description	Notation	Value
Mass of the vehicle	m_v	48×10^3 kg
Mass of the wheelset	m_w	5000 kg
Mass moment of inertia of vehicle body	J_v	25×10^5 $kg.m^2$
Axle distance	$d_1 + d_2$	18 m
Car length	$d_1 + d_2 + 2L_d$	25 m
Velocity of the vehicle	V	140 km/h
Beam length	L	30 m
Force	F	60822 N
Elastic modulus	E_{be}	29.43 GPa
Cross-section area	A	7.94 m^2
Area moment of inertia	I_{be}	8.72 m^4
Mass per unit length	m_{be}	36×10^3 kg/m
Spring stiffness	k_v	1500 kN/m
Damping constant	c_v	85 $kN.s/m$
Damping ratio	ζ	0.025

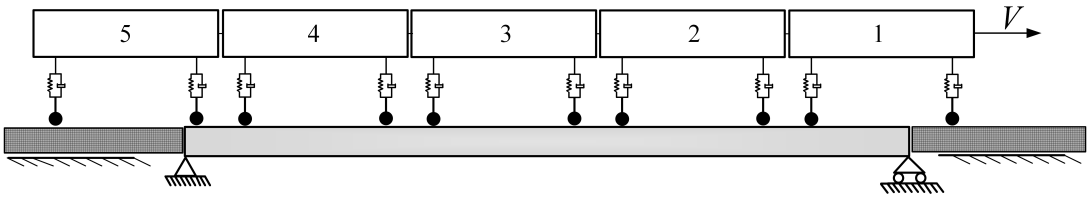

Figure 3.10 A simply supported beam subjected to train consisting of five identical vehicles

Figure 3.11 shows good agreement between the present model and model in Yang et al. (1999).

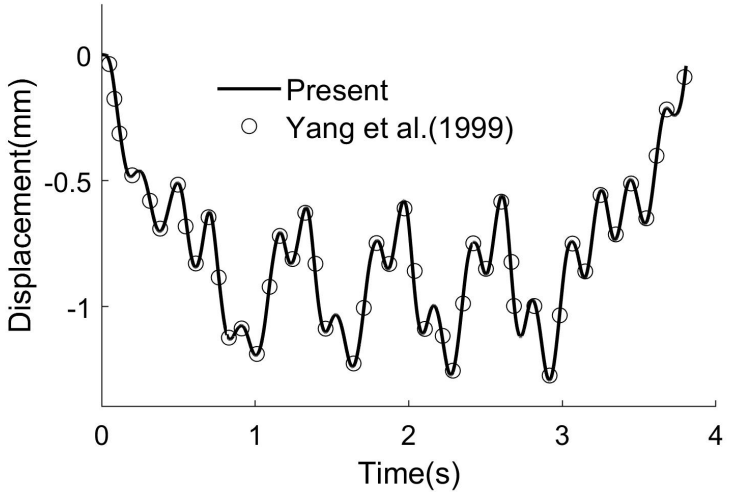

Figure 3.11 Vertical displacement of the midpoint of the beam

3.3 4-axle 2-bogie Multi-body Model with 10 DOF

Dynamic analysis of a structure under vehicular loads requires an accurate model of force induced by the vehicles. The multi-body system, consisting of two bogies, four wheelsets, a vehicle body and a two-layer suspension system, is a more realistic high-speed train model than the previous models.

3.3.1 General Features of the Numerical Model

The problem considered here is a multi-bay frame subjected to moving train, shown in Figure 3.12 (a). Bernoulli-Euler beams forming the frame have the beam (column) length L, the elastic modulus E_{be}, the area moment of inertia I_{be}, mass per unit length m_{be}. Points p_1 and p_2 are corresponding to midpoint of the column and top beam, respectively.

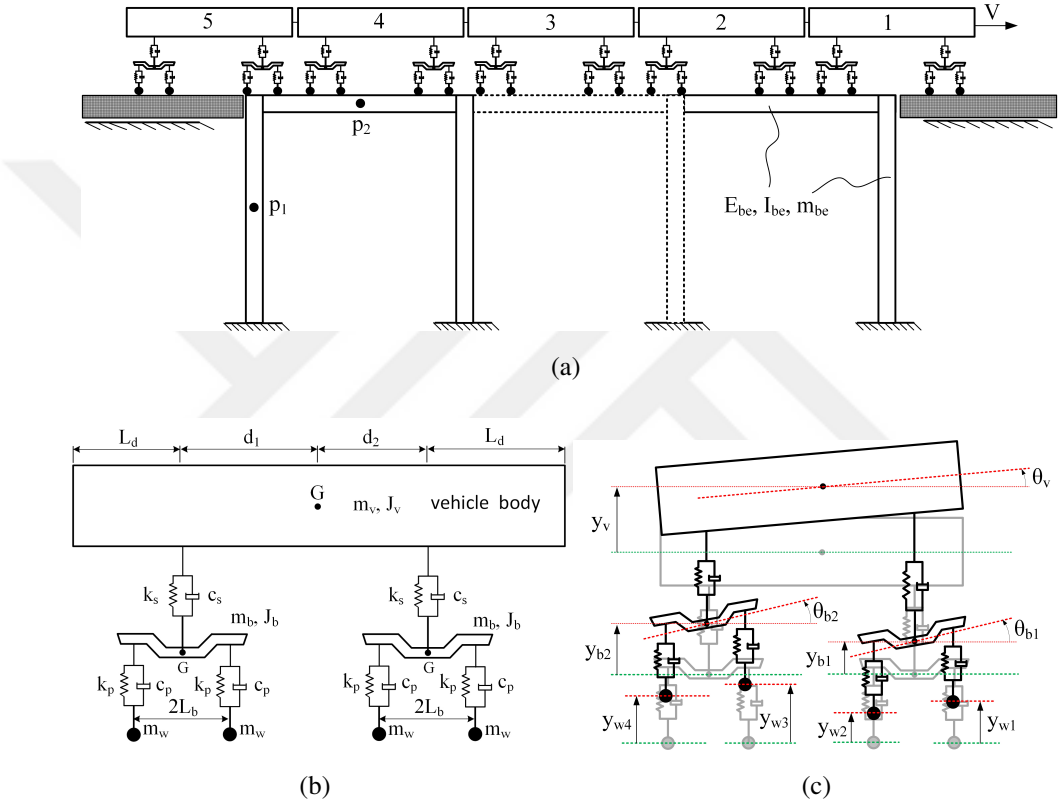

Figure 3.12 Vehicle-structure system: (a) structure model (b) vehicle model, (c)degrees of freedom of the vehicle

The vehicle thought to be as a model of the train consist of primary and secondary suspension systems having stiffness k_p and k_s; damping c_p and c_s. The m_b, m_w and m_v are the respective, the mass of a bogie, the mass of a wheelset and mass of a vehicle body. J_b and J_v are the corresponding mass moment of inertia of a bogie and vehicle body. L_d is the longitudinal distance between the center of gravity of the bogie and the nearest side of vehicle body. d_1 (d_2) is the horizontal distance between the center of

gravity of the vehicle body and of the rear (front) bogie. L_b is the half of bogie axle base. G is the center of gravity of the vehicle body (Figure 3.12 (b)).

As seen Figure 3.12 (c), $y_{wi}(t)$ (i=1,2,3,4) denote the vertical displacement of the i^{th} wheelset. y_{b1} and y_{b2} are the vertical displacements of the bogies and y_v is vertical displacement of the vehicle body. Also, θ_{bi} (i=1,2) and θ_v are rotations of the bogies and the vehicle body. The vehicle has ten unconstrained degrees of freedom. It is assumed that the upward vertical displacements are taken as positive and they are measured from the respective static equilibrium positions.

3.3.2 Theory

A four-axle vehicle travelling at a uniform speed V on a multi-storey frame is investigated, shown in Figure 3.13. x_i (t)(i=1,2,3,4) is the contact point between the frame and i^{th} axle measured from the left end of the top beam. It is assumed that four wheelsets and frame are in contact with elements e_i (i=1,2,3,4) at a time t. q_1^{ei} and q_4^{ei} (i=1,2,3,4) denote the vertical displacements at nodes of element e_i.

The equation of motion of the frame and vehicle are derived from the following generalized Lagrangian equation:

$$\frac{d}{dt}\left(\frac{\partial T}{\partial \dot{u}_k}\right) - \frac{\partial T}{\partial u_k} + \frac{\partial V}{\partial U_k} + \frac{\partial D}{\partial \dot{U}_k} = f_k, \quad k = 1,2,... \tag{3.39}$$

where $\dot{u}$ and u are respective generalized velocity and displacement of the whole system.

The kinetic, potential energy and dissipation function of the integrated system can be written as

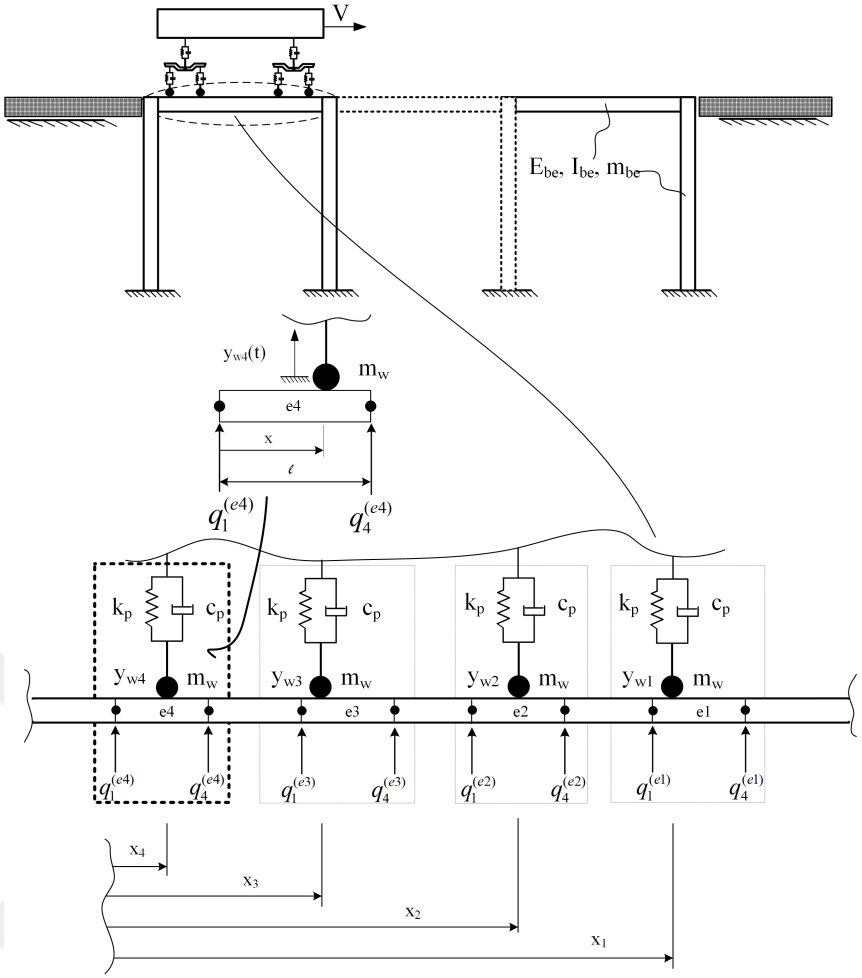

Figure 3.13 A vehicle travelling over a multi-bay frame

$$T = \frac{1}{2}\sum_{i=1}^{4} m_{wi}\dot{y}_{wi}^2 + \frac{1}{2}\sum_{i=1}^{2}\left(m_{bi}\dot{y}_{bi}^2 + m_{bi}\dot{y}_{bi}^2 + J_{bi}\dot{\theta}_{bi}^2\right) + \frac{1}{2}J_v\dot{\theta}_c^2 + \frac{1}{2}m_v\dot{y}_{c1}^2 + \dot{\boldsymbol{q}}_f^T\boldsymbol{M}_f\dot{\boldsymbol{q}}_f \quad (3.40)$$

$$\begin{aligned} V = \frac{1}{2}k_p[&(y_{b1} + L_b\theta_{b1} - y_{w1})^2 + (y_{b1} - L_b\theta_{b1} - y_{w2})^2 \\ &+ (y_{b2} + L_b\theta_{b2} - y_{w3})^2 + (y_{b2} - L_b\theta_{b2} - y_{w4})^2] \\ &+ \frac{1}{2}k_s\left[(y_v + d_1\theta_v - y_{b1})^2 + (y_v - d_2\theta_v - y_{b2})^2\right] + \boldsymbol{q}_f^T\boldsymbol{K}_f\boldsymbol{q}_f \end{aligned} \quad (3.41)$$

$$\begin{aligned} D = \frac{1}{2}c_p[&\left(\dot{y}_{b1} + L_b\dot{\theta}_{b1} - \dot{y}_{w1}\right)^2 + \left(\dot{y}_{b1} - L_b\dot{\theta}_{b1} - \dot{y}_{w2}\right)^2 \\ &+ \left(\dot{y}_{b2} + L_b\dot{\theta}_{b2} - \dot{y}_{w3}\right)^2 + \left(\dot{y}_{b2} - L_b\dot{\theta}_{b2} - \dot{y}_{w4}\right)^2] \\ &+ \frac{1}{2}c_s\left[\left(\dot{y}_v + d_1\dot{\theta}_v - \dot{y}_{b1}\right)^2 + \left(\dot{y}_v - d_2\dot{\theta}_v - \dot{y}_{b2}\right)^2\right] \end{aligned} \quad (3.42)$$

where $\boldsymbol{M}_f$ and $\boldsymbol{K}_f$ are the mass and stiffness matrices of the frame (See Section 2.1.1). $\boldsymbol{q}_f$ and $\dot{\boldsymbol{q}}_f$ are the vectors of nodal displacement and velocity of the frame, respectively.

The total number of degrees of freedom of vehicle is ten. It is assumed that the wheels always keep in contact with the structure. This indicates that the structure and wheelsets do not move independently of each other. Therefore, the vertical displacement/velocity of each wheelset is equal to the vertical displacement/velocity of the point where it contacts the frame:

$$y_{w_i} = N_1(\xi)q_1^{e_i} + N_2(\xi)q_4^{e_i},\ i = 1,2,3,4 \tag{3.43}$$

$$\dot{y}_{w_i} = N_1(\xi)\dot{q}_1^{e_i} + VN_1(\xi)_{,x}q_1^{e_i} + N_2(\xi)\dot{q}_4^{e_i} + VN_2(\xi)_{,x}q_4^{e_i},\ i = 1,2,3,4 \tag{3.44}$$

where the derivative of a function $f(x)$ with respect to x is denoted by $f(x)_{,x}$, $\xi = x/l$ (see Figure **??**) and $N_i(i = 1,2)$ are interpolation functions:

$$N_1 = 1 - 3\xi^2 + 2\xi^3,\ N_2 = 3\xi^2 - 2\xi^3 \tag{3.45}$$

Nodal displacement vector are as follows:

$$\boldsymbol{q}_f^{e_i} = \{q_1^{e_i}, q_2^{e_i}, q_3^{e_i}, q_4^{e_i}, q_5^{e_i}, q_6^{e_i}\},\ i = 1,2,3,4 \tag{3.46}$$

and displacement vector of vehicle is following:

$$\boldsymbol{q}_v = \{y_{b1}, y_{b2}, y_v, \theta_{b1}, \theta_{b2}, \theta_v\} \tag{3.47}$$

Rayleigh damping is commonly used in practice to provide a source of energy dissipation. The damping matrix $\boldsymbol{C}_f$ of the frame can be computed as a weighted sum of mass and stiffness matrices:

$$\boldsymbol{C}_f = \alpha\boldsymbol{M}_f + \beta\boldsymbol{K}_f \tag{3.48}$$

where the coefficients α and β given as:

$$\alpha = \frac{2\zeta\omega_1\omega_2}{\omega_1 + \omega_2},\quad \beta = \frac{2\zeta}{\omega_1 + \omega_2} \tag{3.49}$$

ζ is the damping ratio and, ω_1, ω_2 are the first two natural circular frequencies of the frame.

After some algebraic manipulations, the following equations of motion for the system can be obtained

$$\begin{bmatrix} \boldsymbol{M}_f + \sum_{i=1}^{4} \boldsymbol{M}_{fv}^i & \boldsymbol{0} \\ \boldsymbol{0} & \boldsymbol{M}_v \end{bmatrix} \begin{Bmatrix} \ddot{\boldsymbol{q}}_f \\ \ddot{\boldsymbol{q}}_v \end{Bmatrix} + \begin{bmatrix} \sum_{i=1}^{4} \boldsymbol{C}_{fv}^i & \bar{\boldsymbol{C}}_{vf} \\ \bar{\boldsymbol{C}}_{vf}^T & \boldsymbol{C}_v \end{bmatrix} \begin{Bmatrix} \dot{\boldsymbol{q}}_f \\ \dot{\boldsymbol{q}}_v \end{Bmatrix} + \begin{bmatrix} \boldsymbol{K}_f + \sum_{i=1}^{4} \boldsymbol{K}_{fv}^i & \bar{\boldsymbol{K}}_{vf} \\ \bar{\boldsymbol{K}}_{vf}^T & \boldsymbol{K}_v \end{bmatrix} \begin{Bmatrix} \boldsymbol{q}_f \\ \boldsymbol{q}_v \end{Bmatrix} = \begin{Bmatrix} \boldsymbol{f} \\ \boldsymbol{0} \end{Bmatrix} \quad (3.50)$$

where the subscripts v and f represent the vehicle and the frame, respectively. The index vf (or fv) in matrices is the result of the interaction between the structure and the vehicle. $\boldsymbol{M}_{fv}$, $\boldsymbol{C}_{fv}$ and $\boldsymbol{K}_{fv}$ are the $N \times N$ matrices and $\bar{\boldsymbol{C}}_{vf}$ and $\bar{\boldsymbol{K}}_{vf}$ are $N \times 6$ matrices. The the non-zero columns of these matrices are given by following equations:

$$\boldsymbol{M}_{fv}^i < q_1^{e_i} >= \begin{bmatrix} 0 & . & . & m_w N_1^2 & 0 & 0 & m_w N_1 N_2 & 0 & 0 & .. & 0 \end{bmatrix}^T \quad (3.51)$$

$$\boldsymbol{M}_{fv}^i < q_4^{e_i} >= \begin{bmatrix} 0 & . & . & m_w N_1 N_2 & 0 & 0 & m_w N_1^2 & 0 & 0 & . & . & 0 \end{bmatrix}^T \quad (3.52)$$

$$\boldsymbol{C}_{fv}^i < q_1^{e_i} >= \begin{bmatrix} 0 \\ . \\ . \\ 2V m_w N_1 N_{1,x} + c_p N_1^2 \\ 0 \\ 0 \\ 2V m_w N_{1,x} N_2 + c_p N_1 N_2 \\ 0 \\ 0 \\ . \\ . \\ 0 \end{bmatrix}, \quad \boldsymbol{C}_{fv}^i < q_4^{e_i} >= \begin{bmatrix} 0 \\ . \\ . \\ 2V m_w N_1 N_{2,x} + c_p N_1 N_2 \\ 0 \\ 0 \\ 2V m_w N_2 N_{2,x} + c_p N_2^2 \\ 0 \\ 0 \\ . \\ . \\ 0 \end{bmatrix} \quad (3.53)$$

$$\boldsymbol{K}^{i}_{fv} < q_1^{e_i} >= \begin{bmatrix} 0 \\ . \\ . \\ m_w V^2 N_1 N_{1,xx} + c_p V N_1 N_{1,x} + k_p N_1^2 \\ 0 \\ 0 \\ m_w V^2 N_1 N_{2,xx} + c_p V N_1 N_{2,x} + k_p N_1 N_2 \\ 0 \\ 0 \\ . \\ . \\ 0 \end{bmatrix},$$

$$\boldsymbol{K}^{i}_{fv} < q_4^{e_i} >= \begin{bmatrix} 0 \\ . \\ . \\ m_w V^2 N_{1,xx} N_2 + c_p V N_{1,x} N_2 + k_p N_1 N_2 \\ 0 \\ 0 \\ m_w V^2 N_2 N_{2,xx} + c_p V N_2 N_{2,x} + k_p N_2^2 \\ 0 \\ 0 \\ . \\ . \\ 0 \end{bmatrix} \tag{3.54}$$

where $i = 1, 2, 3, 4$.

$$\bar{\boldsymbol{A}}_{vf} = \begin{bmatrix} 0 & 0 & 0 & 0 & 0 & 0 \\ 0 & -a_p N_1 & 0 & 0 & a_p L_b N_1 & 0 \\ 0 & 0 & 0 & 0 & 0 & 0 \\ 0 & 0 & 0 & 0 & 0 & 0 \\ 0 & -a_p N_2 & 0 & 0 & a_p L_b N_2 & 0 \\ \vdots & \vdots & \vdots & \vdots & \vdots & \vdots \\ 0 & -a_p N_1 & 0 & 0 & -a_p L_b N_1 & 0 \\ 0 & 0 & 0 & 0 & 0 & 0 \\ 0 & 0 & 0 & 0 & 0 & 0 \\ 0 & -a_p N_2 & 0 & 0 & -a_p L_b N_2 & 0 \\ \vdots & \vdots & \vdots & \vdots & \vdots & \vdots \\ -a_p N_1 & 0 & 0 & a_p L_b N_1 & 0 & 0 \\ 0 & 0 & 0 & 0 & 0 & 0 \\ 0 & 0 & 0 & 0 & 0 & 0 \\ -a_p N_2 & 0 & 0 & a_p L_b N_2 & 0 & 0 \\ \vdots & \vdots & \vdots & \vdots & \vdots & \vdots \\ -a_p N_1 & 0 & 0 & -a_p L_b N_1 & 0 & 0 \\ 0 & 0 & 0 & 0 & 0 & 0 \\ 0 & 0 & 0 & 0 & 0 & 0 \\ -a_p N_2 & 0 & 0 & -a_p L_b N_2 & 0 & 0 \\ 0 & 0 & 0 & 0 & 0 & 0 \end{bmatrix} \tag{3.55}$$

$$\boldsymbol{M}_v = diag(m_b, m_b, m_v, J_b, J_b, J_v) \tag{3.56}$$

$$\boldsymbol{A}_v = \begin{bmatrix} 2a_p + a_s & 0 & -a_s & 0 & 0 & -d_1 a_s \\ 0 & 2a_p + a_s & -a_s & 0 & 0 & d_2 c_s \\ -a_s & -a_s & 2a_s 0 & 0 & (d_1 - d_2)a_s & \\ 0 & 0 & 0 & 2L_b^2 a_p & 0 & 0 \\ 0 & 0 & 0 & 0 & 2L_b^2 a_p & 0 \\ -d_1 a_s & d_2 a_s & (d_1 - d_2)a_s & 0 & 0 & (d_1^2 + d_2^2)a_s \end{bmatrix} \tag{3.57}$$

$$\boldsymbol{f} = \begin{bmatrix} 0 & . & . & f_1^{e_i} & 0 & 0 & f_4^{e_i} & 0 & 0 & . & . & 0 \end{bmatrix}^T \tag{3.58}$$

where $f_1^{e_i}$ and $f_4^{e_i}$ represent the vehicle loads exerted by each wheelset on the contacting element i and those are determined as follows:

$$\begin{aligned} f_1^{e_i} &= -\left(m_w + \frac{1}{2}m_b + \frac{1}{2}m_v\frac{d_2}{d_1+d_2}\right)gN_1 \\ f_4^{e_i} &= -\left(m_w + \frac{1}{2}m_b + \frac{1}{2}m_v\frac{d_1}{d_1+d_2}\right)gN_2 \end{aligned} \tag{3.59}$$

where g is the acceleration due to gravity.

Notation $\boldsymbol{A} < q_j^{e_i} >$ represents the j^{th} column of the element e_i in the matrix $\boldsymbol{A}$. If $\boldsymbol{A}$ and a in matrices $\bar{\boldsymbol{A}}_{vf}$ and $\boldsymbol{A}_v$ in Eqs. (3.55) and (3.57) are replaced by $\boldsymbol{C}$ and c (or $\boldsymbol{K}$ and k), matrices $\bar{\boldsymbol{C}}_{vf}$ and $\boldsymbol{C}_v$ (or matrices $\bar{\boldsymbol{K}}_{vf}$ and $\boldsymbol{K}_v$) can be determined.

When the vehicle runs on the structure, matrices with double subscript and the vector of $\boldsymbol{f}$ are always changing. As a consequence of this, equation (3.50) becomes a second-order differential equation with variable coefficients. Those time-variable coefficients should be updated every time interval before the numerical integration process is applied. equation (3.50) can then be solved by using the Wilson-theta time integration scheme with $\theta = 1.4$ (See Section 2.2.2).

3.3.2.1 Validation of the Model

The validation of the present model is carried out in reference Lou et al. (2005). A simply supported beam subjected to a single vehicle is considered (Figure 3.14). Physical properties are given in Table 3.3.

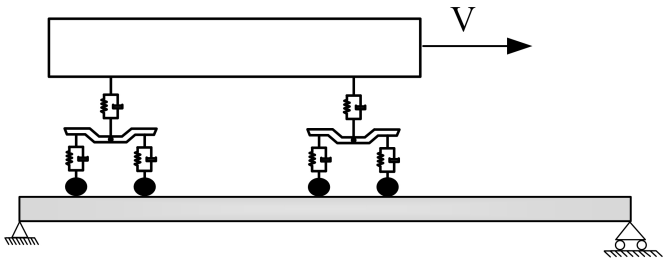

Figure 3.14 A vehicle moving over a simply supported beam

Table 3.3 Parameters of the vehicle and simply supported beam (Lou et al., 2005)

Description	Notation	Value
Vehicle		
Mass of the vehicle body	m_v	$4.175 \times 10^4\, kg$
Mass of a wheelset	m_w	$1.78 \times 10^3\, kg$
Mass moment of inertia of vehicle body	J_v	$2.08 \times 10^6\, kg.m^2$
Horizontal distance between the centre of gravity of car body and of rear bogie	d_1	$8.75\, m$
Horizontal distance between the centre of gravity of car body and of front bogie	d_2	$8.75\, m$
Longitudinal distance between the centre of gravity of bogie and nearest side of vehicle body	L_d	$3\, m$
Stiffness of primary suspension system	k_p	$1.18 \times 10^6\, N/m$
Damping of primary suspension system	c_p	$3.92 \times 10^4\, N.s/m$
Stiffness of secondary suspension system	k_s	$5.3 \times 10^5\, N/m$
Damping of secondary suspension system	c_s	$9.02 \times 10^4\, N.s/m$
Mass bogie	m_b	$3.04 \times 10^3 kg$
Mass moment of inertia of a bogie	J_b	$3.93 \times 10^3\, kg.m^2$
Half of bogie axle base	L_b	$1.25\, m$
Simply supported beam		
Beam length of frame	L	$32\, m$
Mass moment of inertia	I_{be}	$2.88\, m^4$
Mass per unit length	m_{be}	$1.2 \times 10^4\, kg/m$
Young's modulus	E_{be}	$2.943 \times 10^{10}\, Pa$
Damping ratio	ζ	0.02

Figures 3.15 (a)-(b) show good agreement between the present model and the model in Lou et al. (2005).

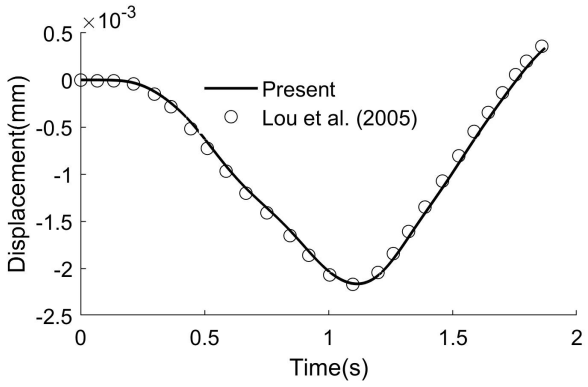

(a)

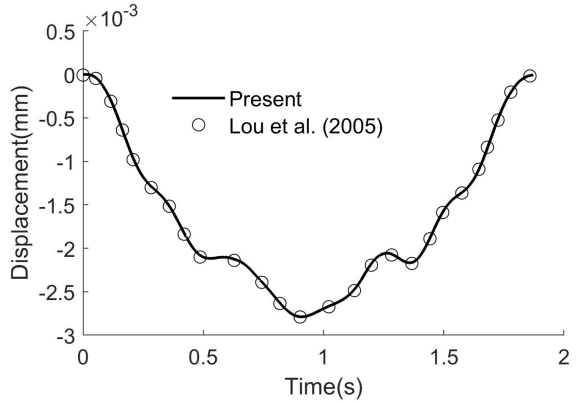

(b)

Figure 3.15 (a)Vertical displacement of the centre of the gravity of car body, (b)vertical displacement of the midpoint of the beam

3.4 Cracked Beam Element

Consider a prismatic isotropic beam, of length l, with an edge crack, which is located at distances l_c from the right end of the beam (see Figure 3.16). a and h is crack depth and thickness of the beam, respectively.

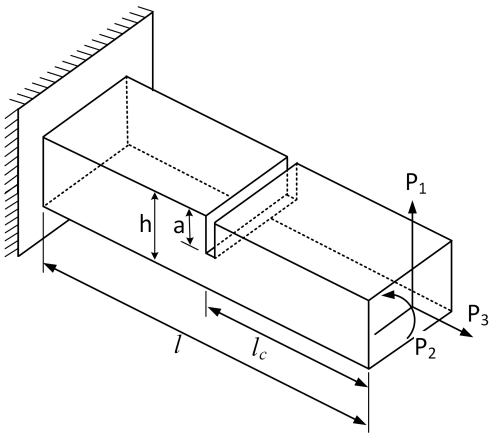

Figure 3.16 A cracked beam element

The derivation of the stiffness matrix of a cracked beam element is determined based on the study presented by Ref. Qian et al. (1990).

The strain energy of a beam without crack and its additional strain energy with crack are given as:

$$W^{(0)} = \frac{1}{2}\int_0^l \left(\frac{(P_1 x + P_2)^2}{EI} + \frac{P_3^2}{EA} \right) dx \tag{3.60}$$

$$W^{(1)} = b\int_0^a \left(\frac{(K_{IP_2} + K_{IP_1})^2 + K_{IIP_1}^2}{E'} \right) da \tag{3.61}$$

where $E' = E$ for plain stress, $E' = E/(1+\nu)$ for plain stress problem ν is Poisson ratio. K_{IP_1}, K_{IP_2} and K_{IIP_1} are stress intensity factors:

$$K_{IP_1} = \frac{6P_1 l_c}{bh^2}\sqrt{\pi a}F_1\ ,\ K_{IP_2} = \frac{6P_2}{bh^2}\sqrt{\pi a}F_1\ ,\ K_{IIP_1} = \frac{P_1}{bh}\sqrt{\pi a}F_2 \tag{3.62}$$

and

$$F_1 = \sqrt{(2h/\pi a)\tan(\pi a/2h)}\frac{0.923 + 0.199[1-\sin(\pi a/2h)]^4}{\cos(\pi a/2h)} \tag{3.63}$$

$$F_2 = \left(3\frac{a}{h} - 2\frac{a^2}{h^2}\right)\frac{1.122 - 0.561a/h + 0.085a^2/h^2 + 0.18a^3/h^3}{\sqrt{1-a/h}} \tag{3.64}$$

Using Castingliano's theorem, the flexibility matrix of the beam without crack can be calculated as

$$c_{ij}^{(0)} = \frac{\partial W^{(0)}}{\partial P_i \partial P_j}\ ,\quad i,j = 1,2,3 \tag{3.65}$$

and the additional flexibility matrix can be obtained from

$$c_{ij}^{(1)} = \frac{\partial W^{(1)}}{\partial P_i \partial P_j}, \quad i, j = 1, 2, 3 \tag{3.66}$$

The total flexibility coefficient is

$$\boldsymbol{C} = \boldsymbol{C}^{(0)} + \boldsymbol{C}^{(1)} \tag{3.67}$$

From the equilibrium conditions, see Figure 3.17,

$$\boldsymbol{p}_{1-6} = \boldsymbol{T}\boldsymbol{p}_{1-3} \tag{3.68}$$

where the transformation matrix is

$$\boldsymbol{T} = \begin{bmatrix} 1 & 0 & 0 & -1 & -l & 0 \\ 0 & 1 & 0 & 0 & -1 & 0 \\ 0 & 0 & 1 & 0 & 0 & -1 \end{bmatrix}^T \tag{3.69}$$

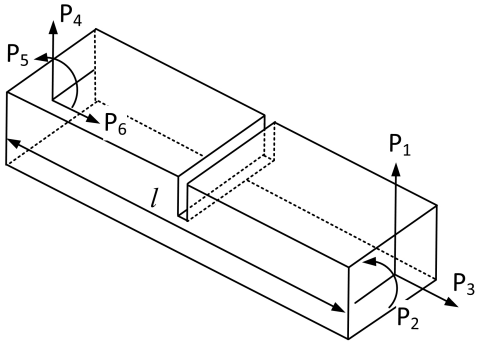

Figure 3.17 Free-free cracked beam element

The stiffness matrix of cracked beam element are calculated thus

$$\boldsymbol{K}_c = \boldsymbol{T}^T \boldsymbol{C}^{-1} \boldsymbol{T} \tag{3.70}$$

3.4.1 Validation the Cracked Beam Model

The finite element results obtained by using MATLAB software have been compared to the those presented by Shifrin & Ruotolo (1999). A cantilever beam with

crack located at the clamped end has been examined (Figure 3.18). The geometric properties of beam are L = 0.8m, rectangular cross-section of width b = 0.02m and height h = 0.02m, crack depth a = 0.002m located at 0.12m from the clamped end. Mechanical properties are Young's modulus E = 210 GPa, Poisson's ratio ν = 0.3 and density ρ = 7800 kg/m^3.

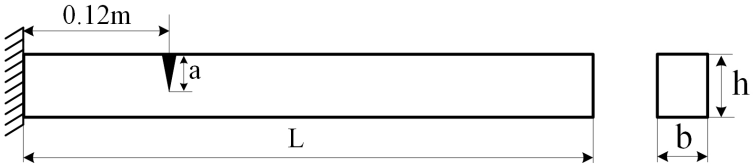

Figure 3.18 Cracked cantilever beam

The comparison between calculated natural frequencies and those given in Shifrin & Ruotolo (1999) demonstrate the accuracy and validity of developed MATLAB program results.

Table 3.4 The first three natural frequencies (Hz) of cracked beam

Present	Shifrin & Ruotolo (1999)
26.1141	26.1231
164.0851	164.0921
459.6195	459.6028

CHAPTER FOUR
CASE STUDY 1: DYNAMIC RESPONSES OF THE VIADUCT-LIKE STRUCTURES SUBJECTED TO VARIOUS TRAIN MODELS

In this chapter, the effect of the vibration modes on the dynamic response is addressed. It is sufficient to consider only the first mode of the structure in the simply supported beam (Yang et al., 1997). However, if the problem involves frame structures consisting of both columns and beams, higher modes should also be considered. It is discussed the influence of higher-order vibration modes on the dynamic response of the structure.

4.1 The dominant mode shapes of the viaduct modelled by a 3-bay frame subjected to a train model with 2-axle and 4 DOF

4.1.1 Dominant Mode Shapes of the 3-bay Frame

The problem shown in Figure 4.1 is considered. The theory presented in Section 3.2 is applied to study given below:

- The first few natural frequencies and corresponding natural frequencies are determined.
- The 3D relationship of velocity-frequency-amplitude graphs is plotted.
- The values of at the peak points in 3D graphs are selected. The critical speeds can then be identified when deflection of the structure reaches the maximum value.
- The effective mode shapes related to the resonance response of the structure are obtained via the time history curves of the points taken.

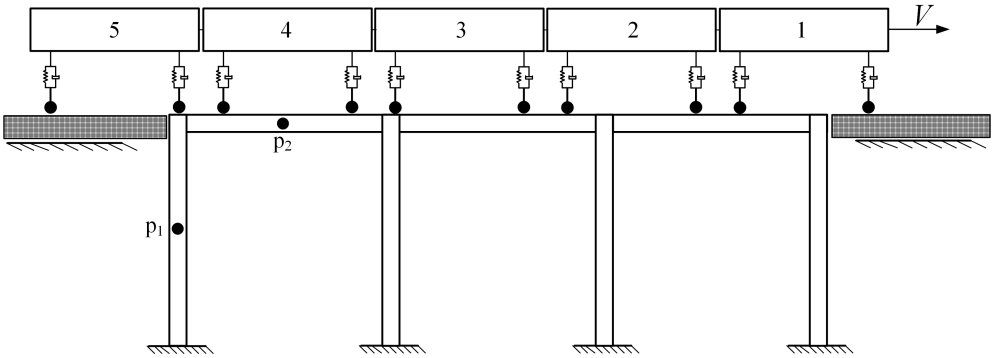

Figure 4.1 3-bay frame subjected to vehicle moving at velocity V

All the parameters which are used in subsequent computations have been given in Section 3.2.2.1.

4.1.2 Modal Analysis of 3-bay Frame

The first few natural frequencies are determined using both ANSYS and the developed MATLAB programs (present work). The beams and columns are modelled as is done in Section 2.4.2. Table 4.1 shows the natural frequencies of the 3-bay frame. The frequencies obtained by using ANSYS program show very good agreement in the present work.

Table 4.1 The first few natural frequencies (f) of 3-bay frame

	3-bay frame	
f (Hz)	Present work	ANSYS
f_1	0.4256	0.4255
f_2	1.7709	1.7675
f_3	2.0219	2.0179
f_4	2.4501	2.4452
f_5	3.0644	3.0559
f_6	3.1410	3.1352
f_7	3.2408	3.2340

The mode shapes corresponding to natural frequencies given in Table 4.1 are plotted. The first mode of the 3-bay frame shown in Figure 4.2 are related to the first bending modes of the columns forming the frame. The vertical displacements of the top beam are negligible in that mode. Due to train moving on the top beam, it can be expected that mode shapes in which vertical displacements of the top beam are effective are important on resonance response. Therefore, the 2^{nd}, 3^{rd}, 4^{th}, 6^{th} and 7^{th} modes of the 3-bay frame may be effective in resonance response of the structure.

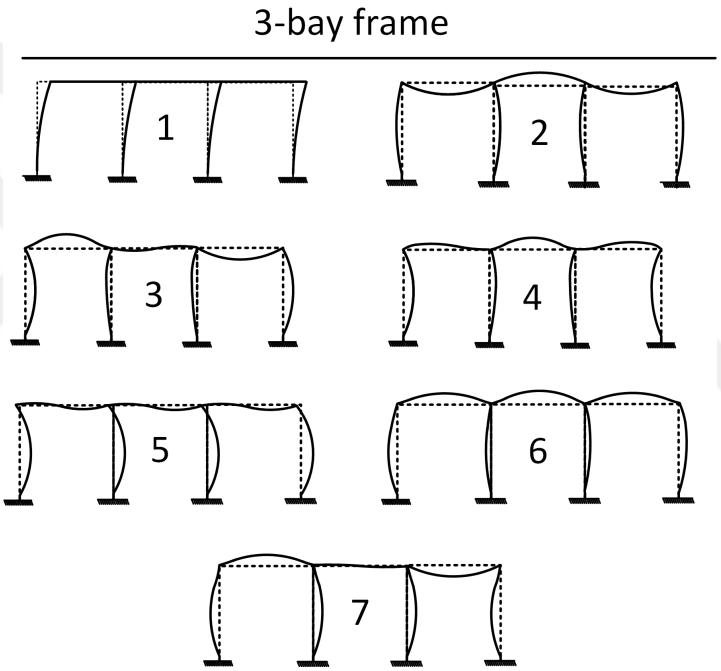

Figure 4.2 Mode shapes of 3-bay frame corresponding to the natural frequencies listed in Table 4.1

4.1.3 Velocity-Frequency-Amplitude Graphs

3D relationship of velocity-frequency-amplitude graphs was plotted with respect to horizontal displacements of the point p_1 and vertical displacements of the point p_2 (see Figure 4.1). The displacement-time history curves of the 3-bay frame were first determined at each velocity ($V = 1, 2, ..., 100$). Then, frequency responses were obtained by applying the Fourier transform to free vibrations. It should be noted that

the number of vehicles is taken as 5 when plotting 3D graphics. However, in order to better visualize resonance, the number of vehicles in the displacement-time history curves was selected as 10.

From Figure 4.3 (a), there are five obvious amplitude peaks. The critical velocity and its corresponding frequency values in Figure 4.3 (a) are: f_1 = 0.426 Hz, V = 11 m/s; f_2 = 1.77 Hz, V = 41 m/s; f_3 = 2.02 Hz, V = 51 m/s and f_7 = 3.24 Hz, V = 80 m/s.

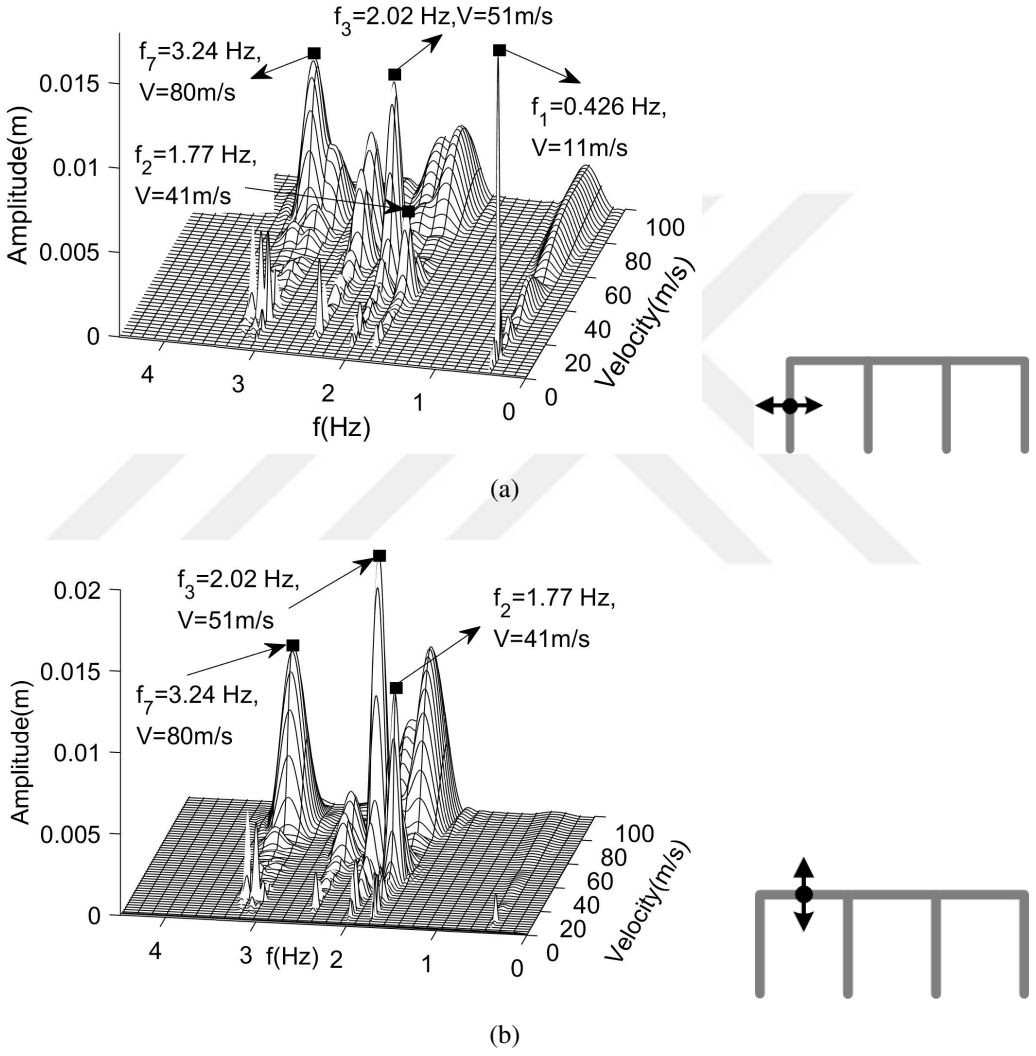

Figure 4.3 3D velocity-frequency-amplitude graphs for 3-bay frame: (a) horizontal displacement of the point 1, (b) vertical displacement of the point 2

From Figure 4.3 (b), it is clear that modes 2, 3 and 7 are effective modes of vibrations in the vertical direction. Points in Figure 4.3 (b) are: f_2 = 1.77 Hz, V = 41 m/s; f_3 = 2.02 Hz, V = 51 m/s and f_7 = 3.24 Hz, V = 80 m/s.

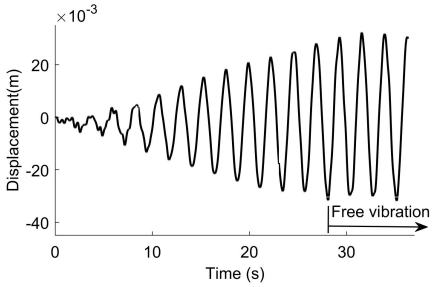

(a1): V = 11 m/s (point p_1)

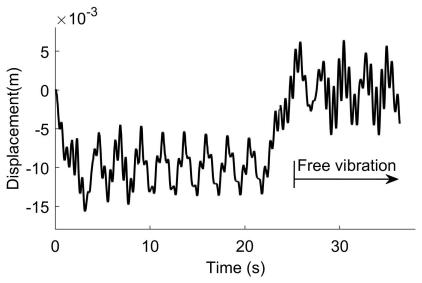

(b1): V = 11 m/s (point p_2)

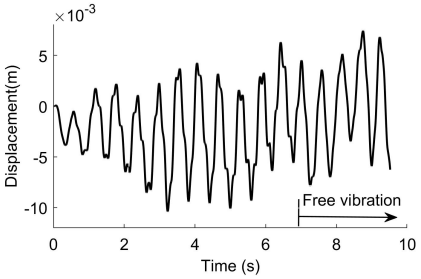

(a2): V = 41 m/s (point p_1)

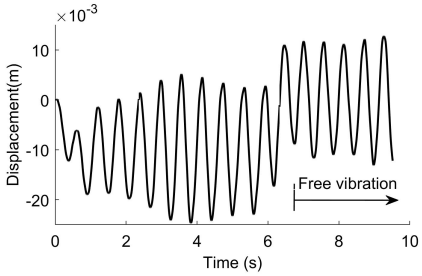

(b2): V = 41 m/s (point p_2)

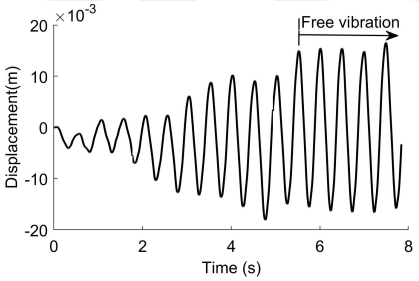

(a3): V = 51 m/s (point p_1)

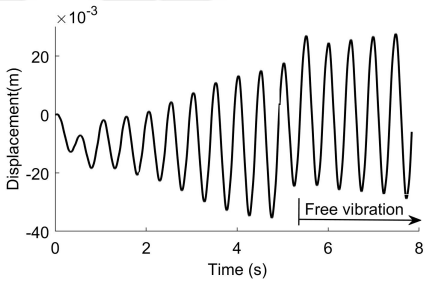

(b3): V = 51 m/s (point p_2)

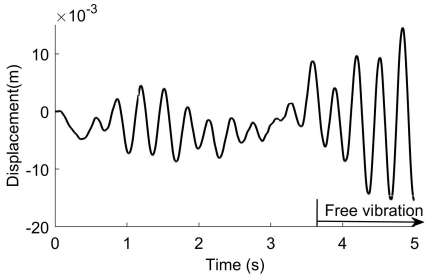

(a4): V = 80 m/s (point p_1)

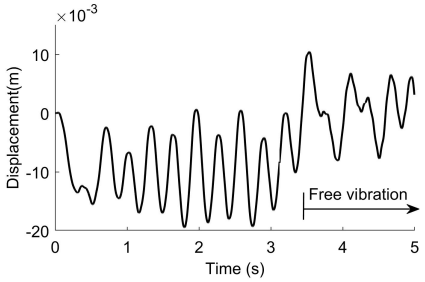

(b4): V = 80 m/s (point p_2)

Figure 4.4 Displacement-time history curves. Figures (ai) and (bi) (i=1,2,3,4) are corresponding to displacements at points p_1 in the horizontal direction and p_2 in the vertical directions, respectively

The time history curves for the above-mentioned velocities are shown in Figures 4.4. Similar to the 1 and 2-bay frames, the resonance vibrations are encountered at the

critical velocity of V = 11 m/s of the train. Figures 4.4 (a2)-(b2) are depicted resonance response at mode 2, as in 1-3 bay frames. The resonance also occurs in the 3^{rd} mode of the 3-bay frame, as shown in Figure 4.4 (a3)-(b3). The resonant behavior is not observed at mode 7.

4.2 Effective Vibration Modes of the Viaduct-like Structures Subjected to the Passage of High-Speed Train

4.2.1 Determination of the Dominant Mode Shapes of the Multi-bay Frame

A multi-bay frame subjected moving train is shown in Figure 4.5. The theory presented in Section 3.3 is applied to the study given below: (1) The first few natural frequencies are calculated and their mode shapes are plotted. (2) The 3D relationship of velocity-frequency-amplitude graphs is established. The values of frequency and velocity at the peak points in 3D graphs are extracted. (3) The mode shapes that affect the resonance response of the structure are obtained by plotting the time history of the points taken.

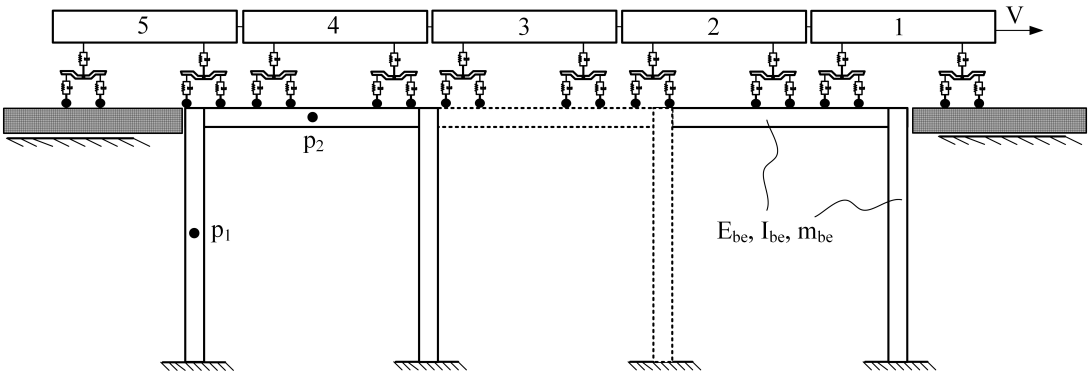

Figure 4.5 A multi-bay frame subjected to vehicle moving at velocity V

All the parameters which is used in subsequent computations have been given in Table 4.2. The values of physical properties are taken from Lou et al. (2005).

Table 4.2 Parameters of the vehicle and multi-bay frame

Description	Notation	Value
Vehicle		
Mass of the vehicle body	m_v	$4.175 \times 10^4\, kg$
Mass of a wheelset	m_w	$1.78 \times 10^3\, kg$
Mass moment of inertia of vehicle body	J_v	$2.08 \times 10^6\, kg.m^2$
Horizontal distance between the centre of gravity of car body and of rear bogie	d_1	$8.75\, m$
Horizontal distance between the centre of gravity of car body and of front bogie	d_2	$8.75\, m$
Longitudinal distance between the centre of gravity of bogie and nearest side of vehicle body	L_d	$3\, m$
Stiffness of primary suspension system	k_p	$1.18 \times 10^6\, N/m$
Damping of primary suspension system	c_p	$3.92 \times 10^4\, N.s/m$
Stiffness of secondary suspension system	k_s	$5.3 \times 10^5\, N/m$
Damping of secondary suspension system	c_s	$9.02 \times 10^4\, N.s/m$
Mass bogie	m_b	$3.04 \times 10^3 kg$
Mass moment of inertia of a bogie	J_b	$3.93 \times 10^3\, kg.m^2$
Half of bogie axle base	L_b	$1.25\, m$
Multi-bay frame		
Beam/column length of frame	L	$25\, m$
Area moment of inertia	I_{be}	$2.9\, m^4$
Mass per unit length	m_{be}	$1.2 \times 10^4\, kg/m$
Young's modulus	E_{be}	$2.87 \times 10^9\, Pa$

4.2.2 Modal Analysis of the Multi-bay Frame

The first few natural frequencies are determined using both ANSYS and the developed MATLAB programs (present work) as in Section 4.1.2. Table 4.3 shows

the natural frequencies of i-bay frame (i=1,2,3).

Table 4.3 The first few natural frequencies (f) of i-bay frame (i=1,2,3)

	1-bay		2-bay		3-bay	
f (Hz)	Present work	ANSYS	Present work	ANSYS	Present work	ANSYS
f_1	0.4714	0.47135	0.4370	0.4370	0.4256	0.4255
f_2	1.8477	1.8442	1.7933	1.7898	1.7709	1.7675
f_3	3.0356	3.0267	2.2309	2.2265	2.0219	2.0179
f_4	3.2412	3.2343	3.0555	3.0469	2.4501	2.4452
f_5					3.0644	3.0559
f_6					3.1410	3.1352
f_7					3.2408	3.2340

The mode shapes corresponding to natural frequencies given in Table 4.3 are plotted. The first modes of the structures shown in Figures 4.6 are related to the first bending modes of the columns forming the frame. The vertical displacements of the top beam are negligible in these modes. Due to train moving on the top beam, it can be expected that mode shapes in which vertical displacements of the top beam are effective are important on resonance response. Therefore, the 2^{nd} and 4^{th} modes of the 1-bay frame; the 2^{nd} and 3^{rd} modes of the 2-bay frame and the 2^{nd}, 3^{rd}, 4^{th}, 6^{th} and 7^{th} modes of the 3-bay frame may be effective in resonance response of the structure.

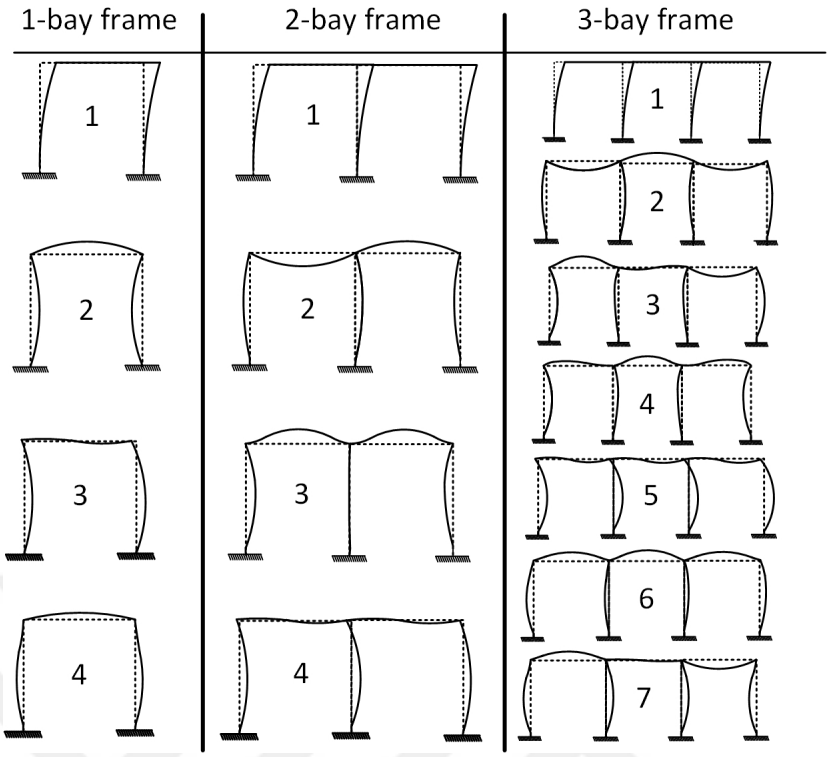

Figure 4.6 Mode shapes of i-bay frame (i=1,2,3) corresponding to the natural frequencies listed in Table 4.3

4.2.3 Velocity-Frequency-Amplitude Graphs

3D relationship of velocity-frequency-amplitude graphs was plotted with respect to horizontal displacements of the point p_1 and vertical displacements of the point p_2 (see Figure 4.5). The displacement-time history curves of the i-bay frame (i=1,2,3) were first determined at each velocity ($V = 1, 2, ..., 100$). Then, frequency responses were obtained by applying the Fourier transform to free vibrations. It should be noted that the number of vehicles is taken as 5 when plotting 3D graphics. However, in order to better visualize resonance, the number of vehicles in the displacement-time history curves was selected as 10.

4.2.3.1 1-bay Frame

Figures 4.7 show the 3D views of the velocity-frequency-amplitude plot. There are 3 peaks in Figure 4.7 (a). The velocities corresponding to the peaks of amplitude may be viewed as the critical velocities at which the resonance vibration may occur. Those velocities and frequencies can be read as f_1 = 0.47 Hz, V = 11 m/s; f_2 = 1.847 Hz, V = 45 m/s; and f_3 = 3.04 Hz, V = 73 m/s.

From Figure 4.7 (b), two peak amplitudes can be extracted as f_2 = 1.847 Hz, V = 45 m/s and f_4 = 3.24 Hz, V = 77 m/s.

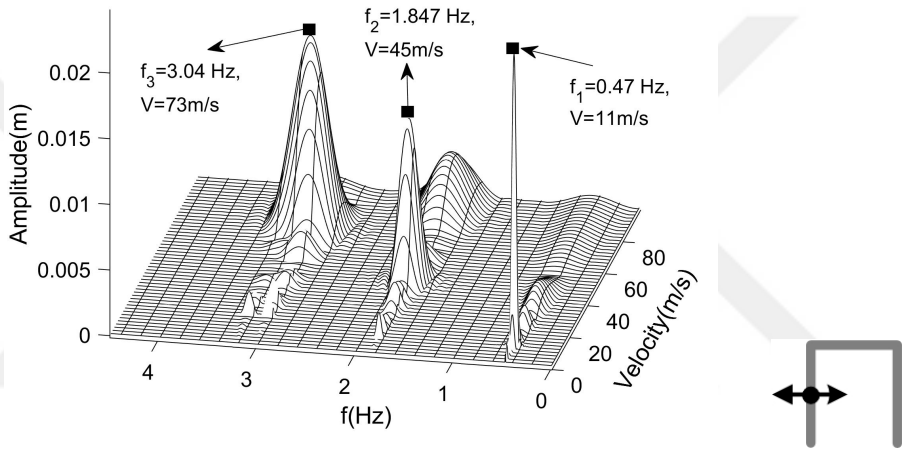

(a)

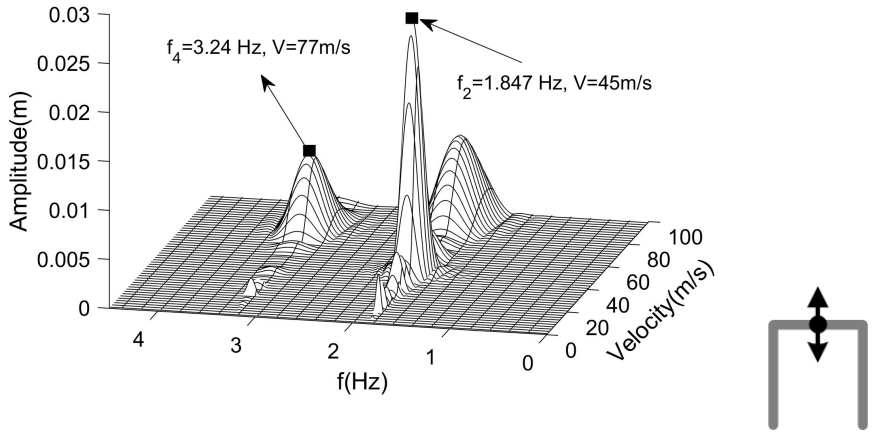

(b)

Figure 4.7 3D velocity-frequency-amplitude graphs for 1-bay frame: (a) horizontal displacement of the point 1, (b) vertical displacement of the point 2

Figures 4.8 shows displacement-time history curves for velocities determined from Figure 4.7. Figure 4.8 (a1) shows resonance behavior in the horizontal direction. From Figures 4.8 (a1) and (b1), the velocity V = 11 m/s has excited the first mode of vibrations.

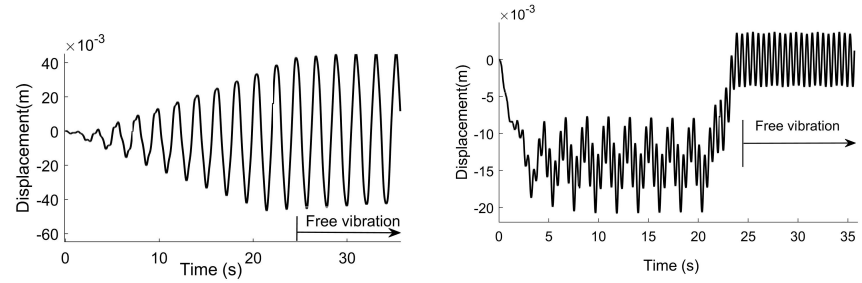

(a1): V = 11 m/s (point p_1)

(b1): V = 11 m/s (point p_2)

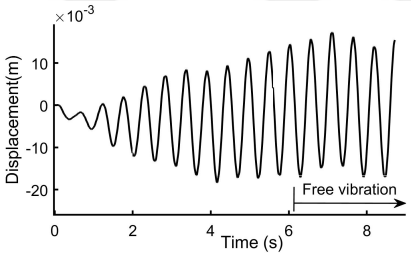

(a2): V = 45 m/s (point p_1)

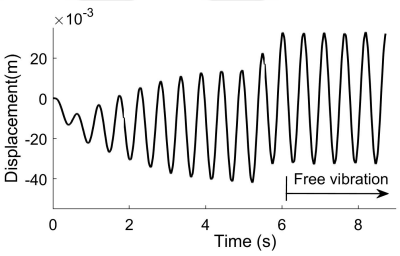

(b2): V = 45 m/s (point p_2)

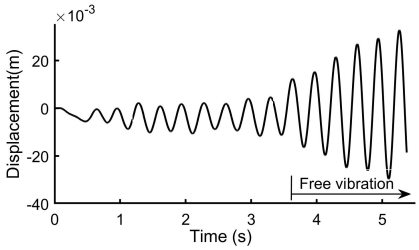

(a3): V = 73 m/s (point p_1)

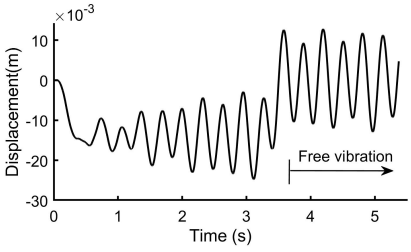

(b3): V = 73 m/s (point p_2)

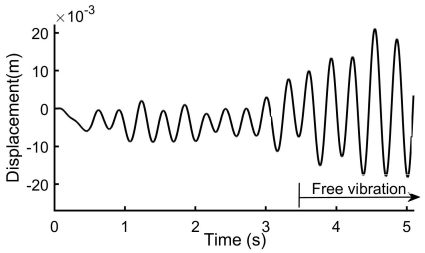

(a4): V = 77 m/s (point p_1)

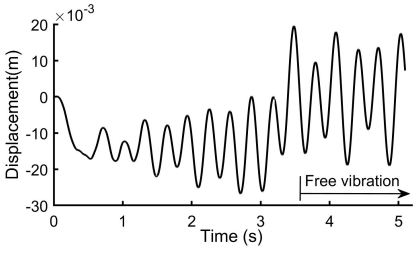

(b4): V = 77 m/s (point p_2)

Figure 4.8 Displacement-time history curves. Figures (ai) and (bi)(i=1,2,3,4) are corresponding to displacements at points p_1 in the horizontal direction and p_2 in the vertical directions, respectively

The resonant responses both in the horizontal and vertical directions are encountered when the speed of the train having a velocity of V = 45 m/s. This critical speed excites the 1-bay frame in 2^{nd} mode of vibrations. The amplitude of vibration in the vertical direction takes place the maximum value when comparing with Figures 4.8 (b1), (b3) and (b4). The resonance behavior related to 3^{rd} and 4^{th} modes cannot be appeared by a train within these velocity ranges, as indicated in Figures 4.8 (a3), (b3), (a4) and (b4).

4.2.3.2 2-bay Frame

Figures 4.9 illustrate the 3D relationship of velocity-frequency-amplitude graphs. The four possible resonance peaks are determined in Figure 4.9 (a). The velocity and frequency values corresponding to these peak amplitudes are as follows: f_1 = 0.437 Hz, V = 11 m/s; f_2 = 1.79 Hz, V = 42 m/s; f_3 = 2.23 Hz, V = 57 m/s and f_4 = 3.05 Hz, V = 74 m/s. It is clear that the largest amplitude occurs when f_1 = 0.437 Hz, V = 11 m/s. This means that the first mode can be the dominant mode in the vibrations of point p_1 in the horizontal direction.

It is seen in Figure 4.9 (b) that mode 2 is effective in vibrations in the vertical directions of the structure within the speed range of interest. The amplitudes peaks in the figure are: f_2 = 1.79 Hz, V = 42 m/s and f_3 = 2.23 Hz, V = 57 m/s.

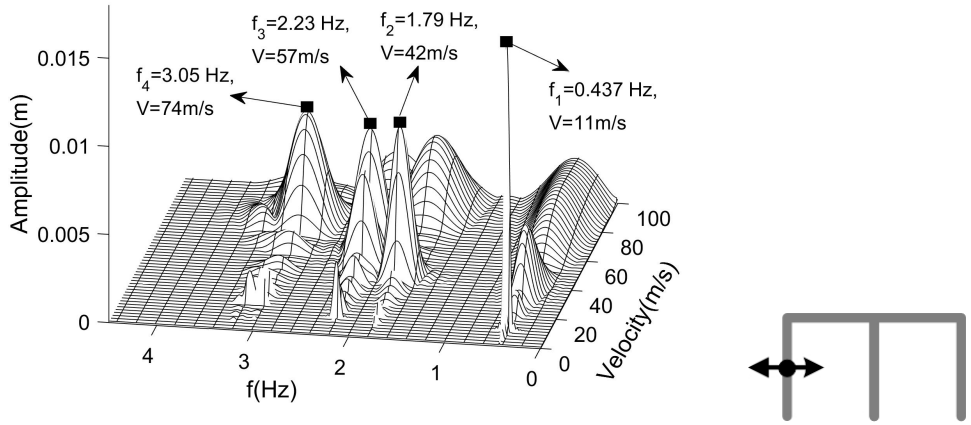

(a)

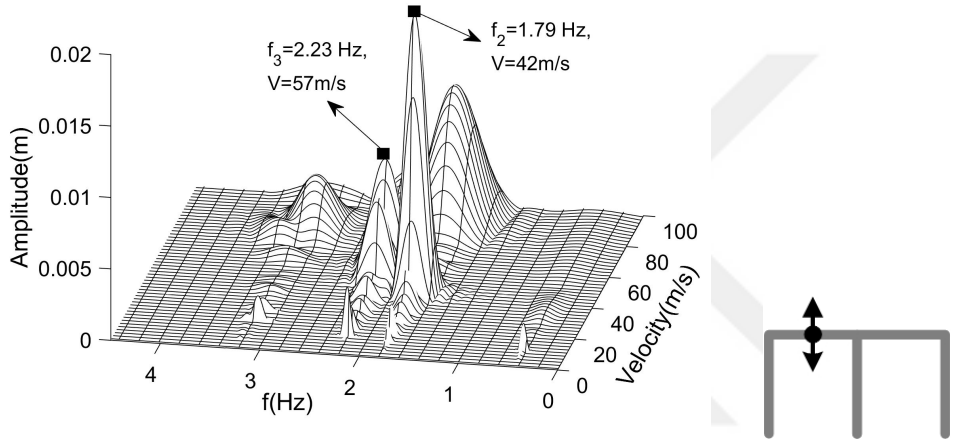

(b)

Figure 4.9 3D velocity-frequency-amplitude graphs for 2-bay frame: (a) horizontal displacement of the point 1, (b) vertical displacement of the point 2

Figure 4.10 (a1) shows the resonant response in the horizontal direction. From Figures 4.10 (a1) and (b1), the 1^{st} mode in which the vibrations of the structure in the horizontal direction are dominant is excited. Figures 4.10(a2) and (b2) illustrate resonance response associated with the 2^{nd} mode. In Figures 4.10 (a3), (b3), (a4) and (b4), the resonant response does not occur for those critical velocities.

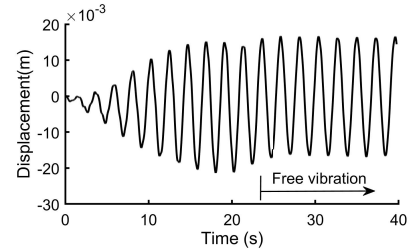

(a1): V = 11 m/s(point p_1)

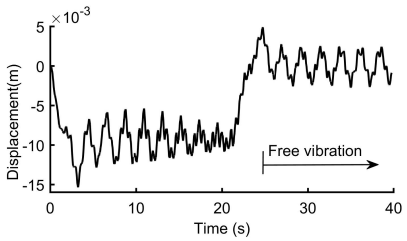

(b1): V = 11 m/s (point p_2)

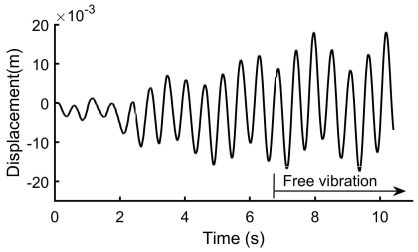

(a2): V = 42 m/s (point p_1)

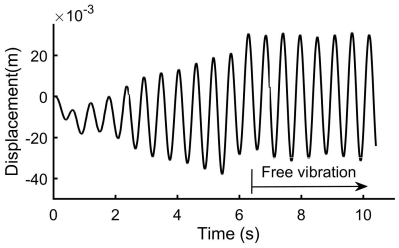

(b2): V = 42 m/s (point p_2)

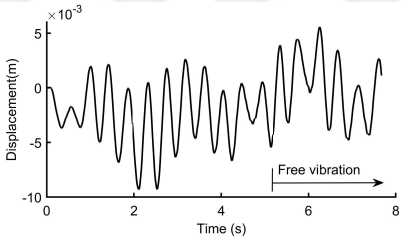

(a3): V = 57 m/s (point p_1)

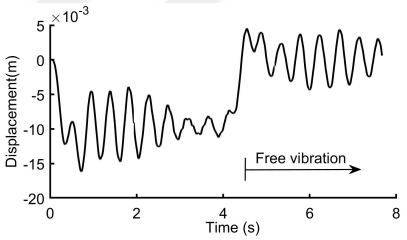

(b3): V = 57 m/s (point p_2)

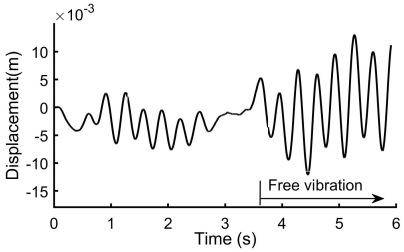

(a4): V = 74 m/s (point p_1)

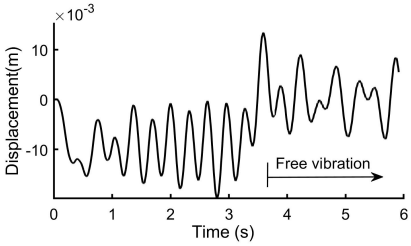

(b4): V = 74 m/s (point p_2)

Figure 4.10 Displacement-time history curves. Figures (ai) and (bi)(i=1,2,3,4) are corresponding to displacements at points p_1 in the horizontal direction and p_2 in the vertical directions, respectively

4.2.3.3 3-bay Frame

There are five obvious amplitude peaks in Figure 4.11 (a). When the number of the bay of the frame increases, the natural frequencies are getting closer to each other. As

a result of this, the peaks in the 3D graphs have become closer to each other, as clearly seen in Figures 4.7, 4.9 and 4.11.

The critical velocity and its corresponding frequency values in Figure 4.11(a) are: f_1 = 0.426 Hz, V = 11 m/s; f_2 = 1.77 Hz, V = 39 m/s; f_3 = 2.02 Hz, V = 49 m/s; f_4 = 2.45 Hz, V = 55 m/s and f_7 = 3.24 Hz, V = 77 m/s.

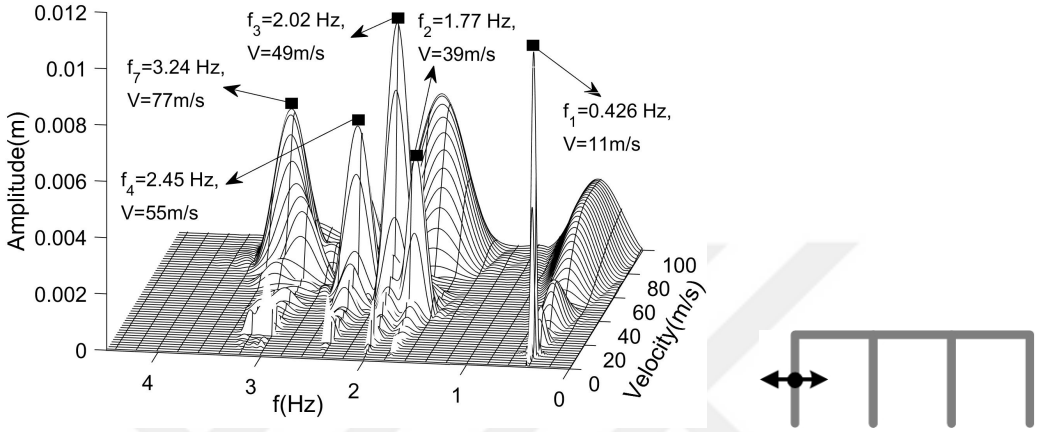

(a)

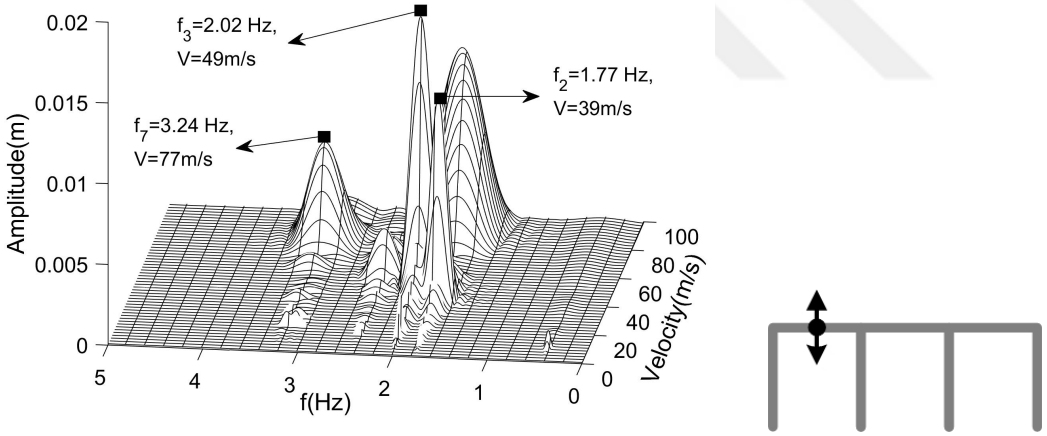

(b)

Figure 4.11 3D velocity-frequency-amplitude graphs for 3-bay frame: (a) horizontal displacement of the point 1, (b) vertical displacement of the point 2

From Figure 4.11 (b), it is clear that modes 2, 3 and 7 are effective modes of vibrations in the vertical direction. Points in Figure 4.11b are: f_2 = 1.77 Hz, V = 39 m/s; f_3 = 2.02 Hz, V = 49 m/s and f_7 = 3.24 Hz, V = 77 m/s.

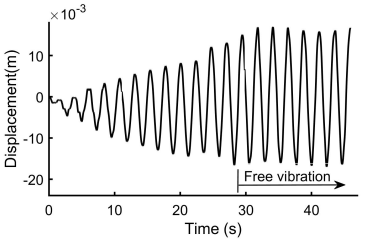

(a1): V = 11 m/s (point p_1)

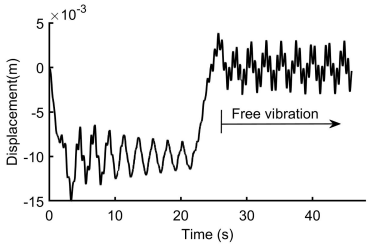

(b1): V = 11 m/s (point p_2)

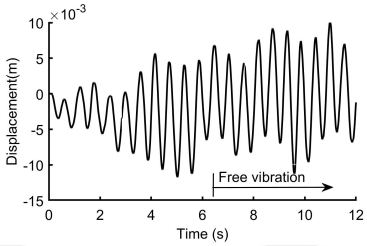

(a2): V = 40 m/s (point p_1)

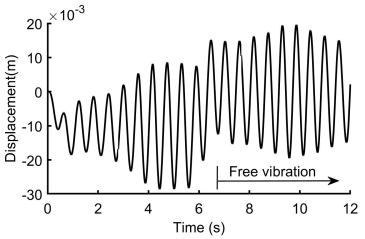

(b2): V = 40 m/s (point p_2)

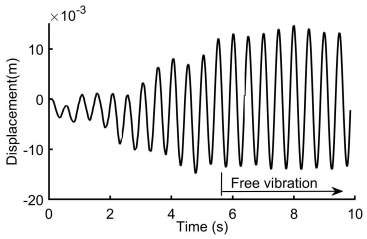

(a3): V = 49 m/s (point p_1)

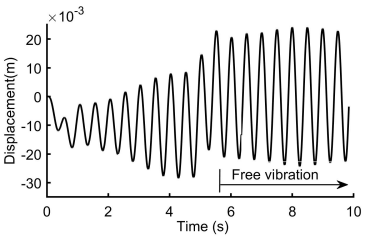

(b3): V = 49 m/s (point p_2)

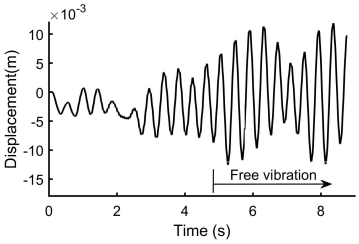

(a4): V = 55 m/s (point p_1)

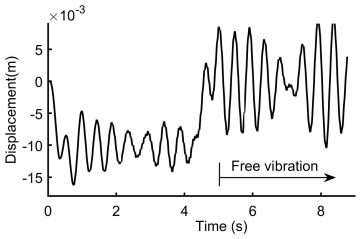

(b4): V = 55 m/s (point p_2)

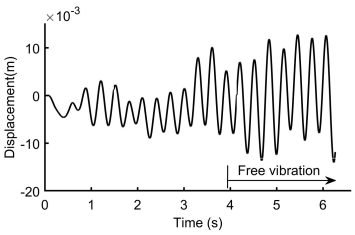

(a5): V = 77 m/s (point p_1)

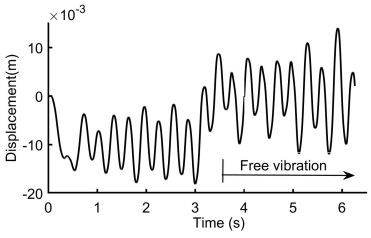

(b5): V = 77 m/s (point p_2)

Figure 4.12 Displacement-time history curves. Figures (ai) and (bi) (i=1,2,3,4,5) are corresponding to displacements at points p_1 in the horizontal direction and p_2 in the vertical directions, respectively

Figure 4.12 shows the displacement-time curves for the above-mentioned velocities. As in 1 and 2-bay frames, the resonance vibrations are encountered at the critical velocity of V = 11 m/s of train. The mode 2 of 1-3 bay frames are similar modes that cause resonance response, as shown in Figures 4.12 (a2)-(b2). Unlike the 1 and 2-bay frames, the resonance effect also occurs in the 3^{rd} mode of the 3-bay structure, as shown in Figure 4.12 (a3)-(b3). It is obvious in Figures 4.12 (a4)-(a5) and Figures 4.12 (b4)-(b5) that resonant behavior is not observed at the critical speeds of V = 55 m/s, 77 m/s.

The first natural frequencies of the i-bay (i = 1,2,3) frame are very close to each other. It is reasonable to expect that critical speeds are also very close to each other. But note that the critical speed values that excite this mode are the same, 11 m/s, due to the graphs plotted in increments of 1 m/s.

It is seen in Figures 4.7, 4.9 and 4.11 that the maximum amplitude decreases as the number of bay increases.

CHAPTER FIVE
CASE STUDY 2: EFFECT OF CRACK LOCATION ON DYNAMIC RESPONSES

The effect of the crack location on the dynamic response of complex structures presented here. When the structure is subjected to high amplitude vibrations for a long time, the fatigue-induced crack formation can occur. The presence of a crack changes the stiffness and damping of the structure. The stiffness decreases and this implies a reduction of the natural frequency of the structure. Depending on the location of the crack, the reduction effect in stiffness or natural frequency varies. Three-dimensional graphics are used to illustrate the effect of crack on dynamic response.

5.1 The Resonant Vibration of a Cracked Multi-bay Frame Subjected to Moving Oscillators

5.1.1 Description of the Numerical Model

A multi-bay frame subjected to moving oscillators has been illustrated in Figure 5.1. x_i(t) (i=1,2,...,K) is the contact point between the frame and i^{th} oscillator measured from the left end of the top beam. L_c is the location of the crack measured from the left end of the top beam. L_f is the distance between consecutive oscillators. Bernoulli-Euler beams forming the frame have beam (column) length L, elastic modulus E, area moment of inertia I and mass per unit length m. The oscillators consist of a spring of stiffness k_v, the mass of a wheelset m_w and a sprung mass M_v. $y_i(t)$ (i=1,2,...,K) denotes the vertical displacement of the i^{th} sprung mass. It is assumed that the upward vertical displacements are taken as positive and that they are measured from the respective static equilibrium positions.

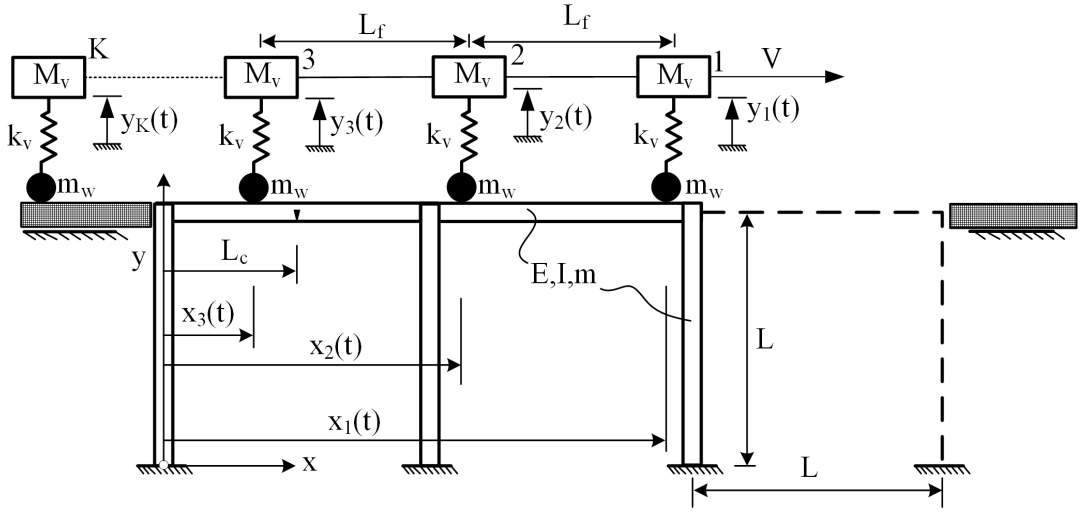

Figure 5.1 A cracked multi-bay frame subjected to moving oscillators

5.1.2 Cracked Multi-bay Frames Subjected to Moving Oscillators

This section is devoted to the numerical evaluation of the expressions established in the preceding sections. For the numerical applications, the following values are chosen for the physical data of the frame and vehicle model as seen in Figure 5.1. The distance between consecutive oscillators is fixed and equals L_f = 26m. The properties m, M_v, k_v, I and E have been given in Section 3.2 are unaltered. The crack is located at the center of each element. When calculating the displacement of the center point of the beam or column, Equation (3.2) (with $\xi = 0.5$) needs to be used because this point does not correspond to a node. The mass of a wheelset m_w = 450kg, crack ratio a/h = 0.4, element length of finite element model l = 5m, total length of beams and columns is L = 35m. The number of oscillators moving on the frame is K = 10. The rail irregularity is neglected in calculations.

5.1.3 Single-bay Frame

The frame is discretized into 21 elements and points shown in Figure 5.2 denote examined possible crack locations. It is assumed that there is only one crack in the structure. Analyses are performed by changing the crack location from point 1 to point

21.

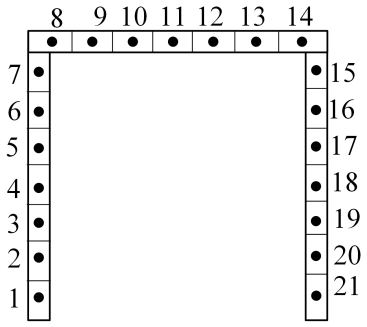

Figure 5.2 Locations of crack on the finite element model

The study presented here, based on the theory given in Section 3.1, is applied to 1-bay frame. The effect of crack location on dynamic response is shown using 3D relationship of the crack location-velocity-maximum displacement plot. Then, using the 3D plot, the critical speed of the oscillator which excites the structure at resonance condition can be determined.

Figures 5.3 to 5.5 show the 3D views of the effect of crack locations and oscillator velocity on the maximum displacements. The maximum displacements in Figures 5.3 and 5.4 are taken at point 4 in the horizontal direction and point 11 in the vertical direction. The maximum displacements in Figure 5.5 belong to the fifth sprung mass (y_5). The distance between the two points in Figure 5.2 is 5m.

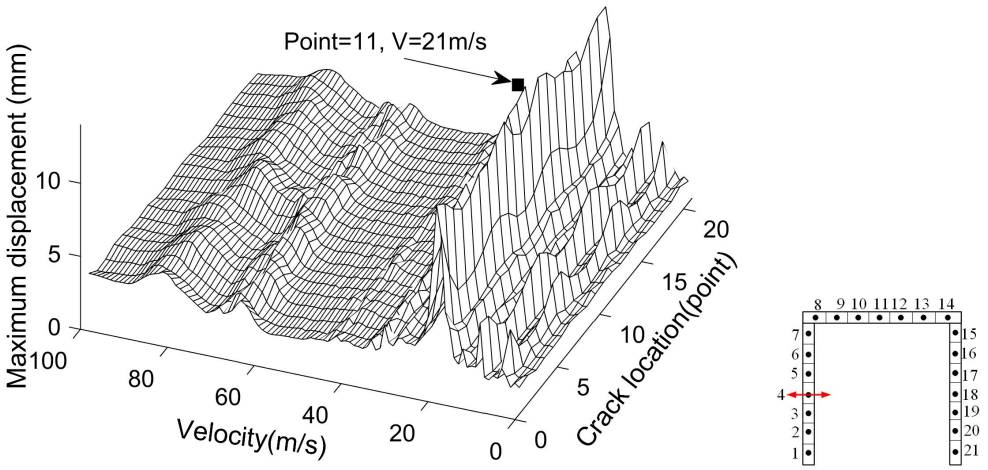

Figure 5.3 Maximum horizontal displacements of point 4

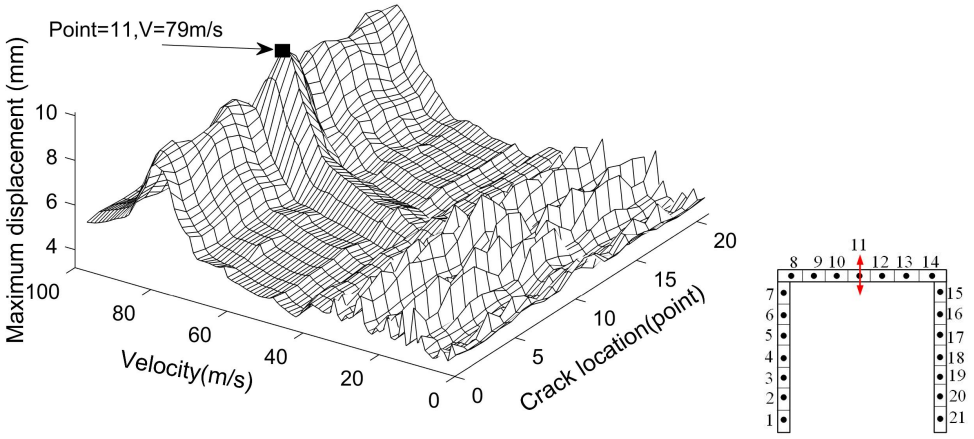

Figure 5.4 Maximum vertical displacements of point 11.

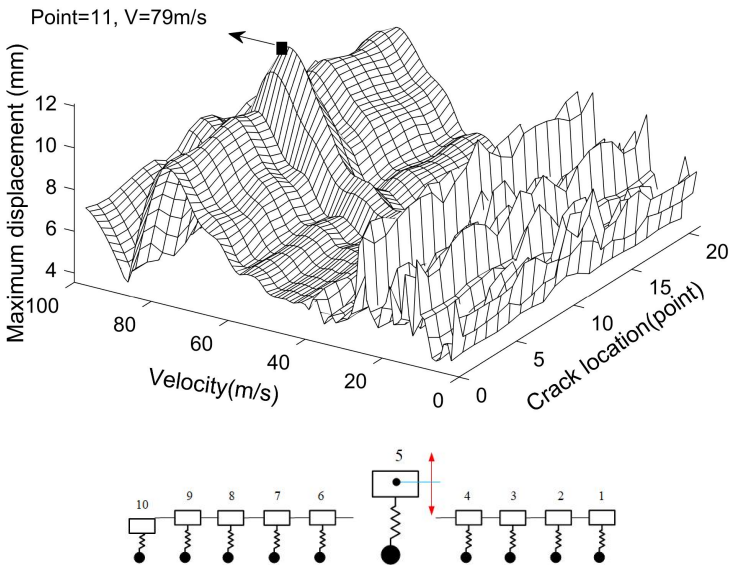

Figure 5.5 Maximum vertical displacements of the fifth sprung mass (y_5)

It is known from the existing literature that the critical velocity that causes resonance can be calculated for a simply supported beam from Yang et al. (1997):

$$V_{cr} = \frac{f_{n_i} L_f}{k}, \quad k = 1,2,3, \quad i = 1,2,\ldots \tag{5.1}$$

From Figure 5.3, it is seen that there is no significant effect of the crack position on the maximum dynamic response. It has been determined that the maximum displacement in the axial direction is related to the first natural frequency of structure and L_f. This relation is expressed approximately by the formula (5.1) with $k = 1$. The

speed value obtained from here is the critical speed that will excite the structure in the resonance condition.

For example, let's examine the situation where the crack is located at point 11. In this case, the first natural frequency of the 1-bay frame is 0.7909 Hz and L_f = 26 m. Then, V_{cr} can be computed as V_{cr} = 0.7909(26) = 20.56 m/s. Figure 5.6 shows that resonance arises in the horizontal direction for this specific speed and L_f values.

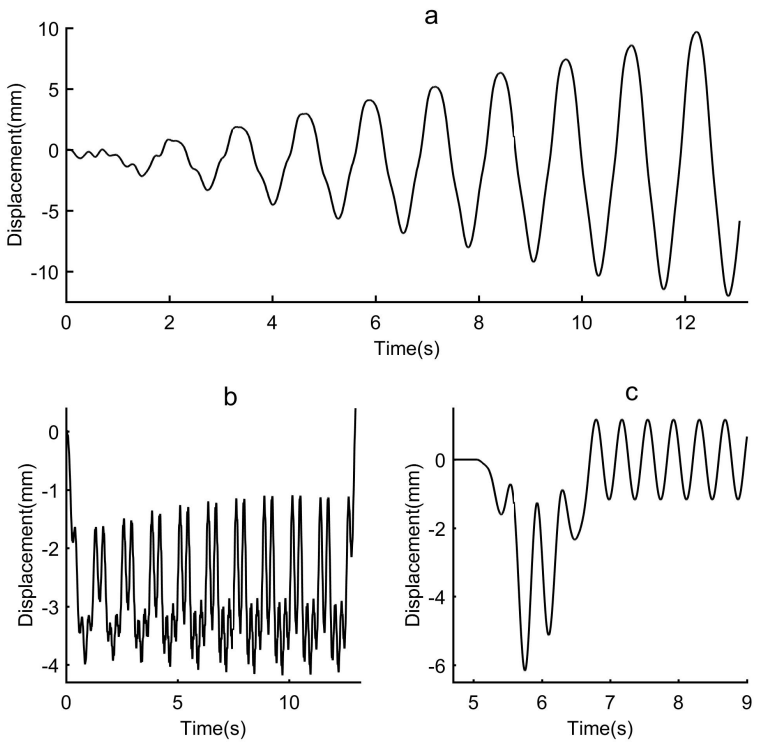

Figure 5.6 1-bay frame, a) horizontal displacement of point 4, b) vertical displacement of point 11, c) vertical displacement of the fifth sprung mass (y_5)

It is clear from Figure 5.4 that the crack location affects the maximum displacements in the vertical direction. The crack located at point 11 gives the largest maximum vertical displacements calculated for the same point. In addition, similar dynamic behavior has been observed for maximum vertical displacements at point 11 and the fifth sprung mass.

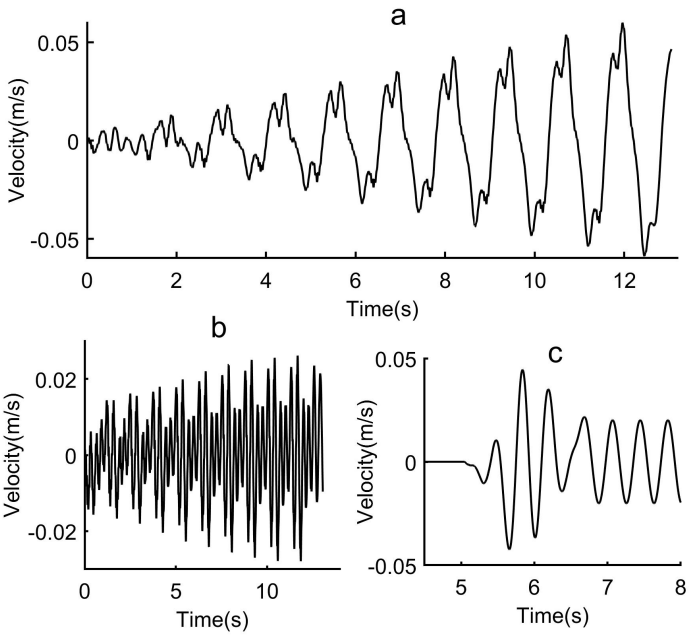

Figure 5.7 1-bay frame, a) horizontal velocity of point 4, b) vertical velocity of point 11, c) vertical velocity of the fifth sprung mass (y_5)

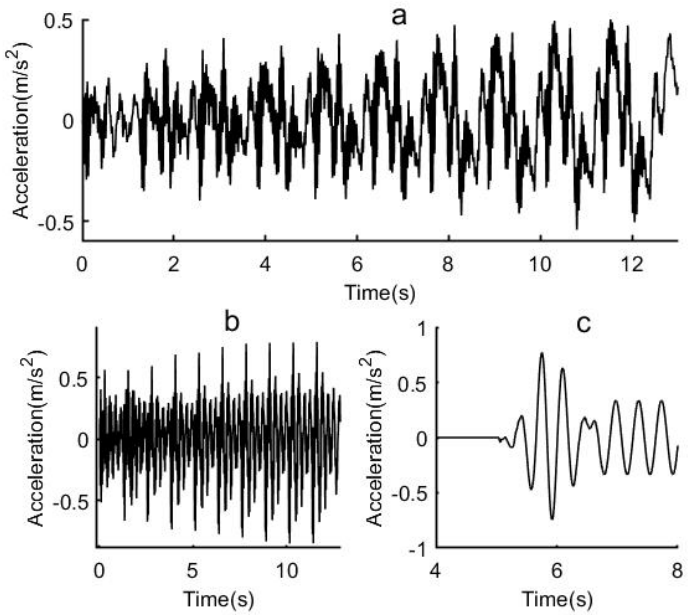

Figure 5.8 1-bay frame, a) horizontal acceleration of point 4, b) vertical acceleration of point 11, c) vertical acceleration of the fifth sprung mass (y_5)

The critical speed for vertical displacement of point 11 is related to the second natural frequency of the frame. It can be computed, following the procedure

mentioned above, as $V_{cr} = f_{n2}L_f = (2.9726)26 = 77.29$ m/s. The dynamic response in the vertical direction at point 11 illustrating the resonant behavior is shown in Figure 5.9 (a). Compared with Figure 5.6, it has been found that the amplitude of the vibration in the axial direction at point 4 gets a smaller value, in addition, the displacement of the vehicle takes a larger value, as seen in Figures 5.6 (b)-(c). Figures 5.7-5.8 show the velocity and acceleration responses for critical velocities. The responses have the same dynamic characteristic as in Figure 5.6. Passenger comfort assessment depends on the vertical acceleration of the vehicles body. The following limits are defined for passenger comfort in EN 1990: Eurocode: 1 m/s^2 acceleration is very good, 1.3 m/s^2 acceleration is good and 2 m/s^2 acceleration is acceptable (EN 1990, 2002). In Figure 5.8 (c), the maximum acceleration value is below 1 m/s^2. Based on the above limits, passenger comfort can be defined as very good.

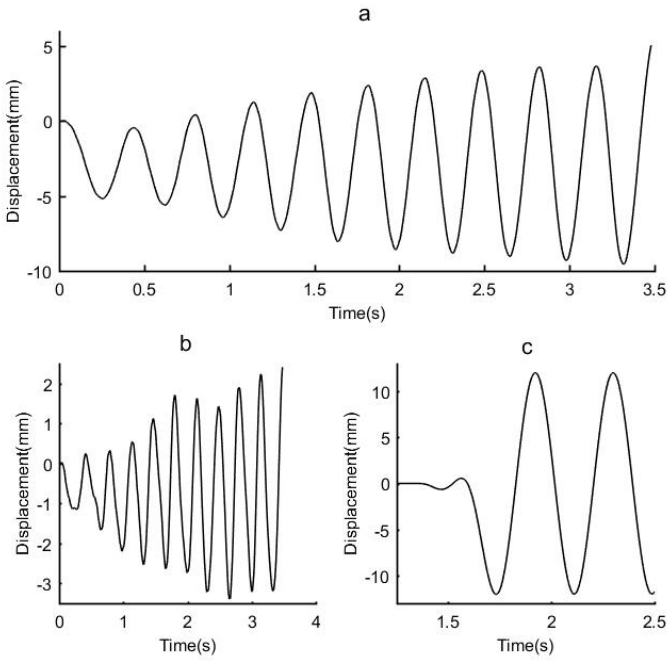

Figure 5.9 1-bay frame, a) vertical displacement of point 11, b)horizontal displacement of point 4, c) vertical displacement of the fifth sprung mass (y_5)

The velocity and acceleration responses for second critical speed are shown in Figures 5.10 and 5.11. The resonance behavior are also observed in the velocity and acceleration graphs. In Figure 5.11 (c), the maximum acceleration value is above

$2\ m/s^2$. This value is above the acceptable limit in terms of passenger comfort.

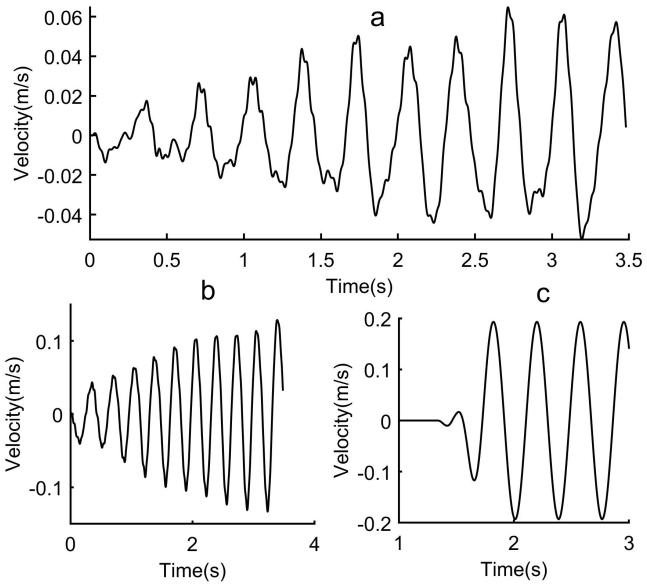

Figure 5.10 1-bay frame, a) horizontal velocity of point 4, b) vertical velocity of point 11, c) vertical velocity of the fifth sprung mass (y_5)

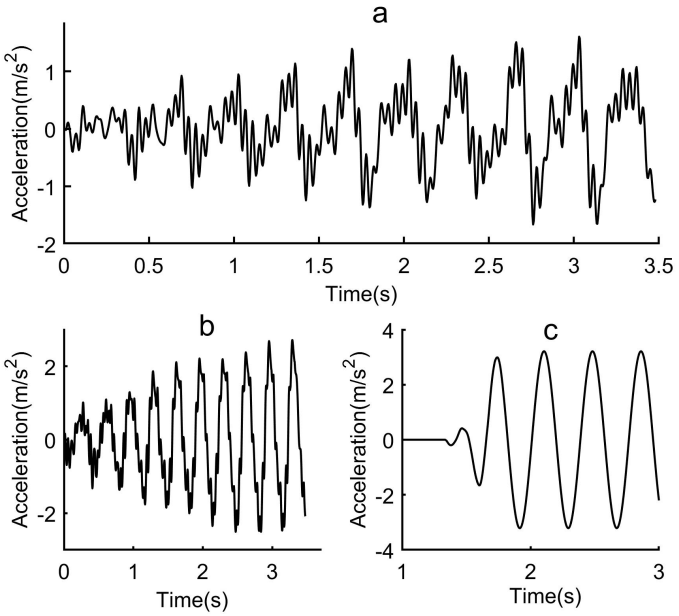

Figure 5.11 1-bay frame, a) horizontal acceleration of point 4, b) vertical acceleration of point 11, c) vertical acceleration of the fifth sprung mass (y_5)

In addition, the critical speeds can be read on the Figures 5.3-5.5. The critical speed values in this case are V_{c1} = 21 m/s and V_{c2} = 79 m/s. The percentage difference

between the formula (5.1) and the 3D graph at the first and second critical speeds are $(21-20.56)/21\times100 = 2.09$ and $(79-77.29)/79\times100 = 2.16$, respectively.

5.1.4 Multi-bay Frame

A similar computation carried out for 2 and 3-bay frames to generalize the procedure to multi-bay frames. The locations of the crack are shown in Figure 5.12 for 2 and 3-bay frames. Just as in the case of 1-bay frame, critical speed values are read from 3D graphics for the case where the crack is located at point 11. The natural frequencies of the structures are also calculated for the crack located at this point.

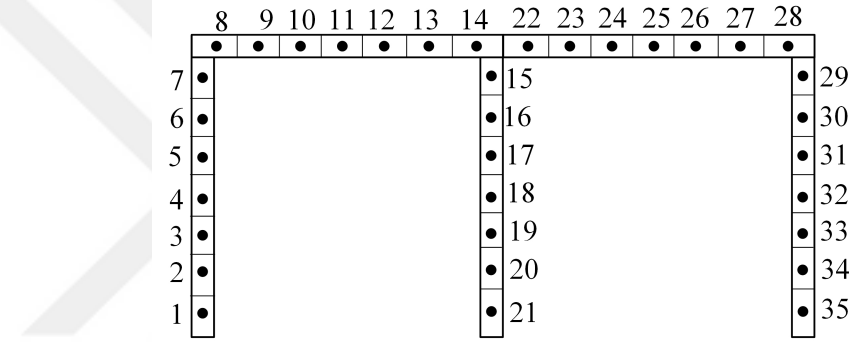

(a)

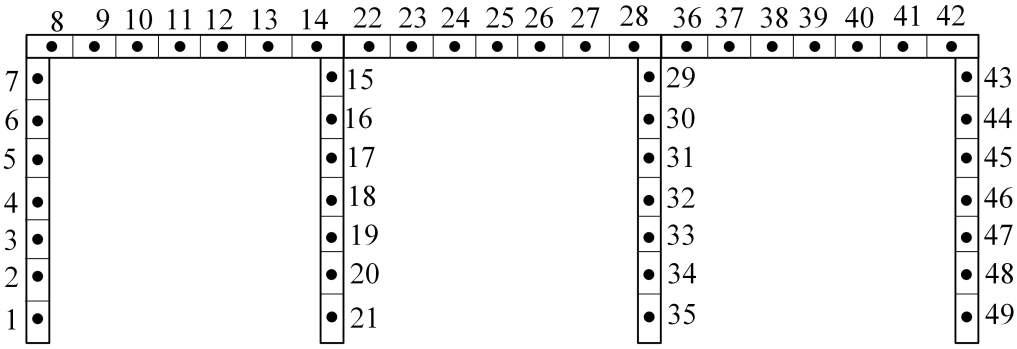

(b)

Figure 5.12 Crack locations, (a) 2-bay frame, (b) 3-bay frame

Figures 5.13-5.15 show 3D crack location-velocity-maximum displacement plots for 2-bay frame. It is seen in Figure 5.13 that crack position has no significant effect on the maximum displacements in the horizontal direction at point 4. Furthermore, it

can be seen that the effect of high speeds in the range of approximately 70 to 80 m/s on maximum displacements is increased compared to Figure 5.3. On the other hand, it is clear from Figures 5.4 and 5.14 that the effect of low velocity, which is the range of approximately 15 to 25 m/s on the maximum displacements in the vertical direction at point 11 decreases. The maximum displacements of the 5^{th} sprung mass are similar to displacements at the point 11 in the vertical direction (Figure 5.15).

The first two natural frequencies of 2-bay frame are 0.7329 and 2.9319 Hz. The critical speeds can be calculated as 19.06 and 76.23 m/s. In addition, critical speeds can be read on Figures 5.13 and 5.14 as 19 m/s and 78 m/s. The percentage differences are $(19.06-19)/19.06\times100 = 0.31$ and $(78-76.23)/78\times100 = 2.27$.

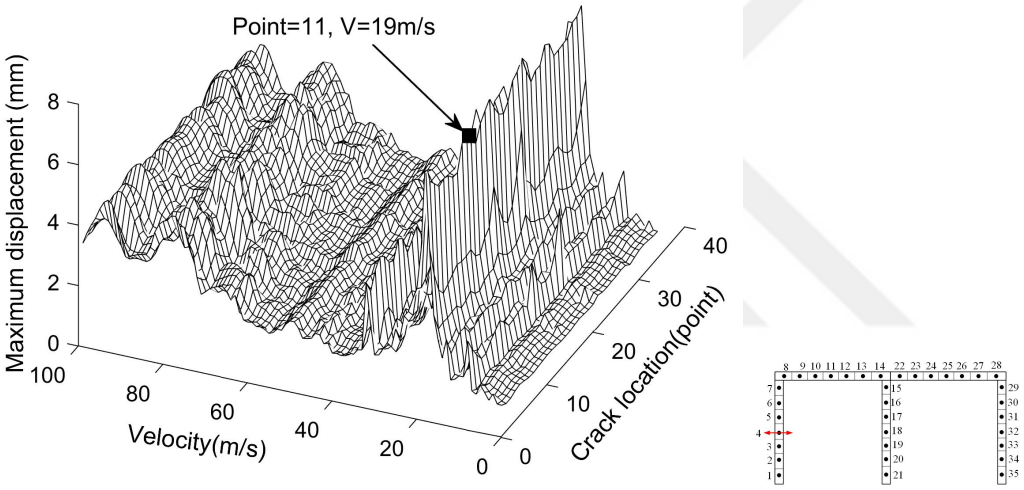

Figure 5.13 Maximum horizontal displacements of 2-bay frame at point 4

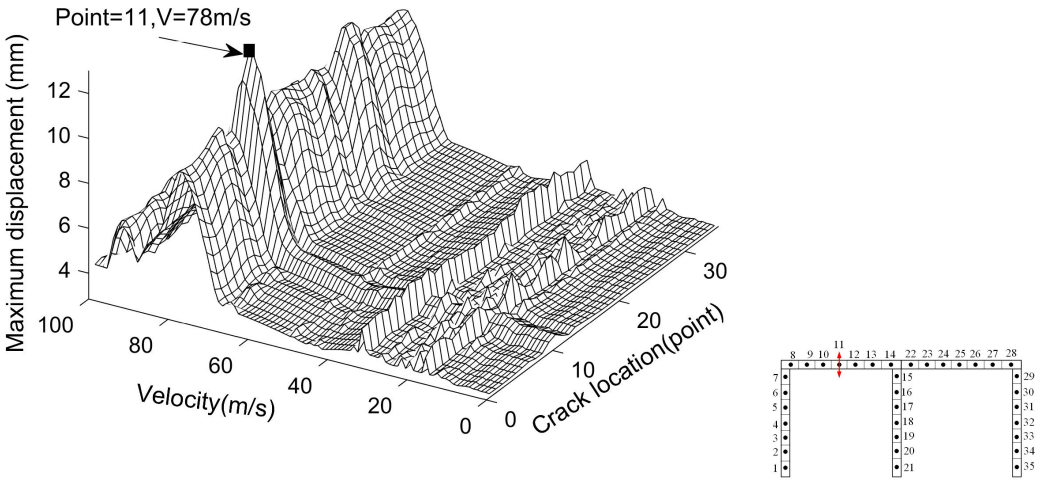

Figure 5.14 Maximum vertical displacements of 2-bay frame at point 11

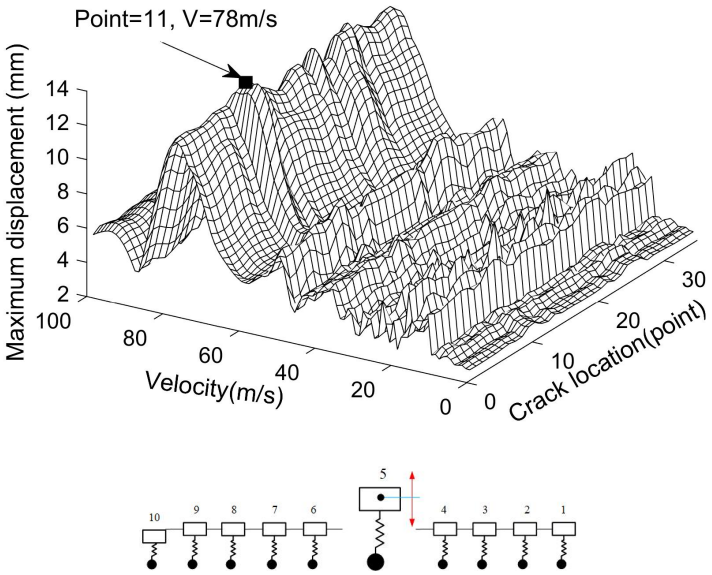

Figure 5.15 Maximum vertical displacements of the fifth sprung mass (y_5)

The 3D crack location-velocity-maximum displacement graphics for 3-bay frame are shown in Figures 5.16-5.18. As shown in Figure 5.16, the maximum displacements in the horizontal direction at high velocity values increased with the increasing number of the bay (see also Figures 5.3 and 5.13). In addition, the effects of the lower velocities on the maximum displacements in the vertical direction have gradually decreased as the number of bay increases, as seen in Figures 5.4, 5.14 and 5.16.

The first two natural frequencies of 3-bay frame are 0.7137 and 2.9164 Hz. The critical speeds computed using Equation (5.1) with $k = 1$ as 18.56 and 75.83 m/s. It is seen in Figures 5.16 and 5.17 that the critical velocity values are 19 and 77. The percentage difference are $(19 - 18.56)/19 \times 100 = 2.31$ and $(77 - 75.83)/77 \times 100 = 1.52$.

As can be seen in Figures 5.3, 5.4, 5.13, 5.14, 5.16 and 5.17, it has been determined that the approximate formula used to calculate the critical speed remains valid regardless of the number of bays. As a result of the increase in the number of bays, the flexibility of the structure is increased and the critical speed values are slightly reduced. The effect of increasing the number of bays will also increase the total number of vehicle loads on the structure and duration of the load interacting with the structure. As a natural consequence of this, dynamic responses can be expected to have larger amplitudes in the vertical direction of top beams.

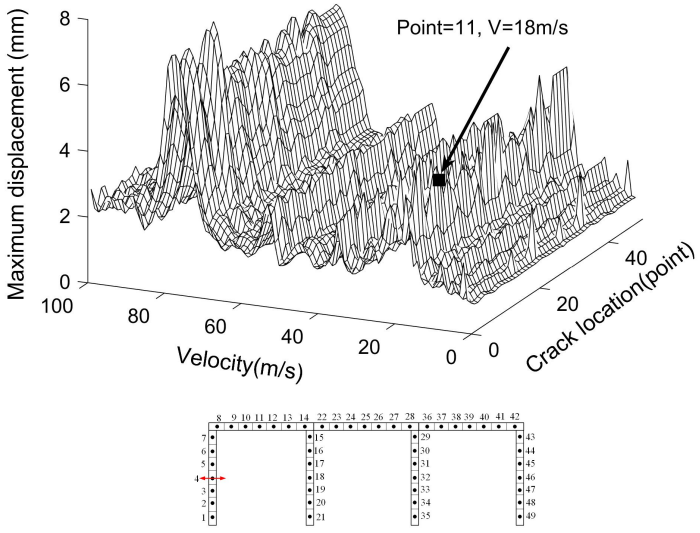

Figure 5.16 Maximum horizontal displacements of 3-bay frame at point 4

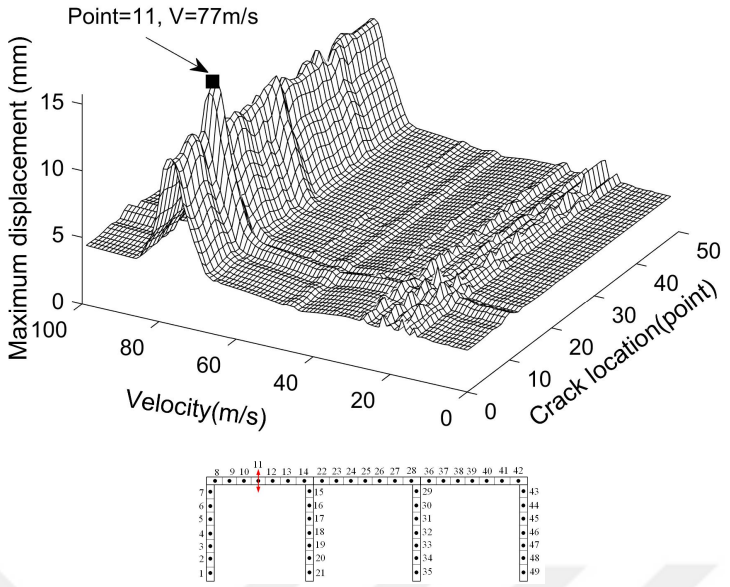

Figure 5.17 Maximum vertical displacements of 3-bay frame at point 11

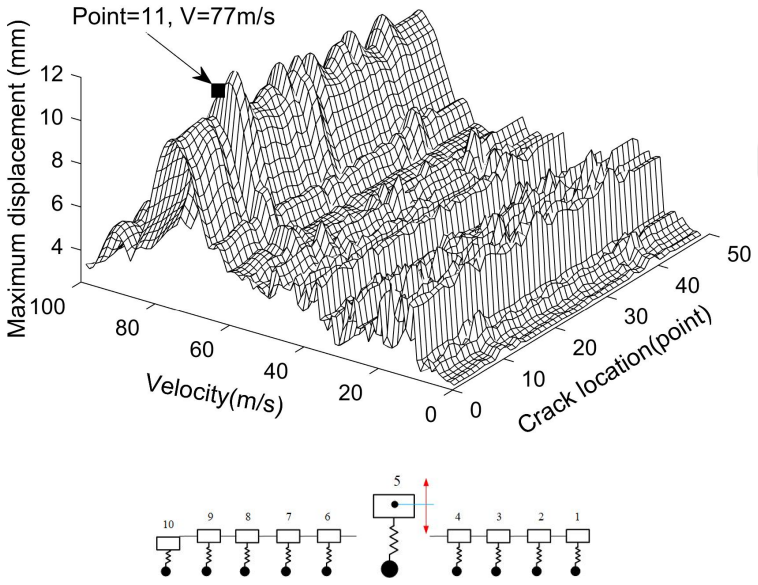

Figure 5.18 Maximum vertical displacements of the fifth sprung mass (y_5)

5.2 Effects of the Crack Location on the Dynamic Response of Multi-storey Frame Subjected to the Passage of High-speed Train

5.2.1 Numerical Model

The problem to be dealt with in the present study is a multi-bay frame with a crack, which is illustrated at the distance L_c from the left end of the top beam, subjected to moving train, shown in Figure 5.19. The physical and geometric properties of the vehicle and structure are given in Section 4.2.1. Also, structural damping is assumed to provide a modal damping ratio of $\zeta = 0.02$ for all modes.

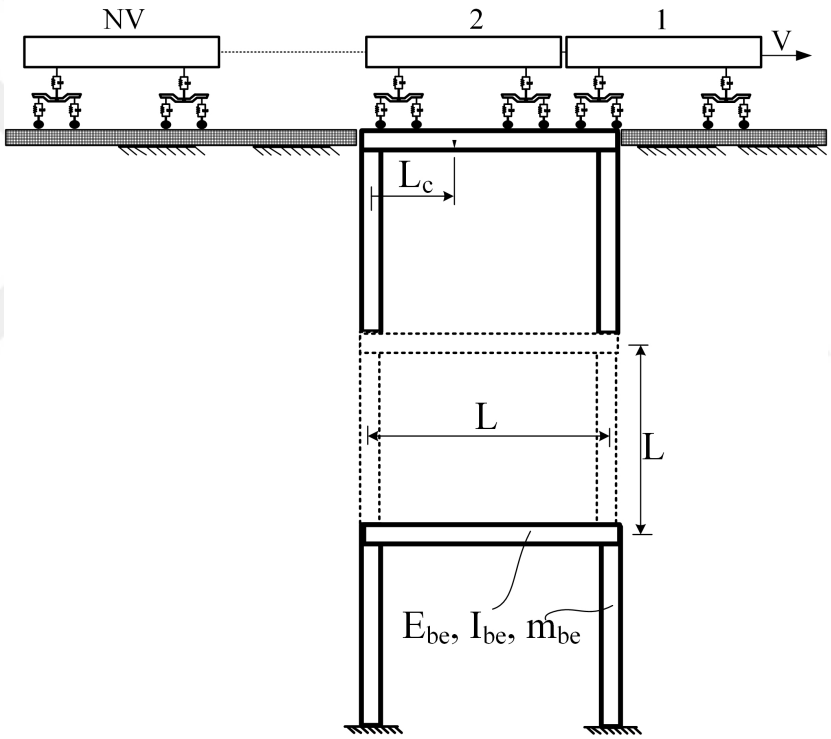

Figure 5.19 A train moving over a multi-storey frame

5.2.2 Cracked Multi-storey Frames Subjected to Moving Train

This section is devoted to the numerical evaluation of the expressions established in the preceding sections.

A i-storey ($i = 1, 2, 3$) cracked frame subjected to train with 5 identical vehicles, as

shown in Figure 5.19 with $NV = 5$, is considered here. The effect of velocity and crack location on the dynamic response was investigated by plotting the velocity (V)-crack location-dynamic magnification factor (DMF) plot. The DMF is defined as the ratio of the maximum dynamic deflection to the maximum static deflection. The maximum static deflection is computed at the midpoint of the top beam, as shown in Figure 5.20.

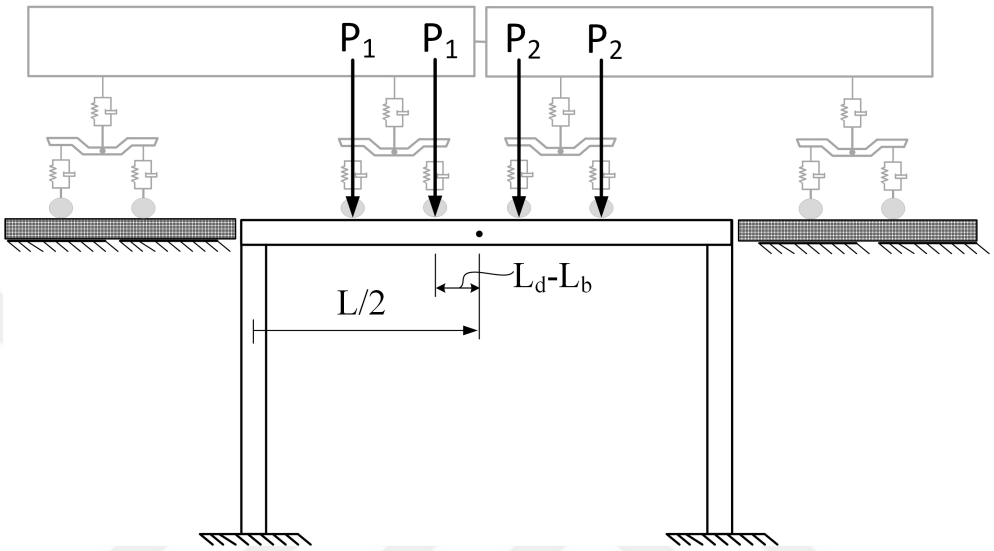

Figure 5.20 The calculation of the maximum static deflection

The loads P_1 and P_2 shown in Figure 5.20 are as follows:

$$P_1 = \left(m_w + 0.5m_b + 0.5m_v \frac{d_1}{d_1 + d_2}\right) g \quad (N) \tag{5.2}$$

$$P_2 = \left(m_w + 0.5m_b + 0.5m_v \frac{d_2}{d_1 + d_2}\right) g \quad (N) \tag{5.3}$$

where g is acceleration due to gravity.

The crack is located at the center of each element, as shown in Figure 5.21. The crack ratio is $a/h = 0.4$. It is assumed that there is only one crack in the structure. The element length of 5m is used. When calculating the DMF of the center point of the top beam (points $8, 23$ and 38 for 1, 2 and 3-storey frames, respectively), Equation (3.43) in Section 3.3.2 (with $\xi = 0.5$) needs to be used because this point does not correspond to a node.

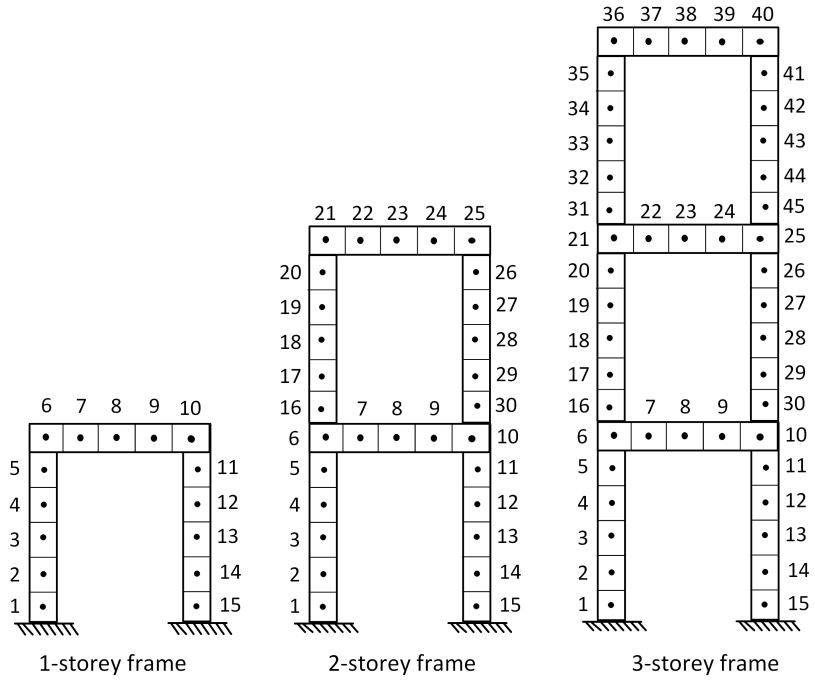

Figure 5.21 Locations of crack on the finite element model

5.2.2.1 1-storey Frame

Figure 5.22 (a) shows the 3D Velocity-Crack location-DMF plotted for 1-storey frame subjected to moving train. As can be seen from Figure 5.22 (a), the position of the crack up to 40 m/s has no effect on DMF. It is clear that the crack is effective in the range of $50-60$ m/s, where DMF takes maximum values. Its maximum value in this range is 2.91. This value is obtained when the speed of the train is 58 m/s and the crack is located at point 8, that is, at the midpoint of the top beam.

The time history graph for the maximum displacement point shown in Figure 5.22 (a) is given in Figure 5.22 (b). When the displacements of point 8 in the vertical direction are examined, the 1-storey frame exhibits resonance behavior at these values. Although the resonance behavior occurred for the frame, it was not observed in the vehicles body in the vertical direction.

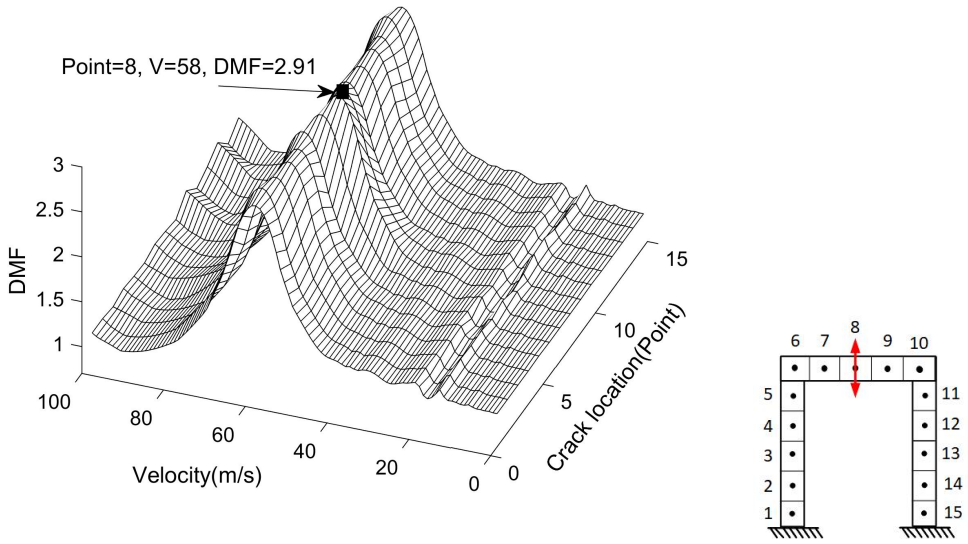

(a)

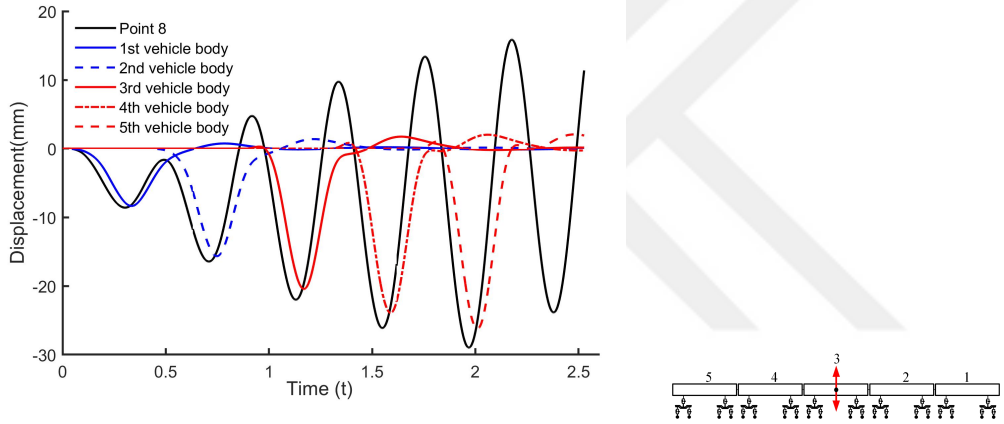

(b)

Figure 5.22 3D graphs: (a) Velocity-Crack location-DMF plot for point 8 of the 1-storey frame, (b) Vertical displacement of point 8 and vehicles body

The variation of the maximum displacements of the 3^{rd} vehicle's body in the vertical direction by changing the speed and crack position is plotted in Figure 5.23 (a). The crack is dominant over the maximum displacements in the speed range of $10-30$ m/s and $40-60$ m/s. Similar to the frame case, the crack located at point 8 has the greatest effect on dynamic response. The highest maximum displacement of the vehicle's body at $V = 55$ m/s of the train speed is achieved as 7.14 mm. The time history plotted for the point shown in Figure 5.23 (a) is given in Figure 5.23 (b). It is clear from Figures 5.23 (a) and 5.23 (b) that the maximum dynamic response of the frame and vehicle do not occur at the same speed but these values are very close to each other.

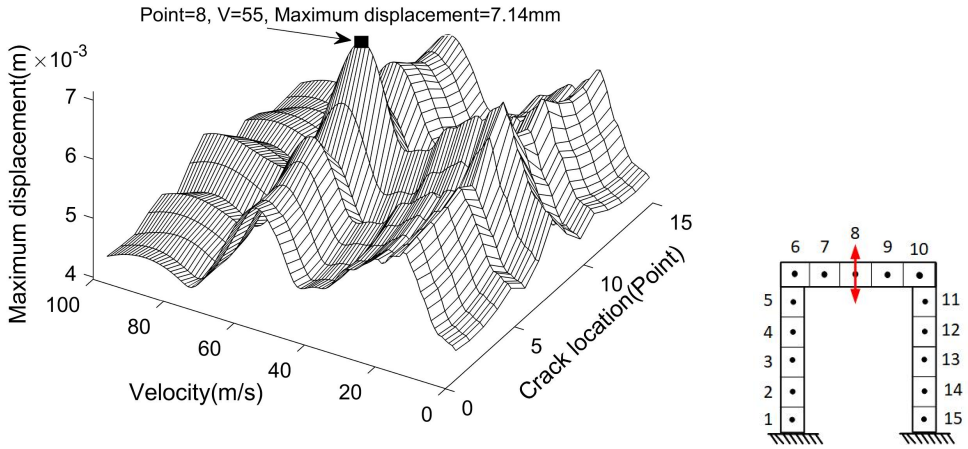

(a)

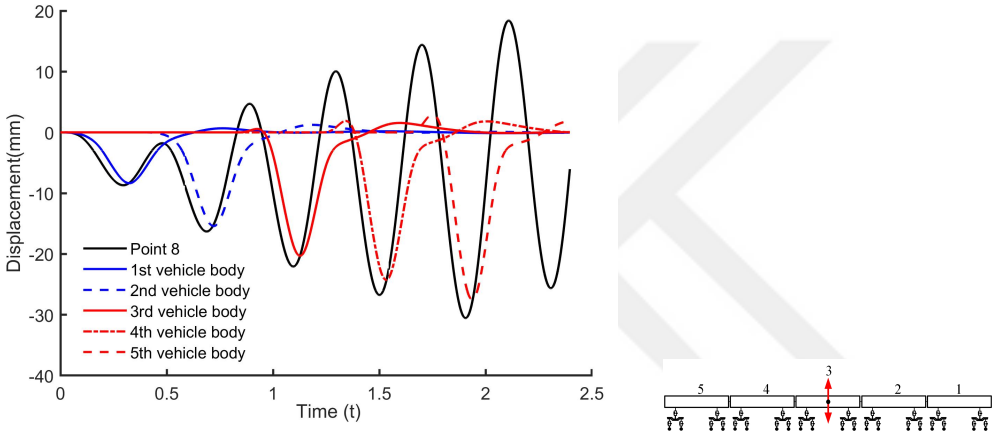

(b)

Figure 5.23 3D graphs: (a) Velocity-Crack location-DMF plot for point 8 of the 1-storey frame, (b) Vertical displacement of point 8 and vehicles body

5.2.2.2 2-storey Frame

Figure 5.24 (a) shows 3D plot of velocity-crack location-DMF for the 2-storey frame. The maximum DMF value of 2.198 is determined for the crack located at point 23 and V = 50 m/s. This point corresponds to the midpoint of the top beam. The maximum DMF and the velocity yielding it are found to be decreased when compared with the analysis for the 1-storey frame.

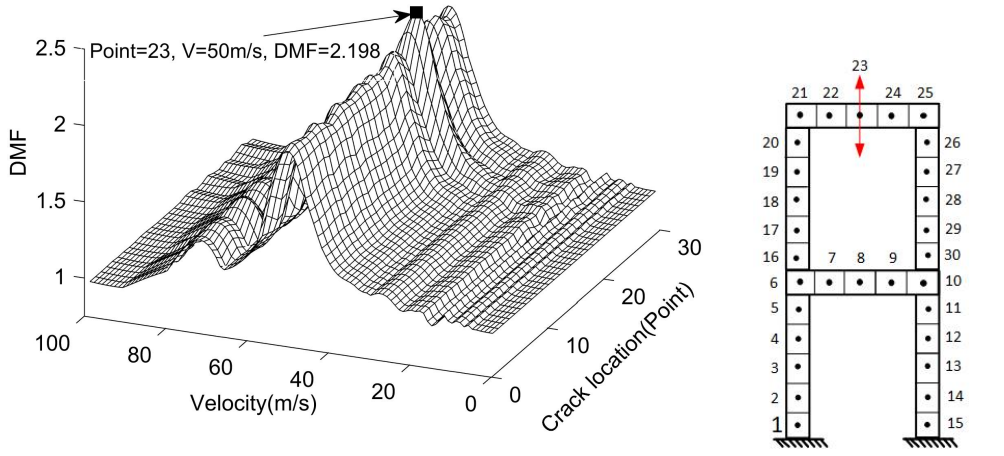

(a)

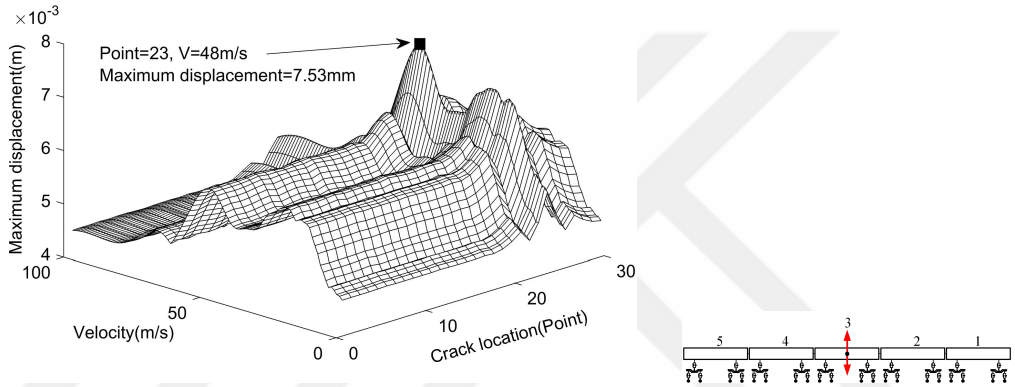

(b)

Figure 5.24 3D graphs: (a) Velocity-Crack location-DMF plot for point 23 of the 2-storey frame, (b)Velocity-Crack location-Maximum displacement plot of the 3^{rd} vehicle's body

From Figure 5.24 (b), one can observe that train speed of 48 m/s. The crack located at point 23 takes place the maximum displacement value as 7.53 mm. It is seen that the maximum displacement value increases slightly compared to the 1-storey frame case. The maximum dynamic responses from Figures 5.24 (a) and 5.24 (b) are at different velocity values. It can be noticed that the maximum displacements value ranges from 4.45 mm to 7.53 mm.

5.2.2.3 3-storey Frame

Figure 5.25 (a) shows the 3D graph of velocity-crack location-DMF for 3-storey frame. DMF values at each speed are calculated at point 38 in the vertical direction. The crack has the maximum effect at the midpoint of the beam (point 38) on which the train moves. Maximum DMF of 1.831 is determined at speed V = 48 m/s. It is observed that the DMF value decreases as the number of storey increases.

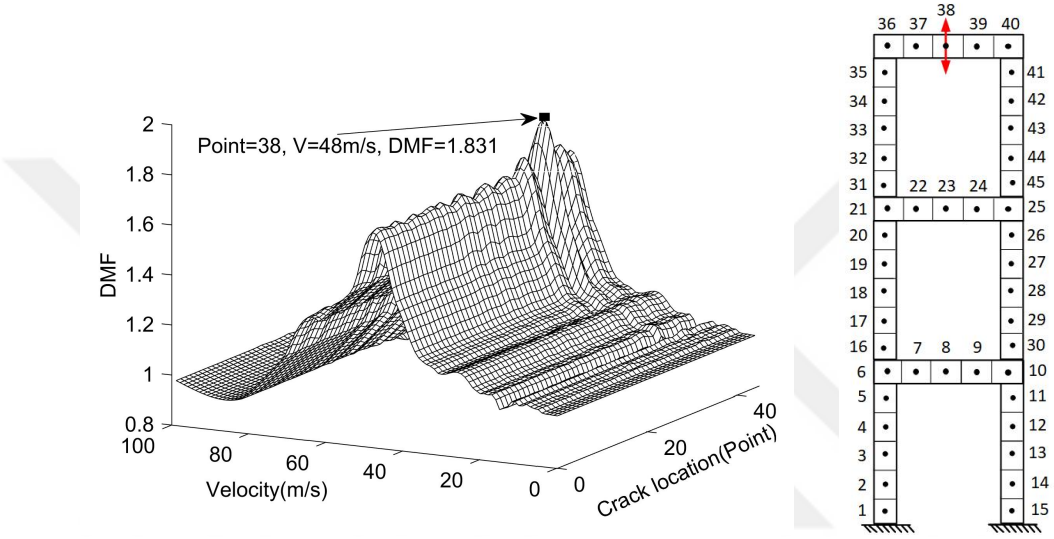

(a)

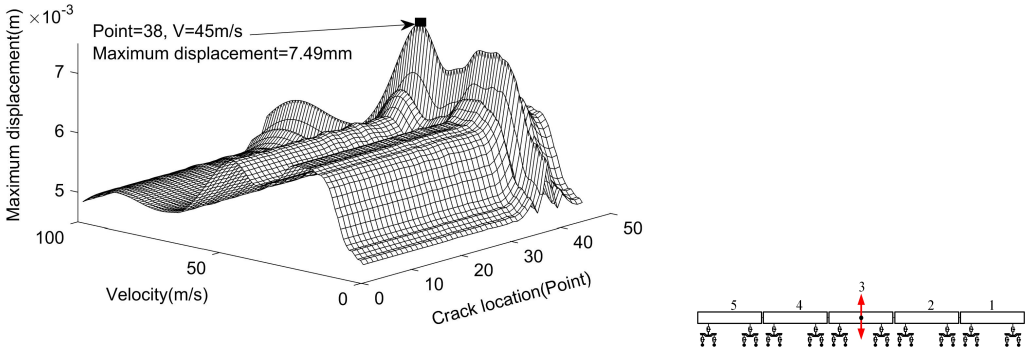

(b)

Figure 5.25 3D graphs: (a) Velocity-Crack location-DMF plot for point 38 of the 3-storey frame, (b)Velocity-Crack location-Maximum displacement plot of the 3^{rd} vehicle's body

The maximum displacement of the 3^{rd} vehicle's body in the vertical direction appears to be insensitive to the crack position except point 38 (5.25(b)). The presence

of the crack at point 38 has had a large impact on the maximum displacement. The maximum displacements take the maximum value of 7.13 mm at point 38 with train velocity $V = 45$ m/s.

CHAPTER SIX
CONCLUSIONS

In this thesis, the dynamic response of the complex structures subjected to vehicles moving at a constant speed V have been investigated. The complex structure, that is, multi- bay and multi- storey frames, consisting of beams and columns are modelled based on Bernoulli-Euler beam theory. The presence of cracks in the structure is also studied and the crack element is developed using the principle of fracture mechanics. The coupled equations of motion of the system are derived by the generalized Lagrange's equation. The Newmark method and Wilson-theta method are used to integrate the equations of motion.

6.1 Moving Load Model

Section 2.3 introduced the dynamic responses of multi-bay frame structures subjected to a concentrated moving load and successive moving loads with constant intervals. It is determined that the largest maximum transverse deflections are encountered when the speed parameter of the moving single force is about 0.58 for the 1-bay frame and multi-bay frame at the midpoint of the top beam over which the load first passes. Regardless of the number of the bay, the maximum displacement of the midpoint of each top beam occurs when the speed parameter of the moving force is approximately 0.73 in the case of the multi-bay frame structure except for the first bay. For the case of a multi-bay frame under successive moving load with a constant interval, the dynamic response at the point j has a similar dynamic behavior at point $(i - j + 1)$ due to the effect of structural symmetry (i denotes the number of the bay and $j < i$). The force span length L_f which gives the minimum dynamic response is independent of the number of bays forming the frame. The value of L_f corresponding to minimum response determined for a simply-supported beam has also been obtained for multi-bay frames. The second mode or the first beam dominant mode of frame structure has a decisive influence on the dynamic response. The relationship between the critical velocity and the L_f values in the multi-bay frames is linear, as the case

with the critical velocity formulation for a simply-supported beam.

It has been investigated in Section 2.4 that which mode shapes are effective in the resonance response of a multi-storey frame. The analyses are restricted by the vibrations in the vertical direction under the moving load sequence of the structure. The conclusions drawn are as follows: (1) The resonance response of the multi-storey frame takes place in one of the mode shapes where the displacement of the top beam in the vertical direction is significant. (2) Large dynamic magnification factor (DMF) values are obtained in the first mode where the displacement of the top beam was significant. These mode shapes were determined as 2^{nd} mode for 1-storey frame, 3^{rd} mode for 2-storey frame, 4^{th} mode for 3-storey frame and 5^{th} mode for 4-storey frame. This leads to result that if the storey number of the structure is N, the effect of $N+1^{th}$ mode on the resonance response should be taken into account. (3) The increase in the storey number of the structure has also increased the effects of the higher modes on the DMF. For example, the effects of the 5^{th} and 6^{th} modes on dynamic response are close to each other in the 4-storey frame.

6.2 Moving Vehicle Model

6.2.1 Beam element without a crack

In Section 4.1.1, the effect of the mode shapes on the dynamic response of the 3-bay frame subjected to train modelled as a 2-axle system with 4 DOF has been investigated. It has been determined that the dominant modes are the 1^{st}, 2^{nd} and the 3^{rd} modes of the 3-bay frame. Resonance vibrations were not encountered at point p_2 (mid-point of the top beam) in the 5^{th} mode where vertical displacements were negligible.

In Section 4.2, it has been demonstrated the effective mode shapes of the viaduct subjected to 10 DOF multi-body system modelling a train. It is inferred from this study that the first mode of the multi-bay frames is excited when the train is moving at a low speed ($V = 11$ m/s = 39.6 km/h). Also, the resonance phenomenon is encountered in the

2^{nd} mode of the 1 and 2-bay frames and 2^{nd} and the 3^{rd} modes of the 3-bay frame. The amplitude of the resonance vibrations decreases as the number of bays of the frame increases. At the point p_2, resonance vibrations are not displayed in the 3^{rd} mode of the 1-bay frame, the 4^{th} mode of the 2-bay frame, and the 5^{th} mode of the 3-bay frame, except for 1^{st} mode of i-bay frame (i=1,2,3), where vertical displacements are negligible.

6.2.2 Cracked Beam Element

In Section 5.1, the dynamic responses of the cracked multi-bay frame structures subjected to moving oscillators have been analyzed. The various aspects of this work are: (1) The first resonant response of the multi-bay structure is related to the vibration of the column in the horizontal direction. The second resonant response has been found to be associated with the vibration of the beam in the vertical direction. (2) The use of the critical speed formula obtained for the simply supported beam in the multi-bay frame has yielded satisfactory results. (3) The location of the crack on the frame has no apparent effect on the maximum displacements in the horizontal direction. Whereas, in the case crack located at the center point of the top beam, the structure has a greater risk of safety and stability since maximum displacement values in the vertical direction are observed at this location.

The effects of the crack location on the dynamic response of the multi-storey frame have been studied in Section 5.2. Firstly, numerical studies show that the maximum dynamic responses of the vehicle and multi-storey frame have not occurred at the same speed values. This speed value for the vehicle is slightly smaller than the multi-storey frame. If the vehicle moves at these speeds, the resonance behavior occurs for the frame. However, the resonance response is not observed for the body of the vehicles. Secondly, it is determined that as the number of storeys of the structure increases, a decrease in the maximum DMF value is observed. Finally, the position where the crack is most effective on the dynamic response is the midpoint of the top beam on which the train moves.

6.3 Conclusion Overview and Further Research

The dynamic analyses of the complex structures subjected to moving loads and train have been investigated. It has been demonstrated that it is sufficient to consider only the first mode of the structure in the simply supported beam in the literature. Viaduct-like structures consist of both beams and columns and horizontal displacement of the columns is not negligible. The horizontal displacements of the columns are dominant in the first few modes depending on the structure analyzed. Therefore, the effect of higher vibration modes on the dynamic response becomes important. The first mode in which the vertical displacement of the top beam is effective plays an important role in the resonance response of the multi-bay frame.

The presence of the crack affects the dynamic characteristic of the structure. The analyses were made by changing the location of the crack on the structure. When the crack is located at the midpoint of the top beam, it has been found that the crack has the greatest effect on dynamic displacements.

In this thesis, the finite element model of moving a series of load and train-structure interaction for complex structures are determined. As far as known, the practical application of the vehicle-structure interaction model is applied for the first time in such structures. In the author's opinion, the continued studies within this field should be considered rail irregularities, the train-rail-soil interaction, three-dimensional finite element model of train and structure, the effect of acceleration of the moving load and the effect of wind and earthquake excitation.

REFERENCES

Bathe, K.-J. (1996). *Finite element procedures* (2nd Ed.). Upper Saddle River, New Jersey 07458: Prentice Hall.

Biondi, B., Muscolino, G. & Sofi, A. (2005). A substructure approach for the dynamic analysis of train-track-bridge system. *Computers and Structures*, *83*(28-30 SPEC. ISS.), 2271–2281.

Cikurutug bridge, (n.d.). Retrieved September, 03, 2019, from http://http://www.orangesmile.com.

Demirtas, S., Ozturk, H. & Sabuncu, M. (2019). Dynamic response of multi-bay frames subjected to successive moving forces. *International Journal of Structural Stability and Dynamics*, *19*(4), 1950042.

Dimitrakopoulos, E. G. & Zeng, Q. (2015). A three-dimensional dynamic analysis scheme for the interaction between trains and curved railway bridges. *Computers and Structures*, *149*, 43–60.

Dimitrovová, Z. (2016). Critical velocity of a uniformly moving load on a beam supported by a finite depth foundation. *Journal of Sound and Vibration*, *366*, 325–342.

Duan, Y. F., Wang, S. M., Wang, R. Z., Wang, C. Y., Shih, J. Y. & Yun, C. B. (2018). Vector form intrinsic finite-element analysis for train and bridge Dynamic Interaction. *Journal of Bridge Engineering*, *23*(1), 1–15.

EN 1990 (2002): Eurocode - Basis of structural design. [Authority: The European Union Per Regulation].

Fryba, L. (1999). *Vibrations of solids and structures under moving loads* (3rd Ed.). London Thomas Telford: Thomas Telford Ltd.

Guo, W. W., Xia, H., De Roeck, G. & Liu, K. (2012). Integral model for train-track-bridge interaction on the Sesia viaduct: Dynamic simulation and critical assessment. *Computers and Structures*, *112-113*, 205–216.

Henchi, K., Fafard, M. Dhatt, G. & Talbot, M. (1997). Dynamic behaviour of multi-span beams under moving loads. *Journal of Sound and Vibration*, *199*(1), 33–50.

Hubbell, D. & Gauvreau, P. (2018). Frequency domain analysis of train – guideway interaction dynamics. *144*(8), 1–11.

Hughes, M. (2015). *The second age of rail: A history of high-speed Trains*. 97 St George's Place, Cheltenham: History Press Limited.

Johansson, C., Pacoste, C. & Karoumi, R. (2013). Closed-form solution for the mode superposition analysis of the vibration in multi-span beam bridges caused by concentrated moving loads. *Computers and Structures*, *119*, 85–94.

Ju, S. H. & Lin, H. T. (2003). Resonance characteristics of high-speed trains passing simply supported bridges. *Journal of Sound and Vibration*, *267*(5), 1127–1141.

Khalili, S. M. R., Jafari, A. A. & Eftekhari, S. A. (2010). A mixed Ritz-DQ method for forced vibration of functionally graded beams carrying moving loads. *Composite Structures*, *92*(10), 2497–2511.

Kiral, Z. & Kiral, B. G. (2007). Dynamic analysis of a symmetric laminated composite beam subjected to a moving load with constant velocity. *Journal of Reinforced Plastics and Composites*, *27*(1), 19–32.

Kumar, C. P. S., Sujatha, C. & Shankar, K. (2015). Vibration of simply supported beams under a single moving load: A detailed study of cancellation phenomenon. *International Journal of Mechanical Sciences*, *99*, 40–47.

Lee, Y. S. & Kim, S. H. (2010). Structural analysis of 3D high-speed train-bridge interactions for simple train load models. *Vehicle System Dynamics*, *48*(2), 263–281.

Lin, C. C., Wang, J. F. & Chen, B. L. (2005). Train-induced vibration control of high-speed railway bridges equipped with multiple tuned mass dampers. *Journal of Bridge Engineering*, *10*(4), 398–414.

Lin, H. P. & Chang, S. C. (2006). Forced responses of cracked cantilever beams subjected to a concentrated moving load. *International Journal of Mechanical Sciences*, *48*(12), 1456–1463.

Lou, P. Dai, G. L. & Zeng, Q. Y. (2005). Modal coordinate formulation for a simply supported bridge subjected to a moving train modelled as two-stage suspension vehicles. *Proceedings of the Institution of Mechanical Engineers, Part C: Journal of Mechanical Engineering Science*, *219*(10), 1027–1040.

Majka, M. & Hartnett, M. (2008). Effects of speed, load and damping on the dynamic response of railway bridges and vehicles. *Computers and Structures*, *86*(6), 556–572.

Mao, L. & Lu, Y. (2013). Critical speed and resonance criteria of railway bridge response to moving trains. *Journal of Bridge Engineering*, *18*(2), 131–141.

Meirovitch, L. (1986). *Elements of vibration analysis* (2rd Ed.). New York: McGraw-Hill.

Ministry of Transport and Infrastructure of the Republic of Turkey, (n.d.). Retrieved September, 17, 2019, from https://www.uab.gov.tr/uploads / pages / ulasan-ve-erisen-turkiye/3dbf8bb47414193.pdf.

Museros, P. & Alarcón, E. (2005). Influence of the second bending mode on the response of high-speed bridges at resonance. *Journal of Structural Engineering*, *131*(3), 405–415.

Neves, S. G. M., Azevedo, A. F. M. & Calçada, R. (2012). A direct method for analyzing the vertical vehicle-structure interaction. *Engineering Structures*, *34*, 414–420.

Ozturk, H., Kiral, Z. & Kiral, B. G. (2015). Dynamic Analysis of Elastically Supported Cracked Beam Subjected to a Concentrated Moving Load. *Latin American Journal of Solids and Structures*, *13*, 175–200.

Ozturk, H., Yashar, A. & Sabuncu, M. (2015). Dynamic stability of cracked multi-bay frame structures. *Mechanics of Advanced Materials and Structures*, *23*(6), 715–726.

Qian, G. L., Gu, S. N. & Jiang, J. S. (1990). The dynamic behaviour and crack detection of a beam with a crack. *Journal of Sound and Vibration*, *138*(2), 233–243.

Romero, A., Solís, M., Domínguez, J. & Galvín, P. (2013). Soil-structure interaction in resonant railway bridges. *Soil Dynamics and Earthquake Engineering*, *47*, 108–116.

Rostam, M. Javid, F. Esmailzadeh, E. & Younesian, D. (2015). Vibration suppression of curved beams traversed by off-center moving loads. *Journal of Sound and Vibration*, *352*, 1–15.

Shifrin, E. & Ruotolo, R. (1999). Natural frequencies of a beam with an arbitrary number of cracks. *Journal of Sound and Vibration*, *222*, 409–423.

Siemens, Velaro High-Speed Train for TCDD. Retrieved September, 17, 2019, from https://w3.usa.siemens.com/mobility/us/en/passenger-rail/rolling-stock/default/Documents/Velaro-TR-EN.pdf.

Song, Y., Kim, T. & Lee, U. (2016). Vibration of a beam subjected to a moving force: Frequency-domain spectral element modeling and analysis. *International Journal of Mechanical Sciences*, *113*, 162–174.

Su, D., Fujino, Y. Nagayama, T., Hernandez, J. Y. & Seki, M. (2010). Vibration of reinforced concrete viaducts under high-speed train passage: Measurement and prediction including train-viaduct interaction. *Structure and Infrastructure Engineering*, *6*(5), 621–633.

Svedholm, C., Zangeneh, A., Pacoste, C., François, S. & Karoumi, R. (2016). Vibration of damped uniform beams with general end conditions under moving loads. *Engineering Structures*, *126*, 40–52.

Şimşek, M. & Kocatürk, T. (2009). Free and forced vibration of a functionally graded beam subjected to a concentrated moving harmonic load. *Composite Structures*, *90*(4), 465 – 473.

Turkish State Railways(TCDD), Annual Statictics, (n.d.). Retrieved December, 11, 2019, from http://www.tcdd.gov.tr/files/istatistik//20142018yillik.pdf.

Turkish State Railways(TCDD), (n.d.). Retrieved September, 17, 2019, from http://www.tcdd.gov.tr/content/5.

Thambiratnam, D. & Zhuge, Y. (1996). Dynamic analysis of beams on an elastic foundation subjected to moving loads. *Journal of Sound and Vibration*, *198*(2), 149–169.

Wu, J., Whittaker, A. & Cartmell, M. (2000). The use of finite element techniques for calculating the dynamic response of structures to moving loads. *Computers & Structures*, *78*(6), 789–799.

Wu, J., Whittaker, A. & Cartmell, M. (2001). Dynamic responses of structures to moving bodies using combined finite element and analytical methods. *International Journal of Mechanical Sciences*, *43*, 2555–2579.

Wu, Y. S. & Yang, Y. B. (2003). Steady-state response and riding comfort of trains moving over a series of simply supported bridges. *Engineering Structures*, *25*(2), 251–265.

Xia, C. Y., Lei, J. Q., Zhang, N., Xia, H. & De Roeck, G. (2012). Dynamic analysis of a coupled high-speed train and bridge system subjected to collision load. *Journal of Sound and Vibration*, *331*(10), 2334–2347.

Xia, H., Zhang, N. & Guo, W. W. (2006). Analysis of resonance mechanism and conditions of train-bridge system. *Journal of Sound and Vibration*, *297*(3-5), 810–822.

Xiang, T., Zhao, R. & Xu, T. (2007). Reliability Evaluation of Vehicle–Bridge Dynamic Interaction. *Journal of Structural Engineering*, *133*(8), 1092–1099.

Yang, Y.-B., Chang, C.-H. & Yau, J.-D. (1999). An element for analysing vehicle-bridge systems considering vehicle's pitching effect. *International Journal for Numerical Methods in Engineering*, *46*, 1031–1047.

Yang, Y. B., Lin, C. L., Yau, J. D. & Chang, D. W. (2004). Mechanism of resonance and cancellation for train-induced vibrations on bridges with elastic bearings. *Journal of Sound and Vibration*, *269*, 345–360.

Yang, Y. B. & Lin, C. W. (2005). Vehicle–bridge interaction dynamics and potential applications. *Journal of Sound and Vibration*, *284*, 205–226.

Yang, Y.-B., Yau, J.-D. & Hsu, L.-C. (1997). Vibration of simple beams due to trains moving at high speeds. *Engineering Structures*, *19*(11), 936–944.

Youcef, K., Sabiha, T., El Mostafa, D. Ali, D. & Bachir, M. (2013). Dynamic analysis of train-bridge system and riding comfort of trains with rail irregularities. *Journal of Mechanical Science and Technology*, *27*(4), 951–962.

Zheng, D. Y., Cheung, Y. K., Au, F. T. K. & Cheng, Y. S. (1998). Dynamic behaviour of multi-span beams under moving loads. *Journal of Sound and Vibration*, *212*(3), 455–467.

APPENDICES

APPENDIX-1: Nomenclature

$\boldsymbol{M}$, $\boldsymbol{C}$, $\boldsymbol{K}$	Structural mass, damping and stiffness matrices
$\boldsymbol{f}$	Force vector
E	Elastic modulus
ρ	Mass density
$I(x)$	Impact factor
$R_d(x)$, $R_s(x)$	Maximum dynamic and maximum static responses
S_v	Speed parameter
L	Length of the beam/column
I	Area moment of inertia
V	Velocity of moving load/vehicle
L_f	Force span length
$\overline{L}$	Force span length to beam length ratio
DMF	Dynamic magnification factor
ω	Circular natural frequency
V_{cr}	Critical velocity
A	Cross-section area
m	Mass per unit length
f	Natural frequency in Hz
$r(x)$	Rail irregularity function
$y(t)$	Vertical displacement of sprung mass
$y_w(t)$	Vertical displacement of the wheelset
$\boldsymbol{q_f^{ei}}$	Nodal displacement vector of element ei
N_i	Interpolation function
m_v	Mass of the vehicle body
J_v	Mass moment of inertia of vehicle body
d_1	Horizontal distance between the centre of gravity of car body and of rear bogie

d_2	Horizontal distance between the centre of gravity of car body and of front bogie
L_d	Longitudinal distance between the centre of gravity of bogie and nearest side of vehicle body
k_p	Stiffness of primary suspension system
c_p	Damping of primary suspension system
k_s	Stiffness of secondary suspension system
c_s	Damping of secondary suspension system
m_b	Mass of a bogie
J_b	Mass moment of inertia of a bogie
L_b	Half of bogie axle base
ζ	Damping ratio
$\boldsymbol{q_v}$	Displacement vector of vehicle
y_{bi}, y_v	Vertical displacement of the bogie and the vehicle's body
θ_{bi}, θ_v	Rotation of the bogie and the vehicle body
l_c	Location of the crack measured from right end of the beam
a	Crack depth
h	Thickness of the beam
K_{IP_1}, K_{IP_2}, K_{IIP_1}	Stress intensity factors
ν	Poisson ratio
$\boldsymbol{C^{(0)}}$	Flexibility matrix of the beam without crack
$\boldsymbol{C^{(1)}}$	Additional flexibility matrix
$\boldsymbol{K_c}$	Stiffness matrix of cracked beam element